A New Blind Equalization Scheme based on Principle of Minimal Disturbance

by

Bakhtiar Qutub Ali

A Thesis Presented to the
DEANSHIP OF GRADUATE STUDIES

In Partial Fulfillment of the Requirements
for the Degree

MASTER OF SCIENCE

IN

Telecommunication Engineering

KING FAHD UNIVERSITY
OF PETROLEUM AND MINERALS

Dhahran, Saudi Arabia

MAY 2004

KING FAHD UNIVERSITY OF PETROLEUM AND MINERALS

DHAHRAN 31261, SAUDI ARABIA

DEANSHIP OF GRADUATE STUDIES

This thesis, written by **Bakhtiar Qutub Ali** under the direction of his thesis advisor and approved by his thesis committee, has been presented to and accepted by the Dean of Graduate Studies, in partial fulfillment of the requirements for the degree of **MASTER OF SCIENCE IN TELECOMMUNICATION ENGINEERING.**

THESIS COMMITTEE

_____
Dr. Zerguine, A. (Chairman)

_____
Dr. Deriche, M. (Member)

_____
Dr. Duwaish, H. (Member)

_____
Dr. Jamil M. Bakhashwain
Department Chairman

_____
Dr. Mohammad A. Al – Ohali
Dean of Graduate Studies

_____
Date

Dedicated to

My Parents

ACKNOWLEDGEMENTS

In the name of Allah, the Most Gracious and the Most Merciful

I would like to express my deepest gratitude to **King Fahd University of Petroleum and Minerals** for providing me with an environment that made this work possible. I am indebted to the faculty members of the Electrical Engineering Department at KFUPM who have imparted and inculcated the knowledge and attitude to do research in this field.

This thesis would not be in existence if it were not for my colleagues, friends and mentors. I am grateful to Dr. Azzedine Zerguine for his patience, moral support, words of encouragement and valuable advise throughout this work. I am thankful to Dr. Mohammad Deriche for his constructive and positive criticism and thought-provoking contribution in my research. I am also thankful to Dr Hussain Duwaish for patiently reviewing my work.

Acknowledgement is due to my senior fellows Shafayat Abrar for helping me on issues relating to LATEX and MATLAB. I also appreciate the moral support pro-

vided by my peers Aleem, Riyaz, Mazher, Amer, Kaleem, Ameer, Zahed, Baber and Faisal.

Special thanks to my surrogate family; Mazher, Qayyum, Yousuf, Ayub, Hameed, Siraj, Obaid, Farooq and Kashif for making my stay in the University memorable and pleasant.

I would like to thank my parents and my younger brother who were with me to guide in every step of my life.

Contents

List of Tables

List of Figures

THESIS ABSTRACT

Name: Bakhtiar Qutub Ali

Title: A New Blind Equalization Scheme using the Principle of Minimal Disturbance

Degree: MASTER OF SCIENCE

Major Field: Telecommunication Engineering

Date of Degree: May 2004

A generalized blind equalization scheme, insensitive to phase shifts introduced by the channel and small carrier phase offsets, is derived. Multiple constraints optimization techniques have been used in the development of the proposed algorithm. This scheme is an improved version of a dual mode modified constant modulus algorithm (MCMA). It uses the principle of minimal disturbance to induce robustness and stability by avoiding the gradient noise amplification problem. Simulation results performed on baud spaced and fractionally spaced equalizers indicate that the new algorithm gives better convergence rates than the existing Lin's algorithm and that of the MCMA with decision directed mode (MCMA-DD).

Keywords*: blind equalization,CMA, MCMA, multiple constraints, DD mode.*

King Fahd University of Petroleum and Minerals, Dhahran.
May 2004

خلاصة الرسالة

الأسم : بختيار قطب علي

عنوان الرسالة: مخطط اعمى جديد للتعديل باستعمال مبدا الاضطراب الادنى

الدرجة الممنوحة: ماجستير في العلوم

حقل التخصص: الهندسة الكهربائية

تاريخ منح الدرجة: ماي 2004م

في هذه الرسالة, تم تطويرمخطط اعمى جديد غير حساس للازاحة في الطور الناتجة عن القناة وايضا للازاحة في طور الحامل.
لقد تم استعمال تقنيات الامثّلة متعددة القيود في تطوير الخوارزمية المقترحة. هذا المخطط هو نسخة محسنة للخوارزمية ثنائية النمط المغيرة ذات الطويلة الثابتة (MCMA). هذا الاخير يستعمل مبدا الاضطراب الادنى لادخال المرونة و الاستقرار عن طريق تجنب مشكلة تضخم الضجيج التدرجي. نتائج المحاكاة و التي استعمل فيها معدلات ذات تباعد بودي و نسبي تبين ان الخوارزمية الجديدة تعطي سرعة تقارب احسن من خوارزمية Lin و من خوارزمية MCMA ذات نمط القرار الموجه (MCMA-DD).

مفردات: التعديل الاعمى,CMA, MCMA , القيود المتعددة, نمط DD.

درجة الماجستير في العلوم

جامعة الملك فهد للبترول و المعادن

ماي 2004

Chapter 1

Introduction

The desire to move data at high rates across transmission media with limited bandwidth has prompted the development of sophisticated communications systems, for example, voice band modems and microwave radio relay systems. Success in these applications has led to great interest in other communication scenarios in which economic or regulatory considerations limit the available transmission bandwidth. An important example of such an application is the wireless and cable distribution of digital television.

Information-bearing signals transmitted between remote locations often encounter a signal-altering physical channel. Examples of common physical channels include coaxial, fiber optic, or twisted-pair cable in wired communications and the atmosphere or ocean in wireless communications. Each of these physical channels may cause signal distortion, including echoes and frequency-selective filtering of the

transmitted signal. In digital communications, a critical manifestation of distortion is inter-symbol interference (ISI), whereby symbols transmitted before and after a given symbol corrupt the detection of that symbol. All physical channels (at high data rates) tend to exhibit ISI. The presence of ISI is readily observable in the sampled impulse response of a channel; an impulse response corresponding to a lack of ISI contains a single spike of width less than the time between symbols.

Central to the successful employment of most high-data-rate transmission systems is the use of adaptive equalization to counteract the disruptive effects of the signal's propagation from the transmitter to the receiver. Linear channel equalization, an approach commonly used to counter the effects of linear channel distortion, can be viewed as an application of a linear filter (i.e., the equalizer) to the received signal. The equalizer attempts to extract the transmitted symbol sequence by counteracting the effects of ISI, thereby improving the probability of correct symbol detection.

Since it is common for the channel characteristics to be unknown (e.g., at startup) or to change over time, the preferred embodiment of the equalizer is a structure adaptive in nature. The general operating modes of equalizer include tracking and training. First a known, fixed-length training sequence is sent by the transmitter so that the receiver's equalizer may adapt to a proper setting for minimum bit error rate (BER) detection.

The training sequence is typically a pseudo-random binary signal or a fixed pre-

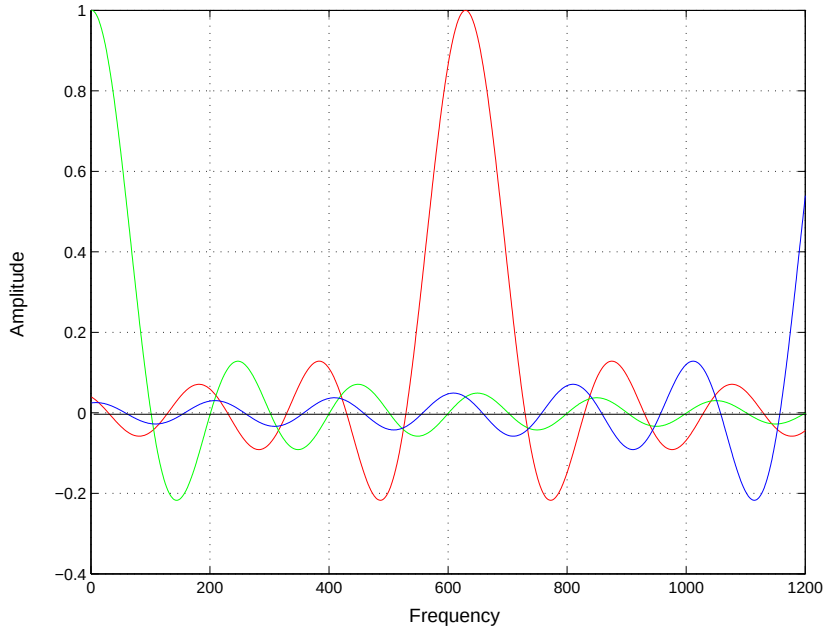

Figure 1.1: Inter-Symbol Interference

scribed pattern. Immediately following this training sequence, the user data (which may or may not include coding bits) is sent, and the adaptive equalizer at the receiver utilizes a recursive algorithm to evaluate the inverse of the channel and estimate the filter coefficients to compensate for the distortion created by multipath in the channel. The training sequence is designed to permit an equalizer at the receiver to acquire the proper filter coefficients in the worst possible channel conditions (e.g., fastest velocity, longest time delay spread, deepest fades etc.) so that when the training sequence is finished, the filter coefficients are near the optimal values for reception of user data. As user data are received, the adaptive algorithm of the equalizer tracks the changing channel. As a consequence, the adaptive equalizer is continually changing its filter characteristics over time. When the equalizer has

been properly trained, it is said to have converged.

Classical equalization techniques employ a time-slot (recurring periodically for time- varying situations) during which a training signal, known in advance by the receiver, is transmitted. The receiver adapts the equalizer so that its output closely matches the known reference training signal. The more recent emergence of digital multipoint and broadcast systems has produced communication scenarios where training is infeasible or prohibited, since the inclusion of such signals sacrifices valuable channel capacity.

1.1 Blind Equalization

Blind adaptive equalizers are those that do not need training to achieve convergence from an acceptable equalizer setting to a desired one. During the 1980's, linear equalization methods capable of blind start up moved from concept into practice. Blind equalization is desirable in multipoint and broadcast systems and necessary in noninvasive test and intercept scenarios. Even in point-to-point communication systems, blind equalization has been adopted for various reasons, including capacity gain and procedural convenience.

During the 1990's blind equalization was incorporated into several emerging communication technologies [2, 3], for example, digital cable TV. Also in the 1990's realization of the ideal capabilities of fractionally-spaced data-adaptive equalizers, espe-

cially blind finite-length varieties [4], have energized the study of finite-length fractionally spaced blind equalizers. The problem of blind equalization can be described using a simple system diagram shown in Figure 1.2 . The complex baseband model of a typical quadrature amplitude modulated signal (QAM) data communication

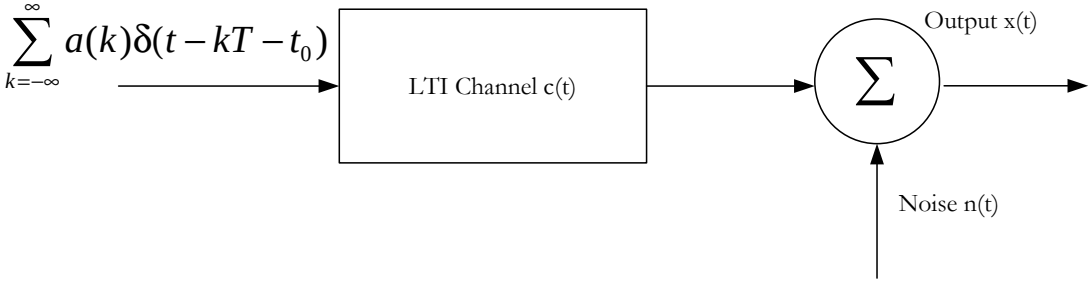

Figure 1.2: Baseband representation of QAM data communication system

system consists of a linear-time invariant(LTI) channel which represents all the interconnections between the transmitter and the receiver at the baseband. The baseband equivalent of the complex valued input data $a(k)$, each element of which belongs to a complex alphabet $\hat{A}$ (or constellation) of a QAM symbol. The data sequence $a(k)$ is sent through a baseband-equivalent complex LTI channel whose output $x(t)$ is observed by the receiver. The function of the receiver is to restore the original data $a(k)$ from the observation $x(t)$ by producing a sequence of estimates for $a(k)$. For a causal and complex LTI communication channel with impulse response $h(t)$, the input/output relationship of the QAM system can be written in

the baseband as:

$$x(t) = \sum_{k=-\infty}^{\infty} a(k)h(t - kT - t_0) + n(t) \tag{1.1}$$

where T is the symbols baud period. Typically the noise $n(t)$ is assumed to be stationary, white, independent of the channel input $a(k)$. When the distortion caused by the nonideal channel impairs the receiver's ability to correctly detect the input sequence, as it is of the the case in practice, equalization is needed to remove the inter-symbol interference (ISI) at the sampling instants such that the transmitted sequence $a(k)$ can be recovered at the receiver. The function of the the receiver is to restore the original data $a(k)$ from the observed signal $x(t)$. Since undesirable ISI is introduced at the channel output $x(t)$ from which a simple memory less decision device may not be able to recover the original data sequence, equalizers need to be applied to remove the unwanted ISI .

Traditional channel equalizers adopt often the minimum mean square error (MMSE) criteria based on the known actual channel input sequence during training. Equalization with training is common to many digital communication systems such as high speed telephone modem, satellite communication systems, digital cellular communication systems. When the channel noise $n(t)$ is of secondary importance, zero forcing (ZF) equalization can be used which essentially attempt to achieve the channel inverse and cancel the ISI. When the channel noise is significant, MMSE equalizers are more effective in reducing the probability of symbol detection error. Both meth-

ods require the identification of the channel frequency response either directly or indirectly. The channel identification process is explicit in non linear channel equalization schemes such as the decision feedback equalizer (DFE) and the maximum likelihood sequence estimator (MLSE) and implicit in linear equalizers where a ZF or MMSE criterion is applied.

The basic problem of blind equalization of a linear channel is nearly identical to that of the system identification without the knowledge of the input signal [5]. Given an output signal of a linear system, the linear system parameters can be uniquely identified if the input signal is persistently exciting. In fact, any constant but finite delay introduced by the channel and equalizer combination is acceptable. once the channel is identified, a desired equalizer can be constructed accordingly. Since the first published work by Sato [6] in 1975, blind equalization has been studied by many researchers and there have been many algorithms proposed.

1.2 Baud Spaced and Fractionally Spaced Equalizers

The 1970's witnessed the emergence of fractionally spaced equalizer (FSE) implementations [7], that is, those that used sampling rates faster than the source-symbol rate. Improved band-edge equalization capabilities and reduced sensitivity to timing synchronization errors were cited as motivation The practical necessity of "tap

leakage" for long FSEs was the most significant adaptive equalizer algorithm modification [8]. Performance analyzes for both fractionally spaced and baud-spaced equalizers commonly included assumptions of effectively infinite equalizer length, which permitted perfect equalization and easy translation between time-and frequency domain interpretations. For performance reasons, fractional spacing of the equalizer became preferred where technologically was feasible. However, performance analysis of blind equalizers remained focused almost exclusively on baud-spaced realizations [9].

For a fractionally spaced equalizer (FSE), the tap spacing of the equalizer is a fraction of the baud spacing (in time) or the transmitted symbol period. As the output of the equalizer has the same rate as the input symbol rate, the output of the FSE needs to be calculated once in every symbol period. In this situation, the FSE can be modeled as a parallel combination of a number of baud spaced equalizers.The over-sampling factor determines the tap spacing of the FSE. If T is the symbol period, then

$$\text{tap spacing} = \frac{T}{\text{over sampling factor}} \tag{1.2}$$

The FSE is an FIR filter and the tap spacing of this filter is T/M, where M is the over-sampling factor. As the sample period of the input sequence is the same as the tap spacing of the filter, the input sequence to the FSE, $x(t)$, needs to be sampled at intervals T/M apart. The expression for the discrete time equivalent

signal $x(n\frac{T}{M})$ is given as

$$x(n\frac{T}{M}) = \sum_{k=-\infty}^{\infty} a(k)h(n\frac{T}{M} - kT - t_0) + n(n\frac{T}{M}) \tag{1.3}$$

where n is an integer

1.3 Motivation

Lin [10] proposed an algorithm using the principle of minimal disturbance and the decision directed mode. The proposed algorithm performed dual operation of simultaneous equalization and phase recovery utilizing the advantage of principle of minimal disturbance to achieve better stability and robustness with respect to various noise characteristics and time-varying channels. Also higher convergence speed and lower steady state error were obtained by means of simple switch between the blind and decision directed modes without increasing the computational complexity.

Tanrikulu *et.al.* [11] proposed constant modulus adaptive blind algorithms which corresponded to an error performance surface, much improved upon that of the existing algorithms. Many undesirable local solutions were avoided by using a deterministic optimization criterion with a soft constraint to obtain an update equation which contains a normalized gradient vector and a particular continuous non-linearity. This approach was extended to multiple constraints to yield faster converging algorithms.

The intended research work is to combine the ideas proposed by Lin and extend

it using the multiple constraints criterion as given by Tanrikulu and his co-workers [11].

1.4 Objectives and Outline of Thesis

In this research work, blind equalizers for digital communication systems will be investigated. The main objective of this thesis is to study different blind equalization algorithms based on constant modulus approach, and then derive a new scheme of blind equalization. The main objectives of this thesis are as follows:

1. To derive a new blind equalization algorithm using the principle of minimal disturbance. The derivation involves solving of the constrained problem as specified by Lin [10] using the method of Lagrange multipliers and extending it using the idea proposed by Tanrikulu et.al.[11], i.e., by using multiple constraints. According to Tanrikulu et. al. [11] the algorithm when optimized using multiple constraints achieves a faster convergence rate. The aim here is to achieve a faster convergence rate than that of the algorithm proposed by Lin.

2. To simulate the new algorithm using MATLAB and test it on complex channels with and without phase offsets. Primarily, the channel considered will be that given in previous work of Picchi and Prati [1]. Moreover the algorithm will be tested on the other channels and its performance will be evaluated for different

scenarios.

3. To simulate the new algorithm using fractionally spaced equalizer. A $T/2$ fractionally spaced equalizer will be considered and the algorithm will be implemented on it. According to the theory this implementation should give improved results when compared to that of the baud spaced equalizer

This thesis is organized as follows: In Chapter 2, a comprehensive literature survey with results regenerated for some well known algorithms will be carried out. Chapter 3 focuses on the derivation of the new blind equalization scheme using the principle of minimal disturbance. In Chapter 4, simulation results for the proposed scheme on various channels under different scenarios for baud spaced equalizers will be presented. Chapter 5 demonstrates the simulation results of the proposed scheme for fractionally spaced equalizer and a comparison will be made with the baud spaced results. Chapter 6 concludes the thesis and summarizes the results of the work. Areas for future work are suggested in this chapter.

Chapter 2

Blind Equalization Algorithms

The concept of blind equalization without a training sequence received its first wide coverage in 1975 when Sato [6] presented a simple linear equalizer for pulse amplitude modulated (PAM) signals under the framework of a discrete system modeled by the equation (1.1)

The major analytical breakthrough of Blind equalization was presented by Benveniste and Goursat [12]. They established the principles of blind deconvolution for analog channel input signals. Benveniste and Goursat officially introduced the term blind equalization in 1982 [13]. In fact, the very term 'blind equalization' can be attributed to them as witnessed by the title of their paper in 1982 [12]. The seminal paper of Benveniste established the connection between the task of blind equalization and the use of higher order statistics of the channel output. Through rigorous analysis, they generalized the original Sato algorithm [6] into a class of

algorithms based on non-MSE cost function exhibiting some desired convergence behavior. More importantly, the convergence properties of the proposed algorithms were carefully investigated. One of the most important issues was to determine whether the channel has been equalized. It was shown by Benveniste *et al* [12] that if the channel input sequence is indpendantly identically distributed(i.i.d.) and the noise is absent, the channel equalization is accomplished if and only if the equalizer output sequence $\{y(k)\}$ has identical distribution as the channel input.

A different generalization of the Sato method came from Godard [14]. Explicitly exploiting the higher order moments of the channel output in its cost functions selection, this new class of adaptive blind equalization can also be applied to complex QAM channel input signals. The work of Triechler and Larimore [2] introduced the philosophy of signal restoration in their cost functions. The constant modulus algorithm (CMA), they presented, assumed a constant modulus input signal and adjusted the blind equalizer accordingly to yield a constant modulus output. Incidentally the CMA happens to be an effective member of the Godard class of algorithms. However, the main drawbacks of CMA were presence of local minima and slow rate of convergence [3],[15]-[16],[17].

The constant modulus algorithm became the most popular and effective blind equalization algorithm for linear T-spaced equalizers. Its convergence behavior also became better understood in time. The convergence of the CMA blind equalizer was first studied by G. Foschini [18] while the local convergence of the CMA was

established by Ding *et al* [19].

The issue of local convergence of Blind Equalization algorithms was investigated by many researchers [3],[15]-[16],[17]. It was then concluded that the presence of local minima are due to the finite length of the equalizer filter and due to the operation of the equalizer at baud rate [16]. Many strategies such as center-tap initialization and tap centering were then proposed [18]. Later on, various blind equalization algorithms were analyzed and a way to counter the parasitic local solutions was proposed [15].

However, for some applications such as the mobile-radio systems a faster convergence of the deconvolution algorithm is needed. Hilal and Duhammel came up with the novel idea of normalizing the CMA [20] by introducing a second order norm of the equalizer input in the denominator of the tap update equation. The normalization factor so introduced caused the algorithm to achieve a faster convergence rate than the un-normalized one. This is in analogy to the case of normalized LMS [21] and LMS [22].

Although CMA remains to be an effective and popular blind equalization algorithm implicitly exploiting the higher order statistics of the channel output there have been many efforts aimed at developing faster algorithms for blind equalization with faster convergence behavior. Notable examples include a stop and go strategy proposed by Prichi and Prati [1] , the so called Bussgang algorithms presented by Godfrey and Rocca [23], Maximum a Posteriori (MAP) symbols estimator based

on the assumption that the effect of the channel distortion and noise is collectively Gaussian; a generalization of CMA by Shalvi and Weinstien [24], and a batch cumulant "super exponential" algorithm again by Shalvi and Weinstein [25].

For a two dimensional system a phase error in an output constellation after equalization is general. This type of phase error pulls down the efficiency of the equalizer significantly because it prevents the decision device from recovering the transmitted data from the output of the equalizer. Therefore, to combat this performance degradation caused by the phase error, a carrier tracking loop is used instead for recovering the carrier phase after the equalizer. In order to combat the phase errors introduced by the channel a modified version CMA was proposed [26].

There are basically two different approaches to the problem of blind equalization. The stochastic gradient descent (SGD) approach which iteratively minimizes a chosen cost function over all possible choices of equalizer coefficients, while the statistical approach uses sufficient stationary statistics collected over a block of received data for a channel identification or equalization. The latter approach often exploits higher order cyclostationary statistical information directly [27]. The intended work is focused on blind equalization method using stochastic gradient approach.

For reasons of practicality and ease of adaptation, linear channel equalization is typically implemented as a linear filter. Denote the equalizer parameter vector at the sample instant k as:

$$\mathbf{w}(k) = [w_{-M}(k), w_{-M+1}(k), w_{-M+1}(k)...w_0(k), w_1(k)...w_{M-1}(k), w_M(k)]^T$$

where $(2M + 1)$ is the length of the equalizer and the superscript T represents the transpose operation, and the input sequence to the equalizer as:

$$\mathbf{x}(k) = [x(k), x(k-1), x(k-2).....x(k-m), x(k-m+1)]^T$$

The output signal of the linear equalizer at the sample instant is thus given by

$$y(k) = \sum_{i=-M}^{M} w_i(k)x(k-i) \tag{2.1}$$

In the ensuing analysis the linear blind equalization system is described.

2.1 Linear Blind Equalization System

The Least Mean Square (LMS) [22] adaptive equalizer employing a training sequence is given by

$$\mathbf{w}(k+1) = \mathbf{w}(k) + \mu e(k)\mathbf{x}(k) \tag{2.2}$$

where μ is a small step size controlling the convergence of the algorithm, and $e(k)$ the difference between the output of the equalizer and the transmitted symbol . Naturally this algorithm requires that the channel input $a(k-v)$ be available, the equalizer iteratively minimizes the $E = |e(k)|^2$ mean square error(MSE) cost func-

tion in which the error is defined as

$$e(k) = y(k) - a(k - v) \tag{2.3}$$

if the MSE is small such that after training the equalizer output $y(k)$ is a close estimate of the true channel input , then the decision device output can replace $a(k - v)$ in a decision directed algorithm that continues to track the modest time variations in the channel dynamics [27].

In blind equalization the channel input $a(k)$ is unavailable, and thus different minimization criteria are explored. The crudest blind equalization scheme is the decision-directed scheme that updates the adaptive equalizer coefficients according to

$$\mathbf{w}(k + 1) = \mathbf{w}(k) + \mu(y_k - Q[y(k)])\mathbf{x}(k) \tag{2.4}$$

where $Q[y(k)] = \hat{a}(k-v)$. The ability of the equalizer to achieve desired convergence results when it is initialized with sufficiently small inter symbol interference (ISI) accounts for the key role that decision-directed algorithm plays in channel equalization. Without direct training, a blind equalization algorithm is therefore used to provide a good initialization scheme for the decision-directed equalizer because of the decision-directed equalizer's poor convergence behavior under high ISI. Thus a better adaptive algorithm is needed for the blind equalization of linear channels when the initial coefficients are far from ideal. The general structure of the blind adaptive algorithm is shown in the Figure 2.1. Blind Adaptive equalization algo-

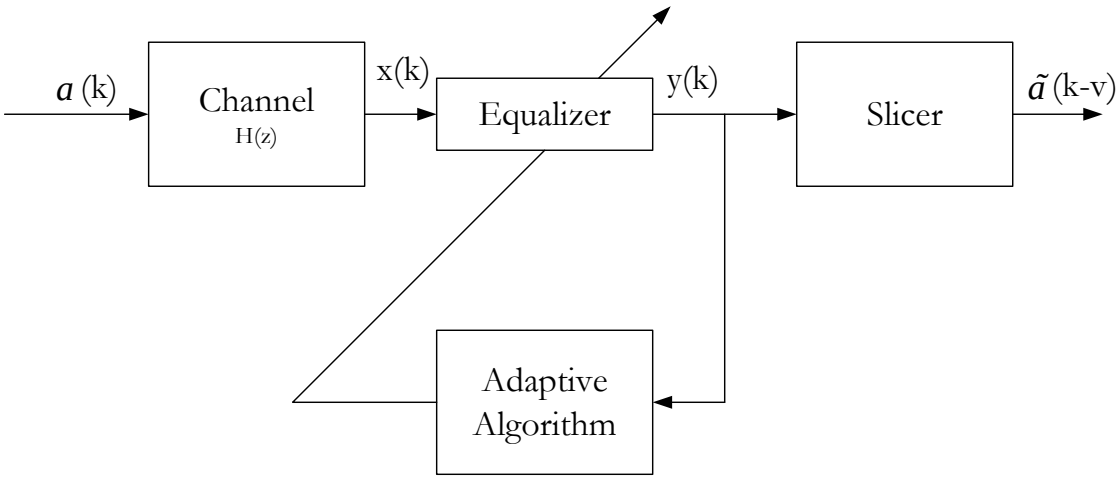

Figure 2.1: Linear Blind Equalization Systems

rithms are often designed by minimizing special non-MSE cost functions that do not directly involve the input $a(k)$ while still reflect the current level of ISI in the equalizer output. Let the mean cost function be defined as

$$J_w = E\{\Psi(y(k))\} \tag{2.5}$$

where $\Psi(.)$ is a scalar function of the equalizer output. The mean cost function $J(w)$ should be specified such that its minimum, the corresponding w results in a minimum ISI or MSE equalizer. Because of the symmetric distribution of $\{a(k)\}$ over alphabet $\hat{A}$ the blind equalizer is unable to distinguish between $\pm a(k-v)$. Thus the function $\Psi(.)$ should be even. In other words, both $y(k) = a(k-v)$ and $y(k) = -a(k-v)$ are acceptable objectives as global minima of the mean cost function.

Using equation (2.5), the stochastic gradient descent minimization algorithm is easily derived and is given by

$$\mathbf{w}(k+1) = \mathbf{w}(k) + \mu \frac{\partial \Psi(y(k))}{\partial \mathbf{w}} \tag{2.6}$$

$$= \mathbf{w}(k) + \mu \Psi^{'}(\mathbf{w}^{H}(k)\mathbf{x}(k)) \tag{2.7}$$

where $\Psi^{'} = \frac{\partial \Psi(x)}{\partial (x)}$ The resulting blind equalization algorithm can be written as

$$\mathbf{w}(k+1) = \mathbf{w}(k) + \mu \Psi^{'}(\mathbf{w}^{H}(k)\mathbf{x}(k)) \tag{2.8}$$

Hence, a blind equalizer can be defined by its cost function or its derivative. The derivative of the cost function is also called as the error function as it replaces the prediction error of the LMS algorithm.

2.2 Sato Algorithm and its Generalization

2.2.1 The Sato Algorithm

The first blind equalizer for multilevel PAM signals was introduced by Sato [6]. In essence, it is identical to the decision-directed algorithm when the PAM input is binary ± 1. For M-level PAM signals, It is defined by the error function

$$e_s(k) = y(k) - R_s \mathtt{sgn}[y(k)] \tag{2.9}$$

where

$$R_s \triangleq \frac{E[|a(k)|^2]}{E[|a(k)|]} \tag{2.10}$$

Clearly the Sato algorithm effectively replaces the input $a(k-v)$ with $R_s\mathtt{sgn}[y(k)]$. The multilevel PAM is viewed as an equivalent binary input signal in this case. The parameter vector is updated via

$$\mathbf{w}(k+1) = \mathbf{w}(k) - [y(k) - a(k-v)]\mathbf{x}(k) \tag{2.11}$$

It is clear that the convergence of the Sato's algorithm clearly depends on how often the errors $y(k) - a(k-v)$ and $e_s(k)$ have identical signs. The Sato algorithm was simulated for a real channel as depicted in Figure 2.2. The equalizer was tested for a 16-QAM constellation as shown in Figure 2.3. The above constellation was passed through the channel as shown in Figure 2.2. The noise variance was assumed to be 0.01 and the signal to noise ratio was taken as 30dB. The equalizer was assumed to have 9 taps. Once the signal was passed through the channel and noise was added, the signal got corrupted as shown in Figure 2.4 and its eyediagram is shown in Figure 2.5 This corrupted signal is then passed through the equalizer inorder to remove the channel distortion at the output of the equalizer is as shown in Figure 2.7 and Figure 2.6 The mean square error and the residual ISI gives an ample idea of when the equalizer is converging and with what steady state error. The MSE and the ISI plots for Sato's algorithm are shown in the Figure 2.8 and Figure 2.9 The Sato's algorithm under the specifications stated above converged around 9500 symbols with a MSE of -17 dB. The residual ISI achieved a steady state of -32 dB.

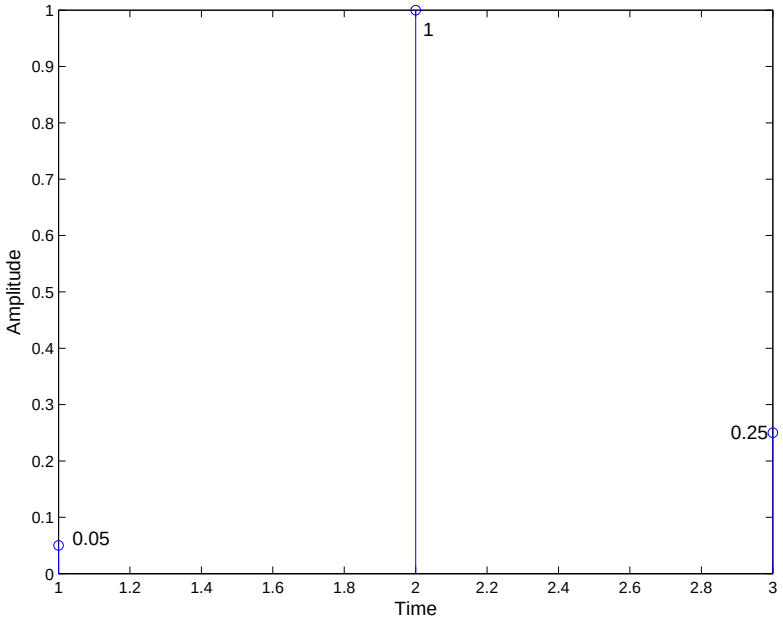

Figure 2.2: Impulse response of the real channel.

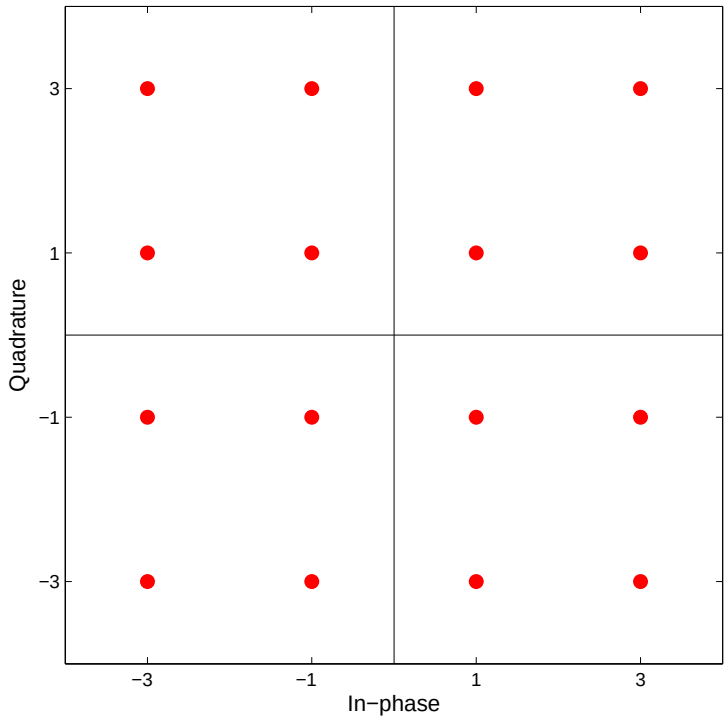

Figure 2.3: 16-QAM signal constellation.

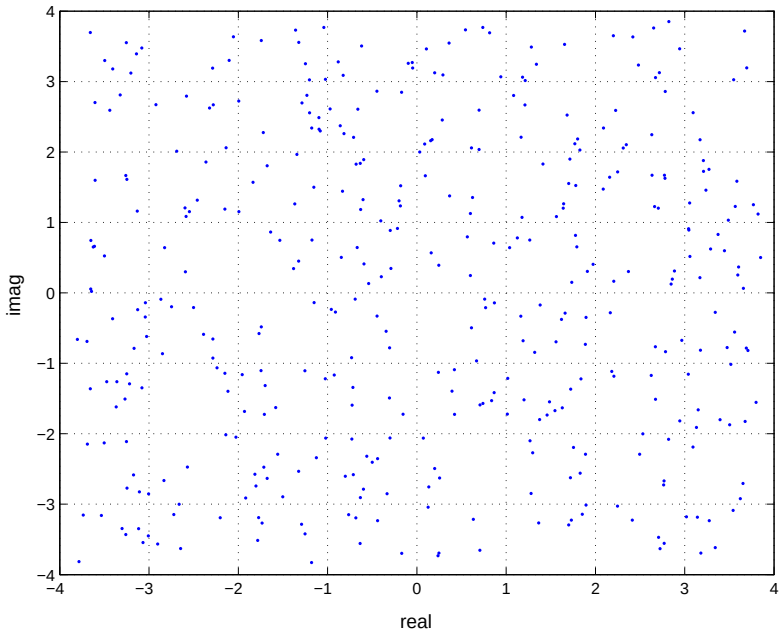

Figure 2.4: Signal constellation before convergence.

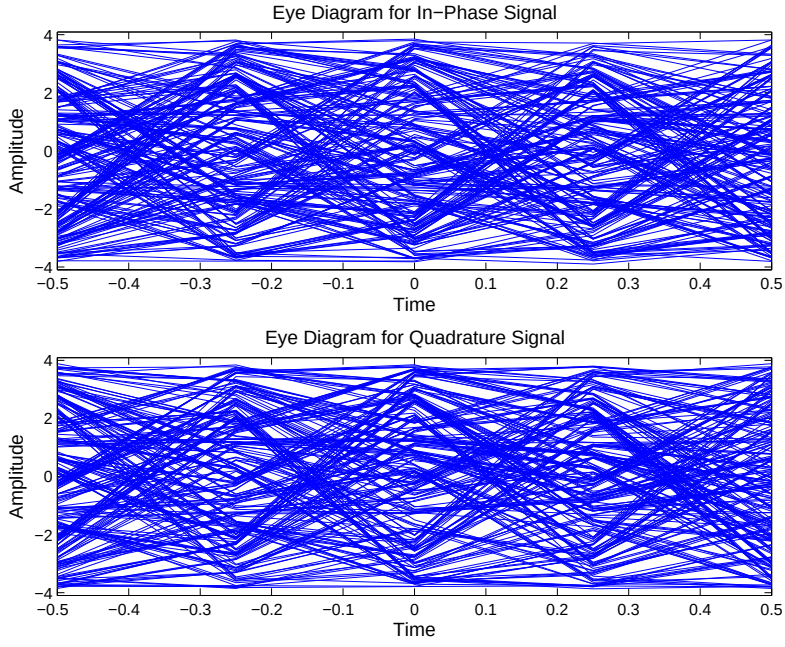

Figure 2.5: Eye-diagram of the signal before convergence.

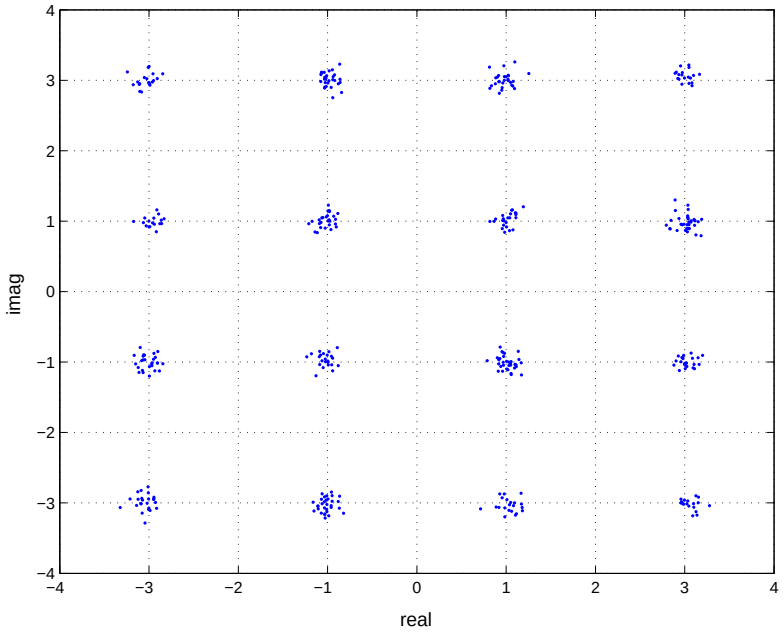

Figure 2.6: Signal constellation after convergence (the last 1000 bits) for Sato's Algorithm.

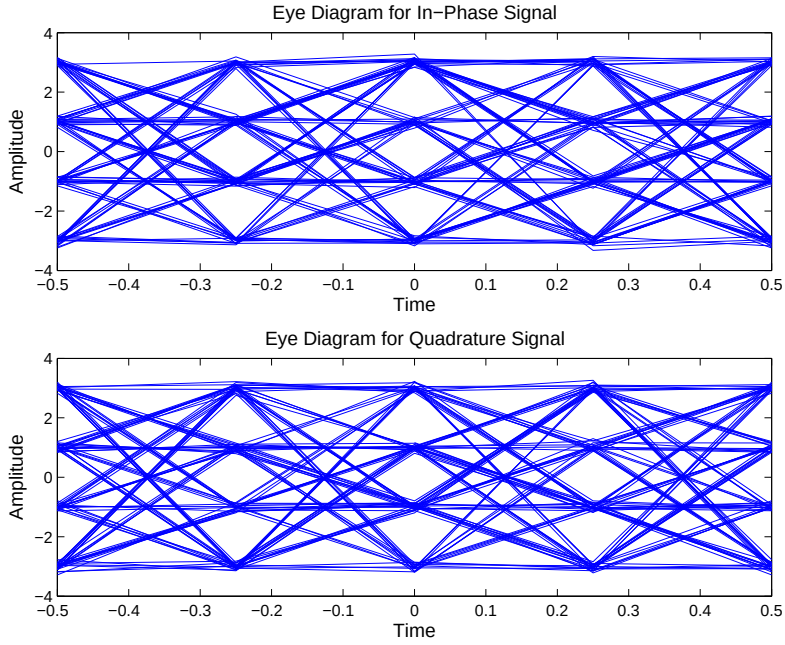

Figure 2.7: Eye-diagram of the signal for last 1000 bits after convergence for Sato's Algorithm.

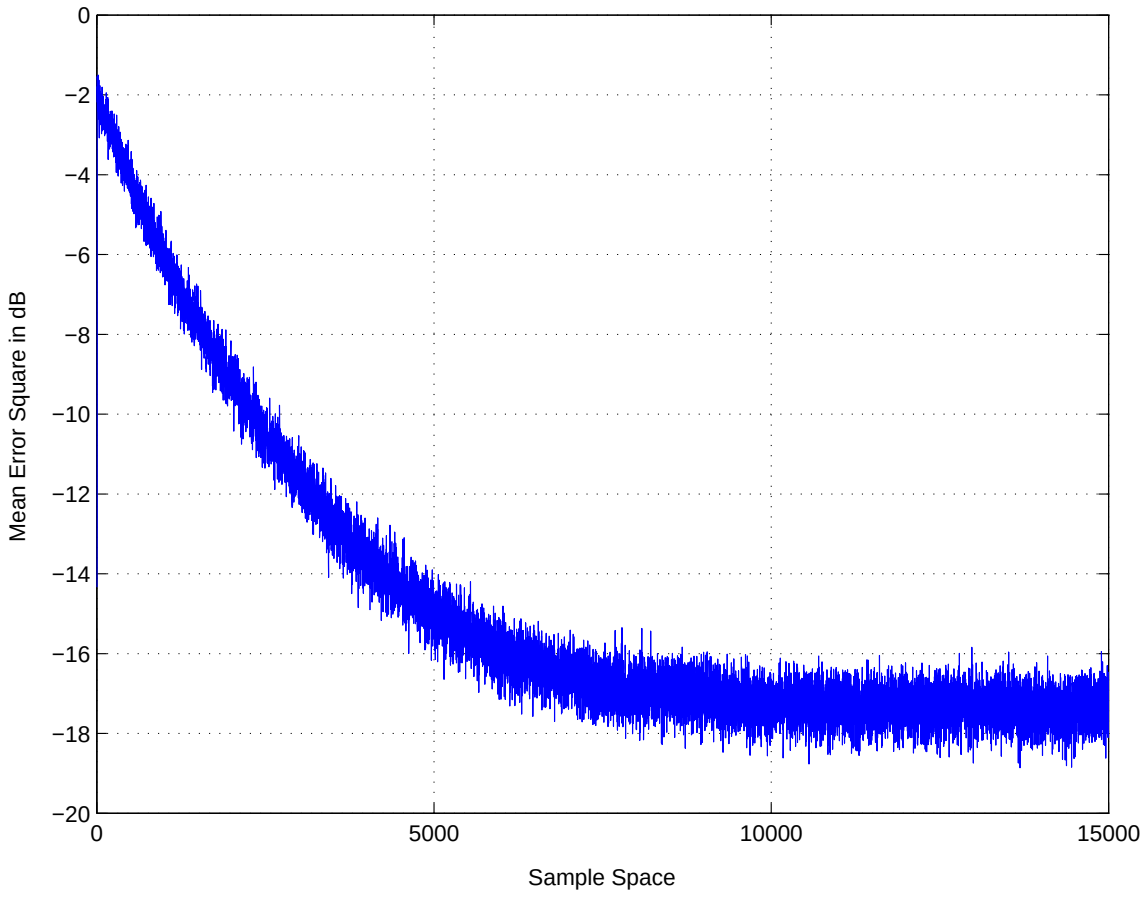

Figure 2.8: The Mean Square Error curve for Sato's Algorithm.

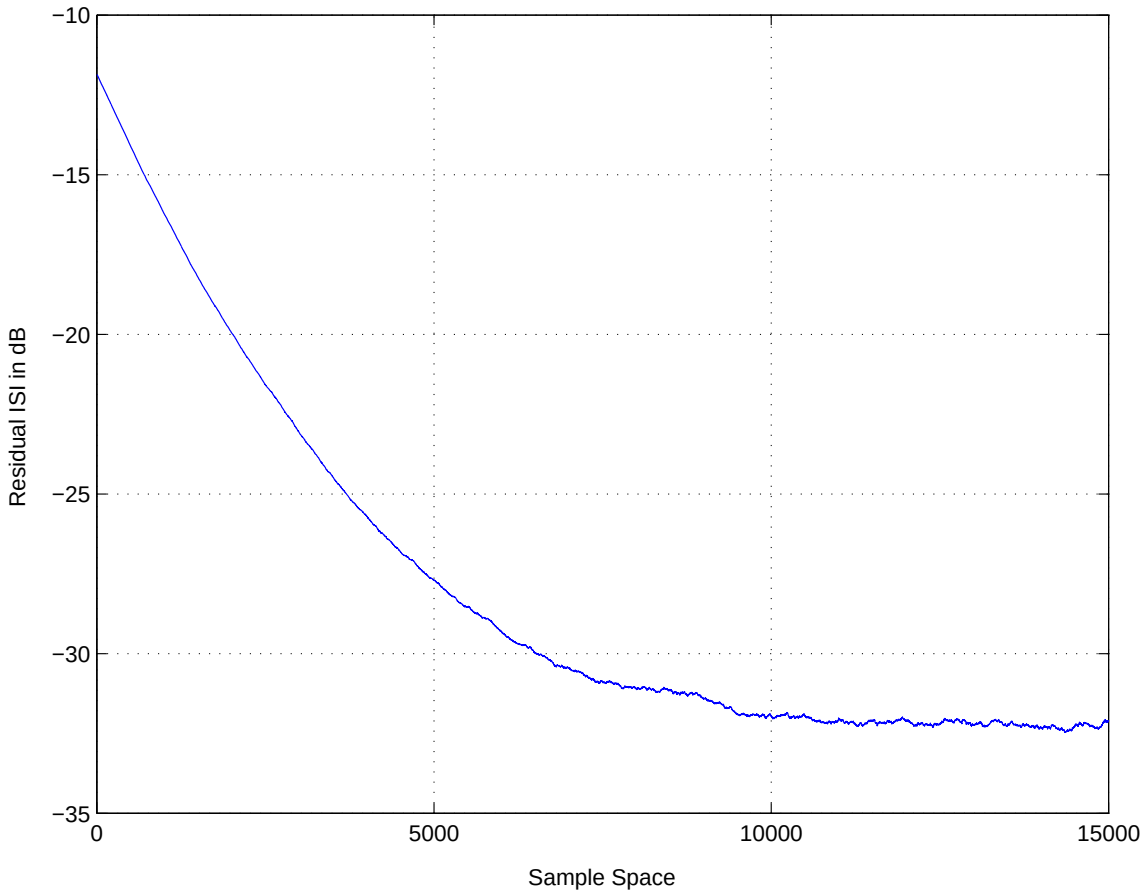

Figure 2.9: The Residual ISI for Sato's Algorithm.

The residual ISI was calculated using the formula [24]:

$$ISI = \frac{\sum_k |h(k) * \mathbf{w}^*(k)| - |h(k) * \mathbf{w}^*(k)|_{max}}{|h(k) * \mathbf{w}^*(k)|_{max}} \tag{2.12}$$

where $h(k)$ represents the channel impulse response and '$*$' represents the complex convolution

2.2.2 BGR Algorithms

The Sato's algorithm was extended by Benveniste, Goursat and Ruget [13] into a class of error functions given by:

$$e_b(k) = \tilde{\psi}[y(k)] - R_b \mathtt{sgn}[y(k)] \tag{2.13}$$

where

$$R_b \triangleq \frac{E\{|\tilde{\psi}[a(k)]a(k)|\}}{E[|a(k)|]} \tag{2.14}$$

In this case, $\tilde{\psi}(x)$ is an odd and twice differentiable function satisfying equation (2.15):

$$\tilde{\psi}(x) \geq 0, \qquad \forall x \geq 0 \tag{2.15}$$

The usage of odd function $\tilde{\psi}(x)$ generalizes the linear function $\tilde{\psi}(x) = x$ in the Sato's algorithm. The end window update equation can be written as

$$\mathbf{w}(k+1) = \mathbf{w}(k) - e_b(k)\mathbf{x}(k) \tag{2.16}$$

2.2.3 Stop-and-Go Algorithms

It is apparent that the convergent characteristics of Blind equalization algorithms are largely determined by the sign of the error signal . In order for the coefficients of the blind equalizer to converge in the vicinity of the optimum MMSE solution achievable by LMS algorithm, the sign of its error signal should agree with the signs of the LMS prediction error . Slow convergence or the convergence of the parameters to local minima of the cost function that do not provide proper equalization, can occur if the signs of these two errors differ sufficiently often. In order to improve the convergence properties of blind equalizer, the so called "stop-and-go" methodology was proposed by Picchi and Prati [1]

The idea behind the stop-and-go algorithm is to allow "to go" only when the error function is more likely to have the correct sign for the gradient descent direction. Given several criteria for blind equalization, one can expect a more accurate descent direction when more than one of the existing algorithms agree on the sign (direction) of the error functions. When the error signs differ for a particular output sample, parameter adaptation is stopped.

In [1], Picchi and Prati combined the Sato and decision directed algorithms to achieve faster convergence results through the corresponding error function.

Consider two algorithms with error functions $\psi_1(y)$ and $\psi_2(y)$. A stop and go

algorithm is defined as follows:

$$\mathbf{w}(k+1) = \begin{cases} \mathbf{w}(k) - \mu\psi_1[y(k)]\mathbf{x}(k), & \text{if } \mathtt{sgn}[\psi_1(y(k))] = \mathtt{sgn}[\psi_2(y(k))]; \\ \mathbf{w}(k), & \text{if } \mathtt{sgn}[\psi_1(y(k))] \neq \mathtt{sgn}[\psi_2(y(k))]. \end{cases} \tag{2.17}$$

2.3 Constant Modulus Algorithms

2.3.1 Constant Modulus (Godard) Algorithm

Integrating the Sato error function $e_s(x)$ shows that the Sato Algorithm has an equivalent cost function:

$$J_s(\mathbf{w}) = E[|y(k)| - R_s]^2 \tag{2.18}$$

This cost function was generalized by Godard into another class of algorithms that are specified by the cost function [14]:

$$J_q(\mathbf{w}) = E[|y(k)|^q - R_q]^2, \qquad q = 1, 2, \ldots \tag{2.19}$$

and

$$R_q \triangleq \frac{E[|a(k)|^{2q}]}{E[|a(k)|^q]} \tag{2.20}$$

This class of Godard algorithms is indexed by a positive integer q. Using the stochastic gradient approach, the Godard algorithms are given by

$$\mathbf{w}(k+1) = \mathbf{w}(k) - \mu(|y(k)|^q - R_q)|y(k)|^{q-2}|y(k)|\mathbf{x}^H(k) \tag{2.21}$$

For q=2 the special Godard algorithm was developed as the "constant modulus algorithm". For channel input signal that has constant modulus $|a(k)|^2 = R_2$, the CMA equalizer penalizes output samples that do not have the constant modulus characteristics. The modulus error is simply

$$e(k) = |y(k)|^2 - R_2 \tag{2.22}$$

and the squaring of the error yields the constant modulus cost function that is identical to the Godard cost function for minimization. This modulus restoral concept has a particular advantage in that it allows the equalizer to be adapted independently of carrier recovery. A carrier frequency offset causes the phase rotation of the equalizer output. Because the CMA cost function is insensitive to the phase of the output $y(k)$, the equalizer parameter adaptation can occur independently and simultaneously with the operation of the carrier recovery system. This property also makes CMA applicable to the analog modulation systems [2].

The Godard's algorithm was simulated for the channel as shown in the Figure 2.2 with SNR= 30 dB. The equalizer was assumed to have 9 complex taps. The noise variance was taken to be 0.01. The following results were obtained: The MSE obtained a steady state value of -17 dB (from Figure 2.12) and the residual ISI obtained the steady state of -30 dB (from Figure 2.13). The algorithm was found to converge around 11,000 symbols. Also the signal constellation and eyediagrams after equalization are plotted in the Figures 2.10 and 2.11.

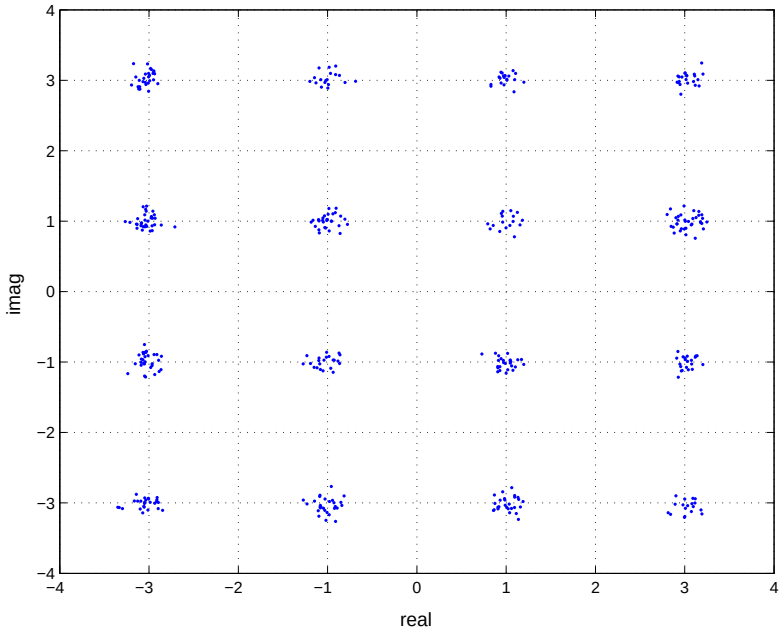

Figure 2.10: Signal constellation after convergence (the last 1000 bits) for Godard's Algorithm.

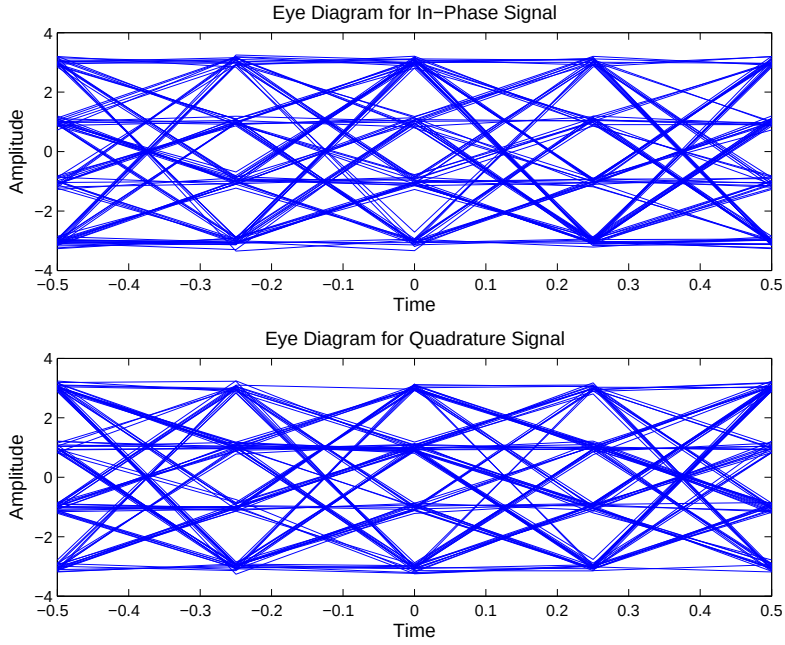

Figure 2.11: Eye-diagram of the signal after convergence (the last 1000 bits) for Godard's Algorithm.

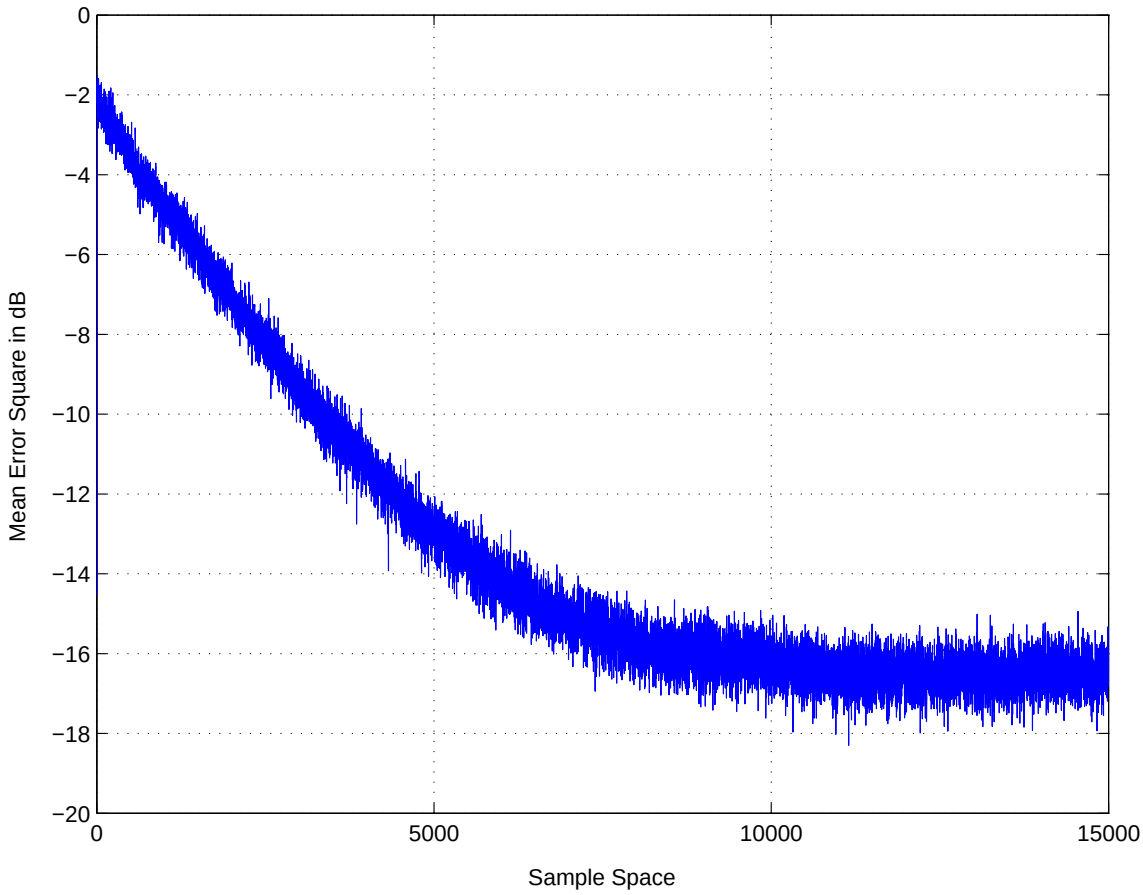

Figure 2.12: The Mean Square Error curve for Godard's Algorithm.

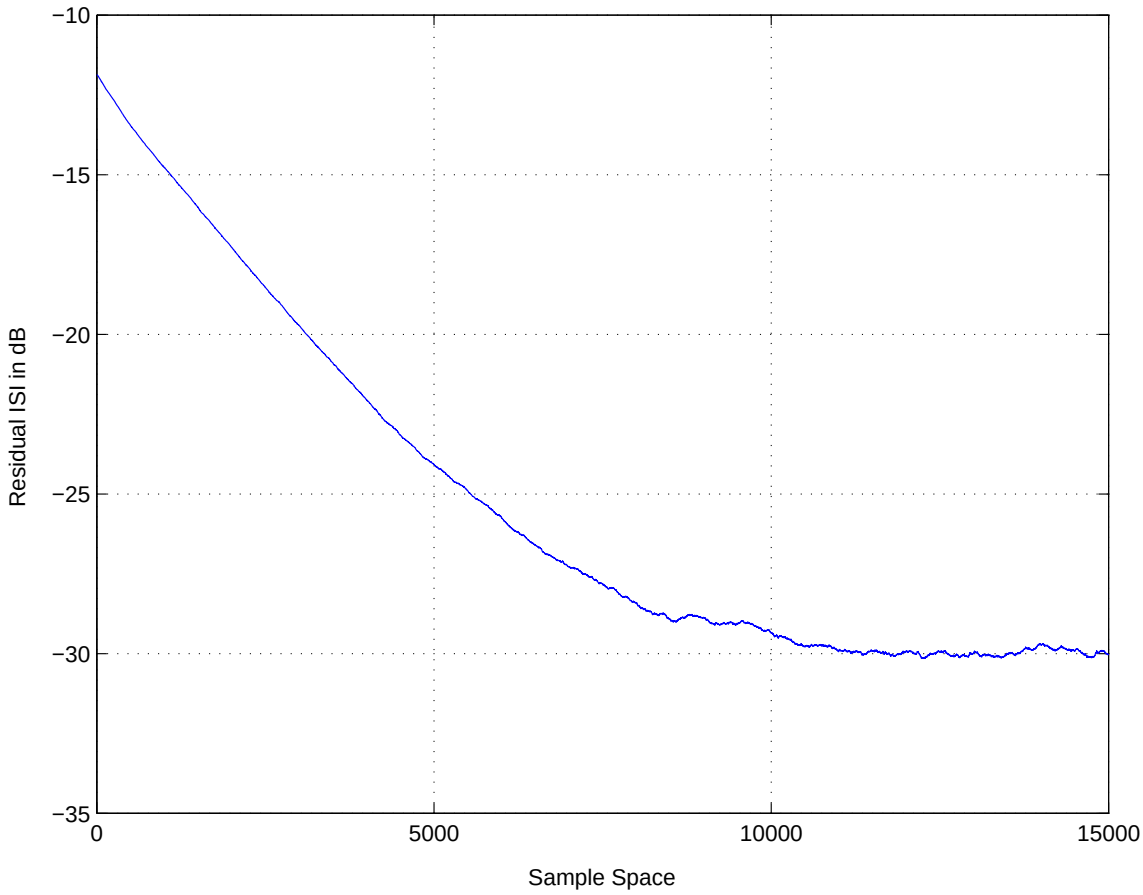

Figure 2.13: The Residual ISI for Godard's Algorithm.

2.3.2 Shalvi and Weinstein Algorithms

Unlike previously introduced algorithms, the method of Shalvi-Weinstein [24] are explicitly based on the higher order statistics of the equalizer output. Define the kurtosis of the equalizer [24]:

$$K_y \triangleq E[|y(k)|^4] - 2\{E[|y(k)|^2]\}^2 \tag{2.23}$$

The Shalvi-Weinstein algorithm maximizes $|K_y|$ subject to the constant power constraint $E[|y(k)|]^2 = E[|a(k)|]^2$. Define $c(k)$ as the combined channel-equalizer impulse response given by:

$$c(i) \triangleq \sum_{k=0}^{m} w(k)h(i-k), \qquad -\infty < i < \infty \tag{2.24}$$

The Shalvi-Weinstein equalizer is equivalent to the following criteria

$$\text{maximize} \quad \sum_{i=-\infty}^{\infty} |c(i)|^4, \qquad \text{subject to} \quad \sum_{i=-\infty}^{\infty} |c(i)|^2 = 1 \tag{2.25}$$

2.3.3 Normalised Constant Modulus Algorithm (NCMA)

The greatest drawback of the CMA is its relatively slow convergence which becomes ever more significant as wireless applications involving rapid changes in the channel characteristic become more prominent. Various enhancements of the CMA offering improved convergence have been investigated [10]-[11],[28]-[29], but most involve significant increases in complexity or computational cost.

The normalized CMA (NCMA) was introduced in order to maximize the convergence speed of the CMA [20]. For blind equalization employing the constant modulus algorithm the constrained optimization problem takes the following form.

$$\min_{\mathbf{w}(k+1)} ||\mathbf{w}(k+1) - \mathbf{w}(k)||^2 \qquad \text{subject to} \qquad |\mathbf{w}^H(k+1)\mathbf{x}(k)|^2 = R_2^2 \tag{2.26}$$

where R_2^2 is the dispersion constant as chosen in equation (2.20) In order to solve the equation (2.26) the method of Lagrange multipliers can be used. The cost function of the NCMA can be written in the following form

$$J(w) = ||\mathbf{w}(k+1) - \mathbf{w}(k)||^2 + \lambda(|\mathbf{w}^H(k+1)\mathbf{x}(k)|^2 - 1) \tag{2.27}$$

Partially differentiating the cost function with respect to the window tap vector $\mathbf{w}$ and equating it to 0 we have

$$2[\mathbf{w}(k+1) - \mathbf{w}(k)] + \lambda\mathbf{x}(k) = 0 \tag{2.28}$$

Thus, the value of λ is obtained as

$$\lambda = -\frac{2[\mathbf{w}(k+1) - \mathbf{w}(k)]}{\mathbf{x}(k)} \tag{2.29}$$

Substituting the value of λ in equation (2.28) and after some manipulations we have,

$$\mathbf{w}(k+1) - \mathbf{w}(k) = \frac{\mathtt{sgn}[y^*(k)] - y^*(k)}{||\mathbf{x}(k)||^2}\mathbf{x}(k) \tag{2.30}$$

where $y(k) = \mathbf{w}^H(k)\mathbf{x}(k)$. Introducing the step size parameter μ the equation (2.30) modifies to

$$\mathbf{w}(k+1) = \mathbf{w}(k) + \mu\frac{\mathtt{sgn}[y^*(k)] - y^*(k)}{||\mathbf{x}(k)||^2}\mathbf{x}(k) \tag{2.31}$$

The above equation is the complete update equation of the normalized CMA. The NCMA speeds up the convergence rate but at a higher MSE and with a slight increase in complexity. Many modifications were made to NCMA [11] It can be observed from Figure 2.16 and Figure 2.17 that NCMA algorithm converges at a faster rate than than the conventional CMA but at a cost of an increase in error floor. The MSE was observed to converge around 7000 symbols at a error floor of -15 dB whereas the ISI was observed to converge at a steady state around -25 dB. When a comparison of NCMA is made with that of the CMA it was found that NCMA converged 4000-4500 symbols before, with a loss of 1 dB. Also the signal constellation and eyediagram after the equalization process are plotted as shown in the Figures 2.14 and 2.15.

2.3.4 Modified Constant Modulus Algorithm (MCMA)

One of the features of the cost function used in CMA is that it is phase blind, i.e., the CMA can converge even in the presence of phase error. Although it is the merit of the CMA, at convergence the equalizer output will have a constant phase rotation. Furthermore, the constellation will be spinning at the carrier frequency offset rate by lack of carrier frequency lock [3]. While this phase-blind nature of the CMA is not a serious problem for the constant phase rotation, for time varying channels such as digital radio channel, the performance of CMA is severely degraded. Kil came up with an idea of dividing cost function as proposed by Godard [14] (in equation

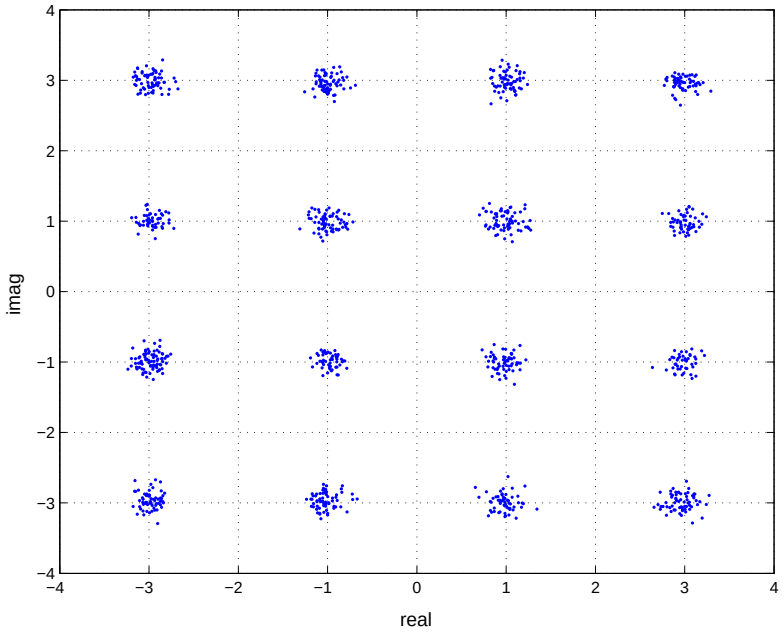

Figure 2.14: Signal constellation after convergence (the last 1000 bits) for NCMA algorithm.

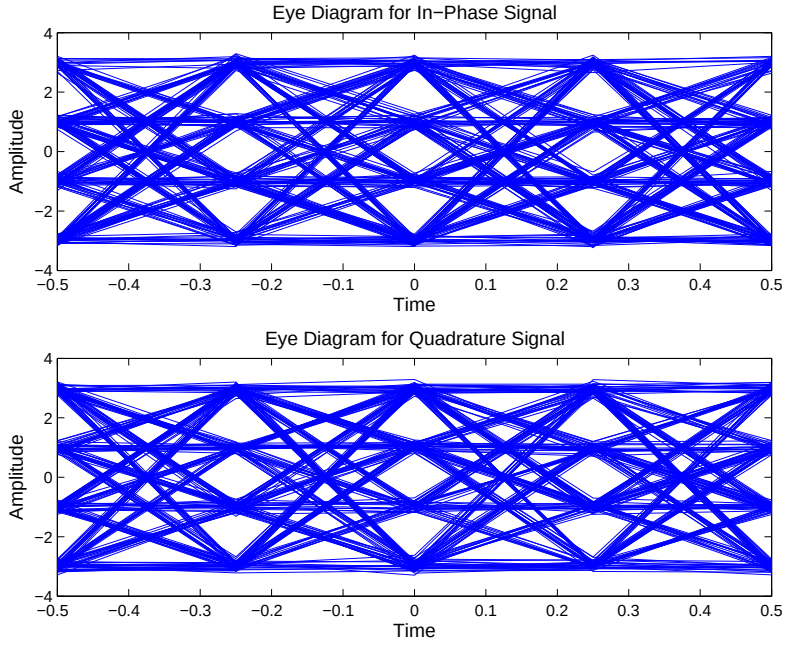

Figure 2.15: Eye-diagram of the signal after convergence (the last 1000 bits) for NCMA algorithm.

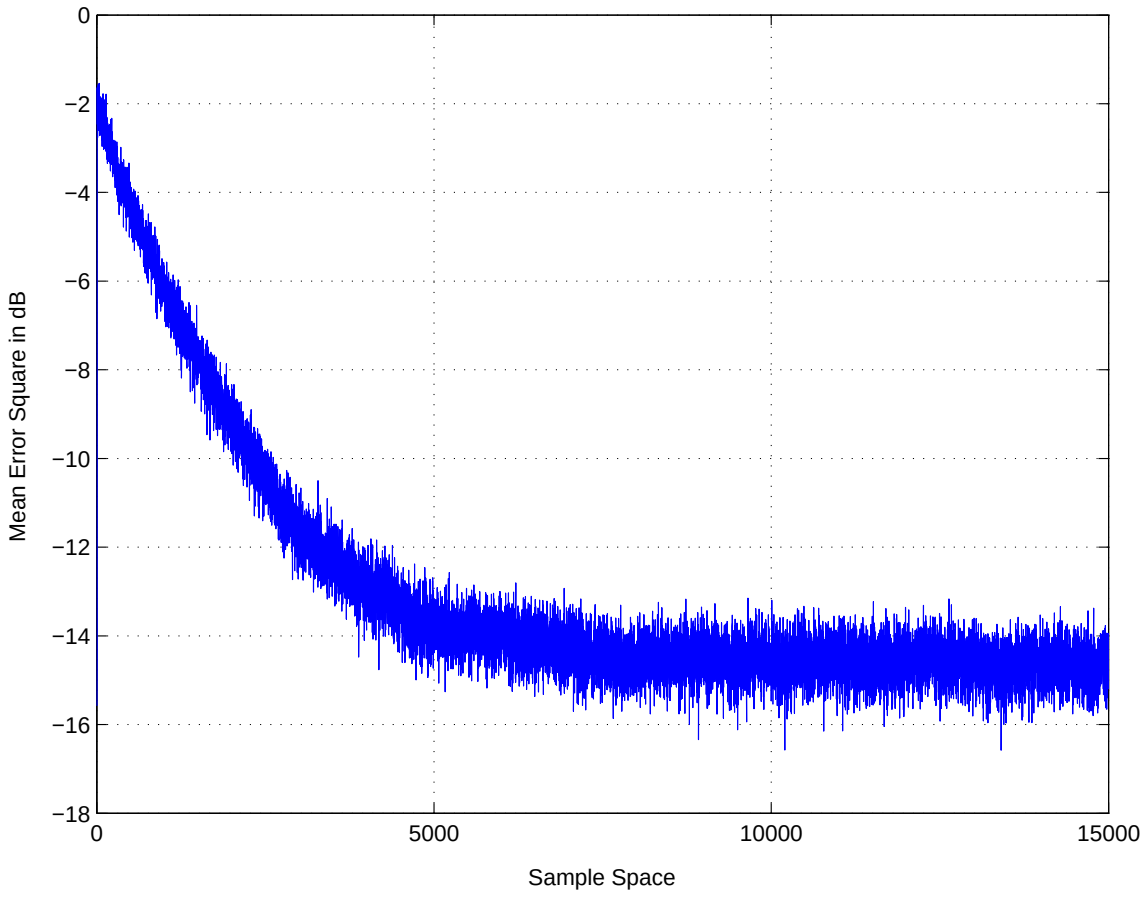

Figure 2.16: The Mean Square Error curve for NCMA algorithm.

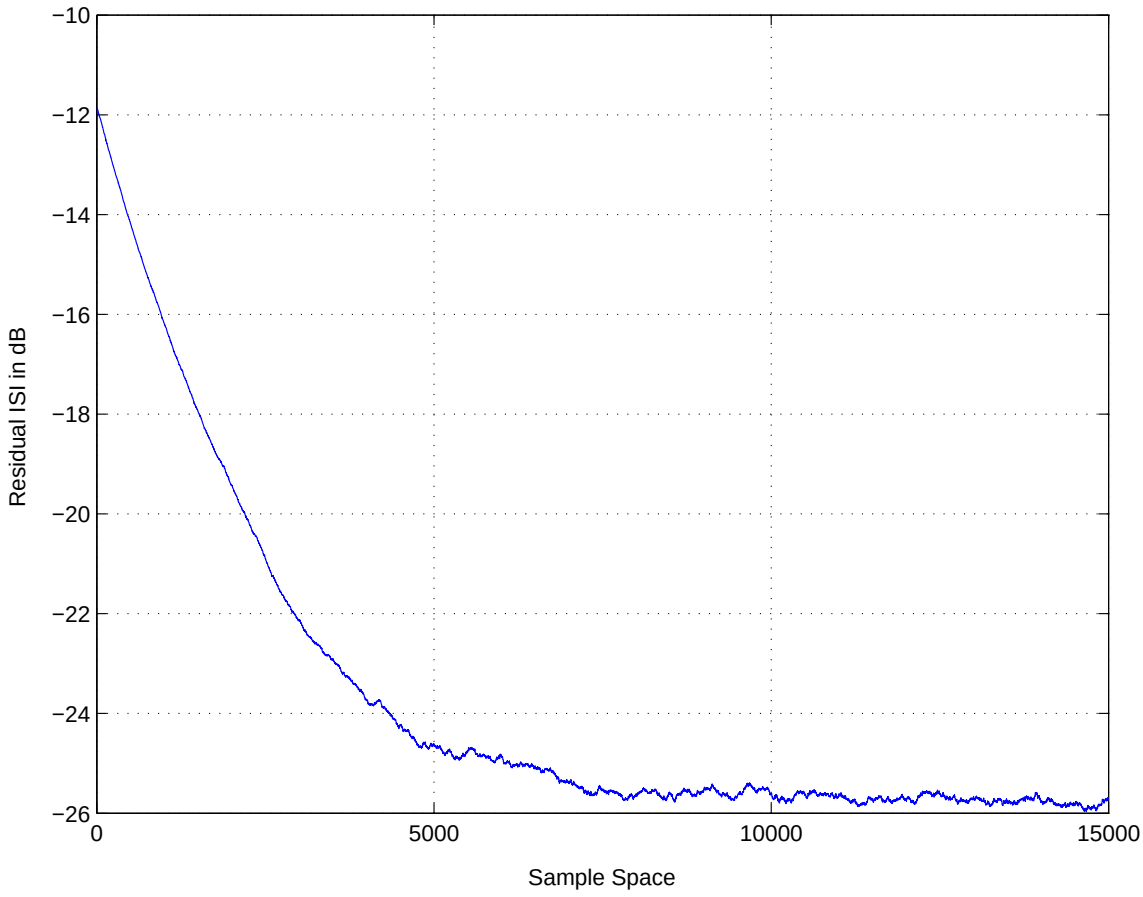

Figure 2.17: The Residual ISI for NCMA algorithm.

(2.18)) into real and imaginary parts for $q = 2$

$$\begin{aligned} J_{2R}(k) &= E[(|y(k)|^2 - R_{2R})^2] \\ J_{2I}(k) &= E[(|y(k)|^2 - R_{2I})^2] \end{aligned} \tag{2.32}$$

where the values of the dispersion constants R_{2R} and R_{2I} are given by:

$$\begin{aligned} R_{2R} &\triangleq \frac{E[|a_R(k)|^4]}{E[|a_R(k)|^2]} \\ R_{2I} &\triangleq \frac{E[|a_I(k)|^4]}{E[|a_I(k)|^2]} \end{aligned} \tag{2.33}$$

The end tap update equation is given as:

$$\mathbf{w}(k+1) = \mathbf{w}(k) - \mu e(k)\mathbf{x}^*(k) \tag{2.34}$$

where the error signal $e(k) = e_R(k) + je_I(k)$ is given by:

$$\begin{aligned} e_R(k) &= y_R(k)(|y_R(k)|^2 - R_{2R}) \\ e_I(k) &= y_I(k)(|y_I(k)|^2 - R_{2I}) \end{aligned} \tag{2.35}$$

The CMA attempts to drive the equalizer output to lie on the circle of radius $\sqrt{R_2}$. Since the cost function is based only on the equalizer output modulus, the equalizer converges independently of the phase error. So if there is no carrier offset the equalizer output will be formed into constellation with arbitrary phase rotation due to channel characteristics. However, if there is an offset the equalizer output will be spinning at the offset rate.

In contrast to the CMA the error function in equation (2.35) separates the equalizer output to real and imaginary parts and then estimates the errors for real and

imaginary parts independently. Under perfect equalization the error $e(k) = 0$ i.e. $y_R(k) = \pm\sqrt{R_{2R}}$ and $y_I(k) = \pm\sqrt{R_{2I}}$. It implies that the MCMA tries to move the real part of the equalizer output lie on the points $\sqrt{R_{2R}}$ and $-\sqrt{R_{2R}}$. Similar is the case with the imaginary part. Since the cost functions employ both the modulus and the phase of the equalizer output, carrier phase recovery is accomplished with blind equalization.

The MCMA was simulated for the channel as shown in the Figure 2.18 and Figure 2.19.The signal to noise ratio was maintained at 30 dB and an equalizer with 9 taps was considered. This channel was taken from the paper by Picchi and Prati [1]. The MCMA was found to converge very well for the channel which offered a phase error to the signal.Figure 2.20 and Figure 2.21 clearly depicts that the some amount of phase error is induced into the signal.Once the signal is passed through the equalizer the phase shift is removed as well as the ISI which can be seen from Figure 2.23 and Figure 2.23. As evident from Figure 2.24 and Figure 2.25, the MCMA converged approximately after 2500 symbols with a steady state MSE of -15 dB and steady state residual ISI of -25 dB.

2.3.5 Dual Mode Modified Constant Modulus Algorithm

In 1995 Kil proposed an improved version of the MCMA by infusing the decision directed mode into the MCMA [30]. The MCMA proposed previously was effective in an aspect of phase recovery with equalization. However, the error signals used

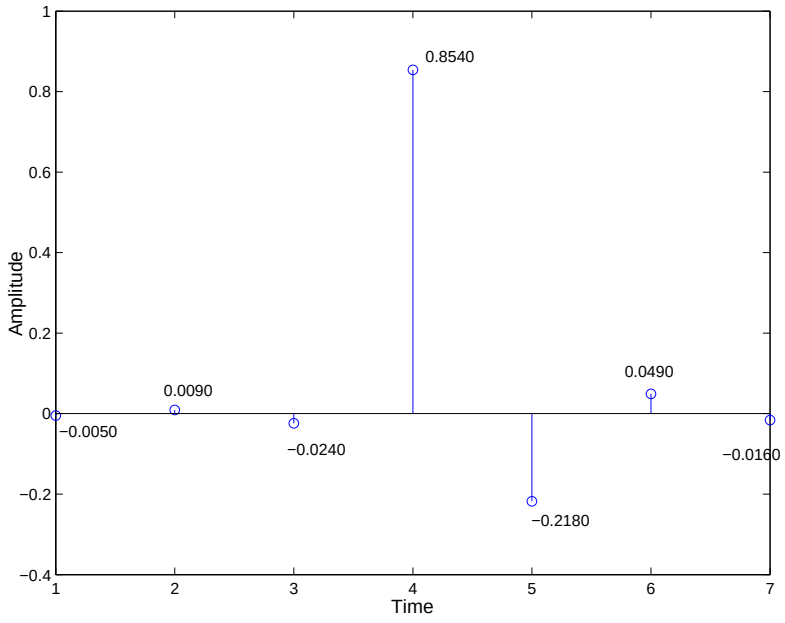

Figure 2.18: Impulse response of the real part of the channel.

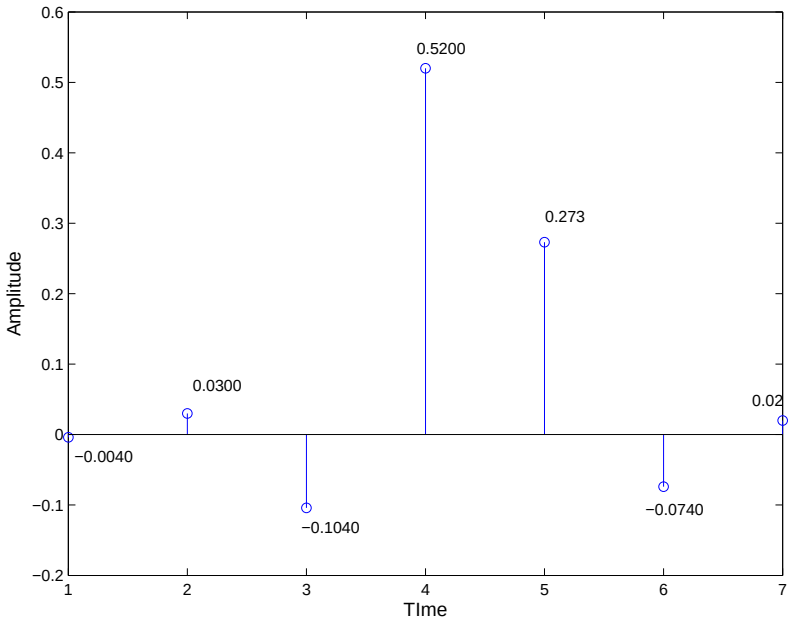

Figure 2.19: Impulse response of the imaginary part of the channel.

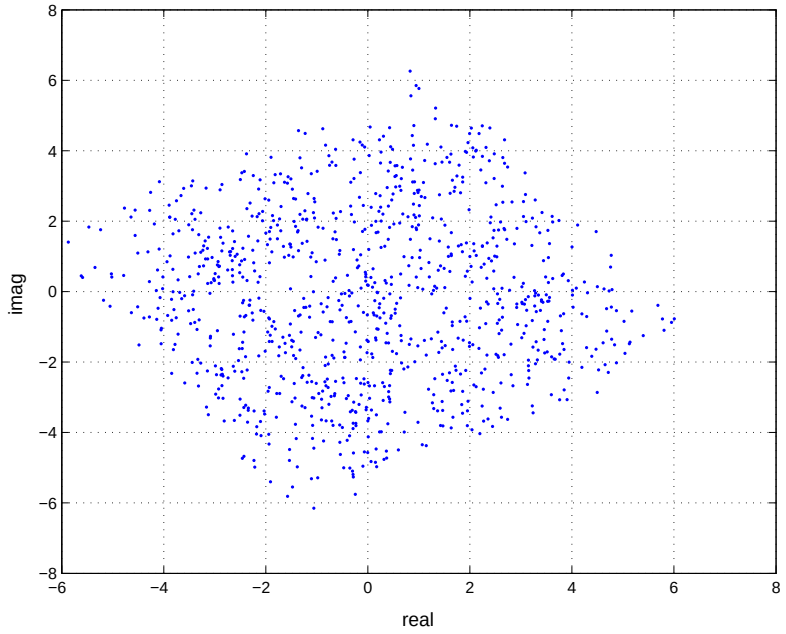

Figure 2.20: Signal constellation after convergence (the last 1000 bits) for MCMA algorithm.

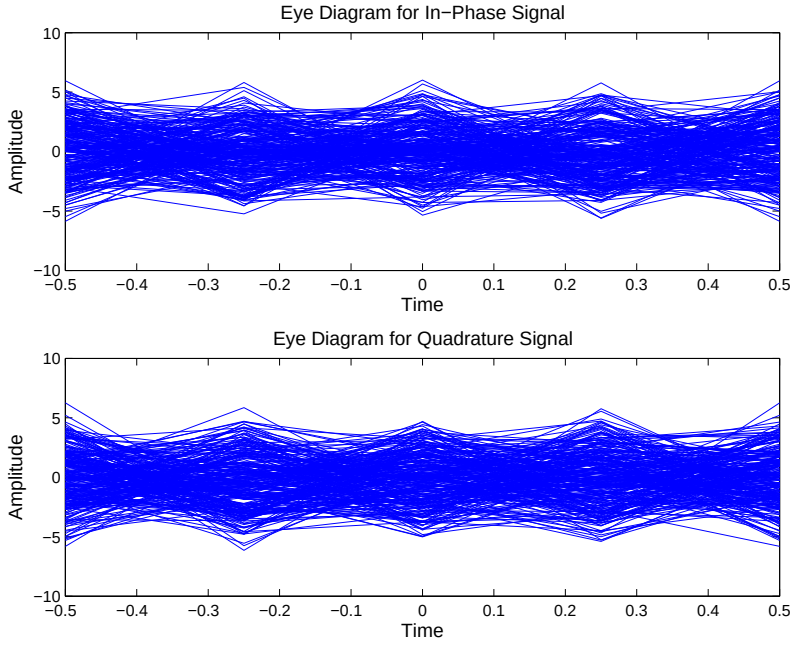

Figure 2.21: Eye-diagram of the signal after convergence (the last 1000 bits) for MCMA algorithm.

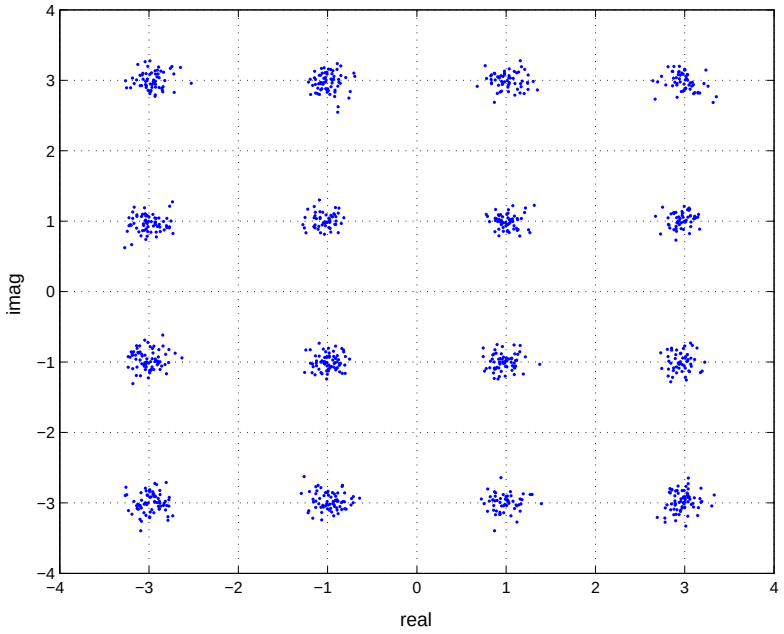

Figure 2.22: Signal constellation after convergence (the last 1000 bits) for MCMA algorithm.

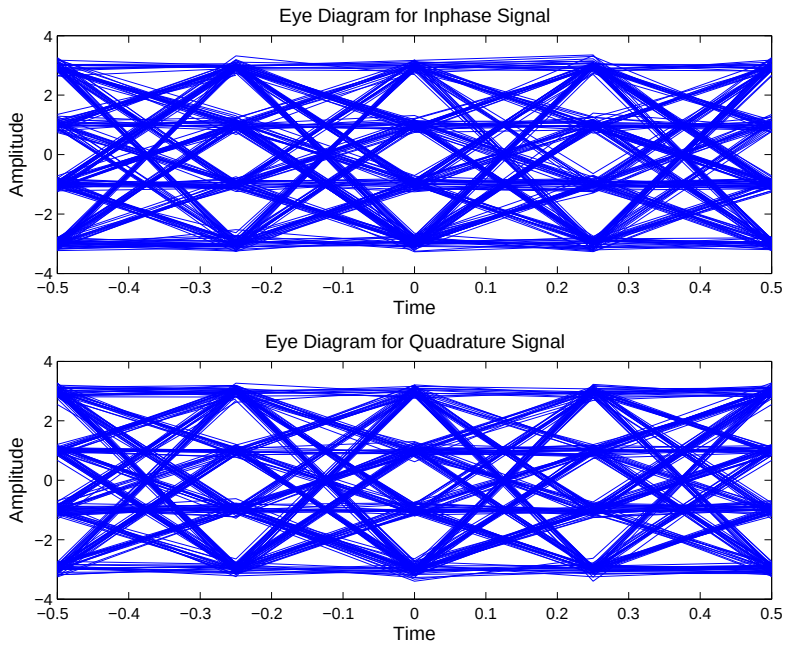

Figure 2.23: Eye-diagram of the signal after convergence (the last 1000 bits) for MCMA Algorithm.

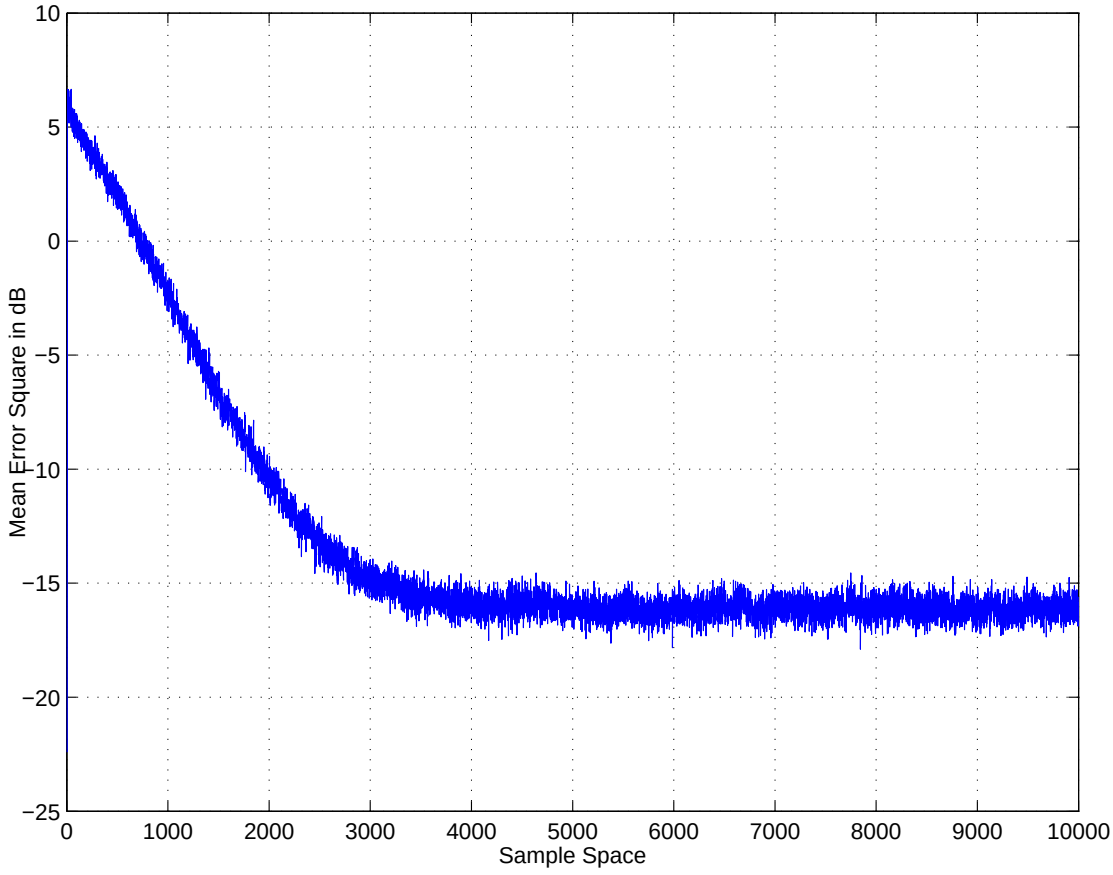

Figure 2.24: The Mean Square Error curve for MCMA algorithm.

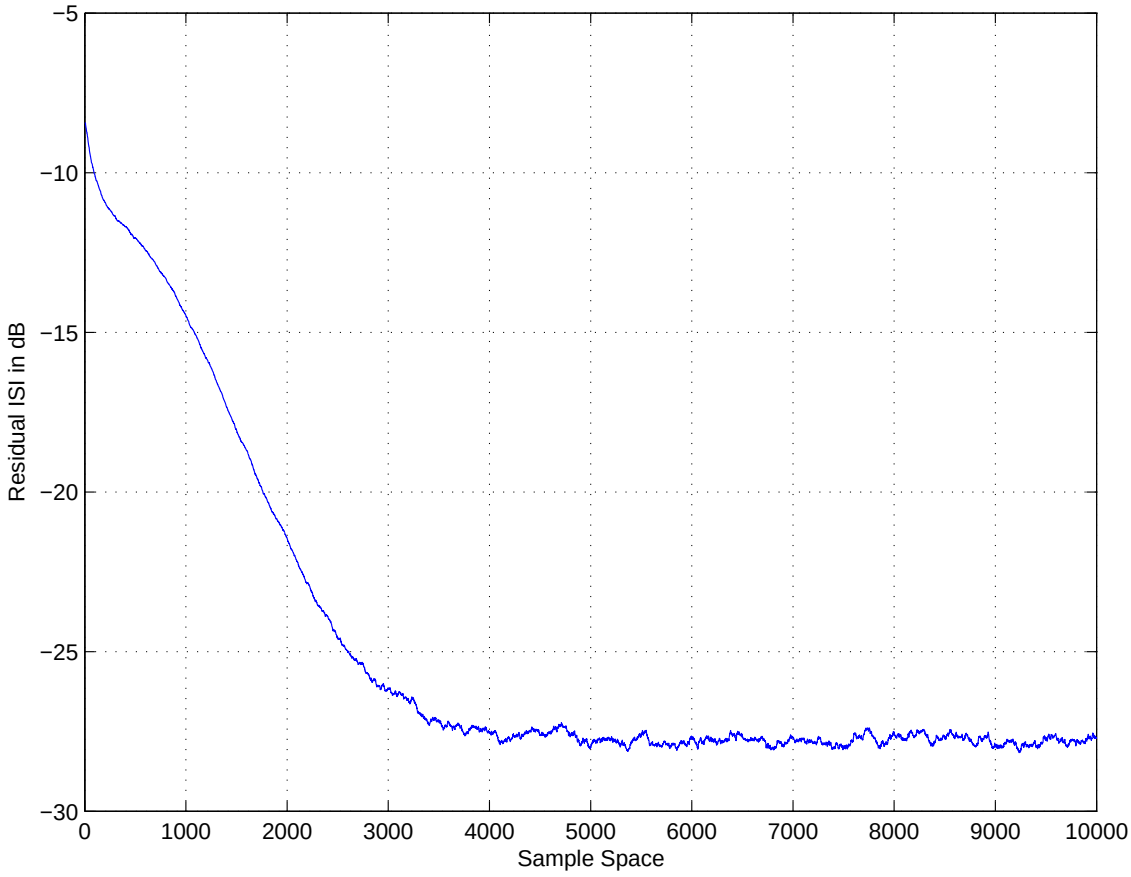

Figure 2.25: The Residual ISI for MCMA algorithm.

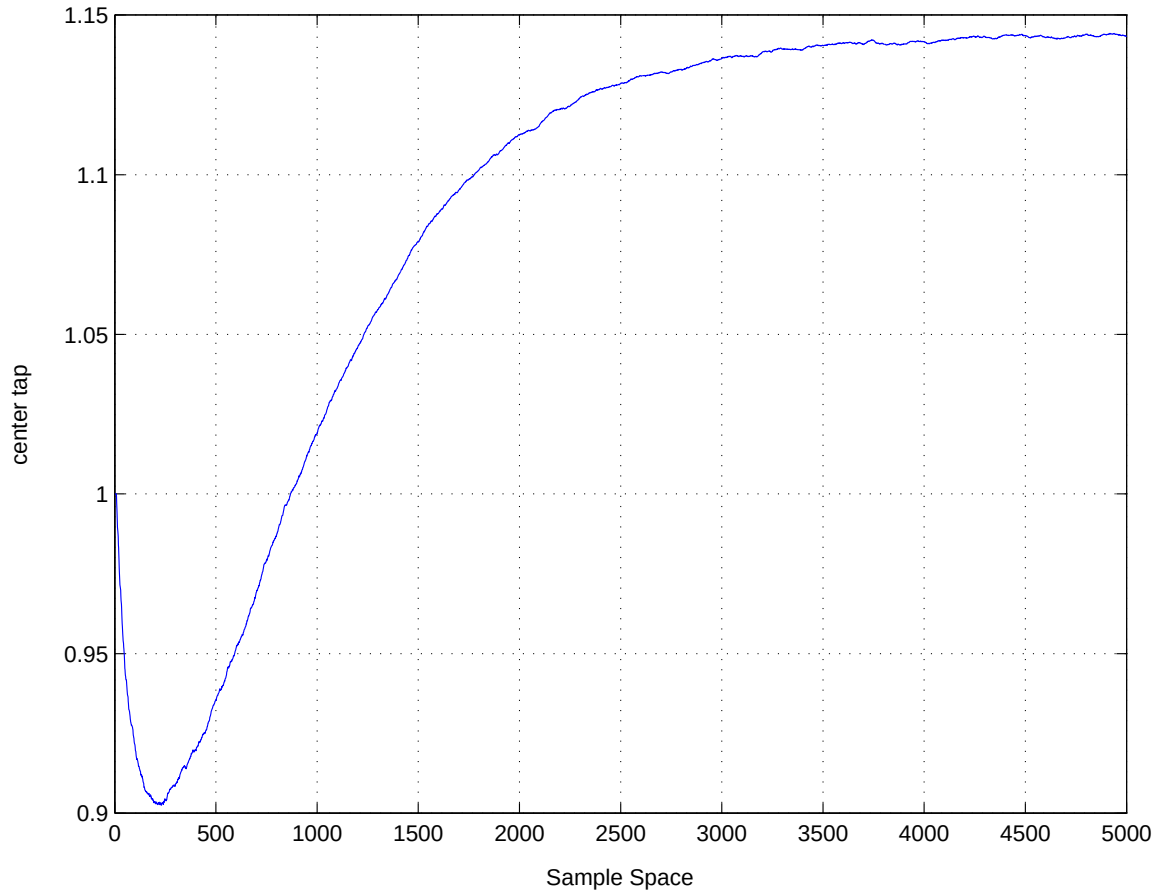

Figure 2.26: Behavior of the center tap of the equalizer for MCMA algorithm.

in MCMA, as in CMA would not be zero even when the channel is perfectly equalized. This in turn results in large output error in the steady state. Therefore Kil switched the MCMA into the decision directed (DD) mode to improve the steady state performance, i.e, the convergence speed and the output error levels, when the eye pattern of the equalizer is opened to some extent by the MCMA. The MCMA is dominant mode in the blind mode and the conventional DD takes over in the tracking mode.

To avoid the weakness of the DD algorithm, the DD mode of operation is confined to the high confidence zones. The confidence zones were selected as shown in Figure 2.27 and Figure 2.28. With this dual mode of operation when perfect equalization is reached, the error signal will be almost equal to zero in the steady state.

The error e_R and e_I can be written as:

$$e_R(k) = \begin{cases} y_R(k) - dec(y_R(k)), & \text{if } y_R(k) \; \epsilon \; C_R \\ y_R(k)(|y_R(k)|^2 - R_R), & \text{otherwise} \end{cases} \tag{2.36}$$

$$e_I(k) = \begin{cases} y_I(k) - dec(y_I(k)), & \text{if } y_I(k) \; \epsilon \; C_I \\ y_I(k)(|y_I(k)|^2 - R_I), & \text{otherwise} \end{cases} \tag{2.37}$$

where C_R and C_I represent the confidence zones for the real and imaginary part of the output of the equalizer respectively and Z_R and Z_I are the confidence zone parameters with $0 < Z_R, Z_I < 1$, which determine the time instants to switch between the MCMA and the DD mode. According to Macchi and Ewada [17] an

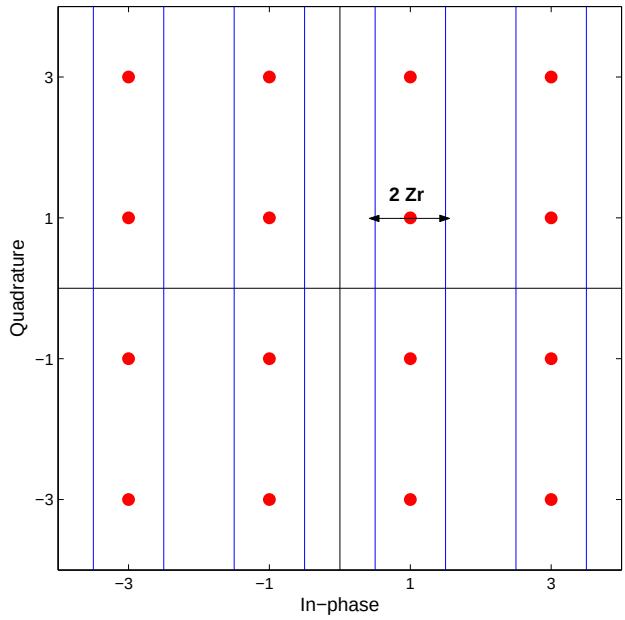

Figure 2.27: Decision zones for real part of the signals.

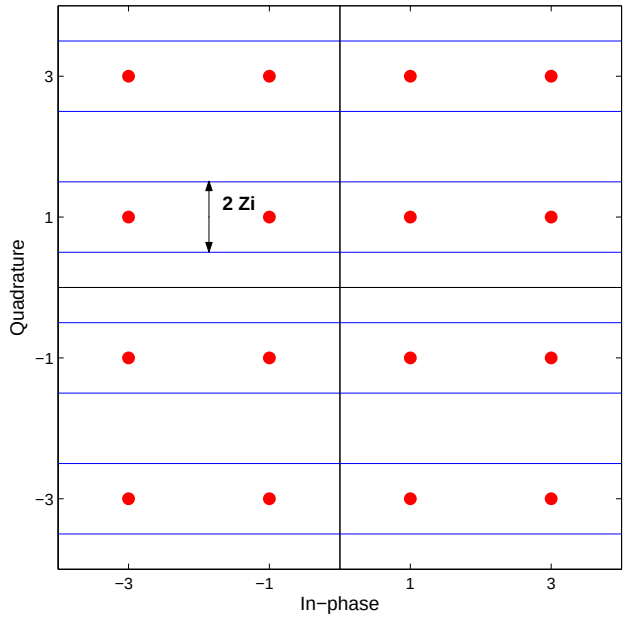

Figure 2.28: Decision zones for imaginary part of the signals.

open eye condition can be expressed as

$$|y(k) - a[k]| < \frac{D}{2}, \qquad \forall k \tag{2.38}$$

where D is the minimum distance between the symbols in the constellation. The dual mode MCMA was simulated for the channel as shown in Figure 2.18 and Figure 2.19. The SNR was maintained at 30 dB and an equalizer with 9 taps was considered. The values of Z_r and Z_i were chosen to be 0.5. As is evident from the Figure 2.31 and Figure 2.32 the equalizer converges around 3200 symbols. Also a mark difference between the constellation after convergence between the MCMA and MCMA-DD can be observed from Figure 2.14 and Figure 2.29

2.4 Summary

The main purpose of this chapter is to introduce the reader to the historical evolution of blind equalization schemes. In brief it can be said that Sato's [6] work formed the basis for all the algorithms that were derived or proposed. Godard [14] extended his work to propose the CMA which suffered from the problem of phase recovery and slow convergence. NCMA [20] was then proposed to speed up the convergence rate followed by MCMA [26] which was able to recover the phase jitter due to complex channels. The tap update functions for some of the algorithms described in this chapter are summarized in Table 2.1

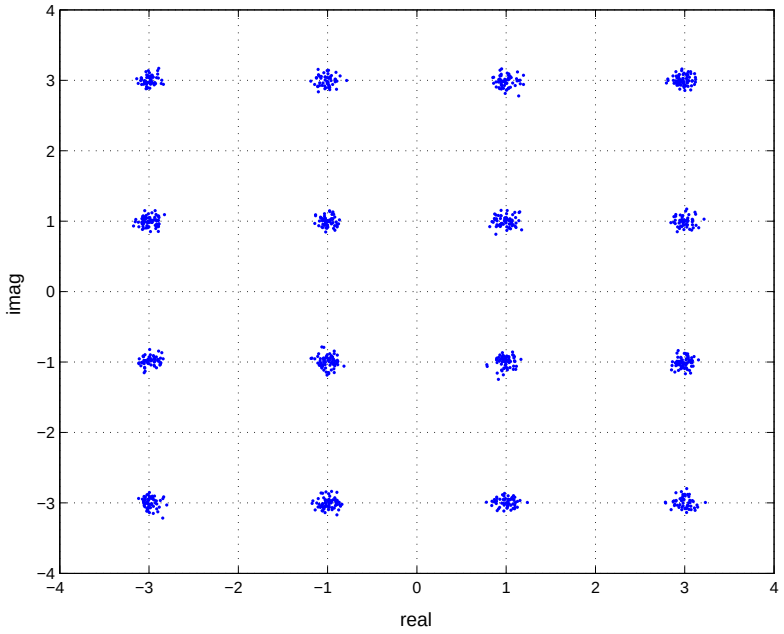

Figure 2.29: Signal constellation after convergence (the last 1000 bits) for MCMA-DD algorithm.

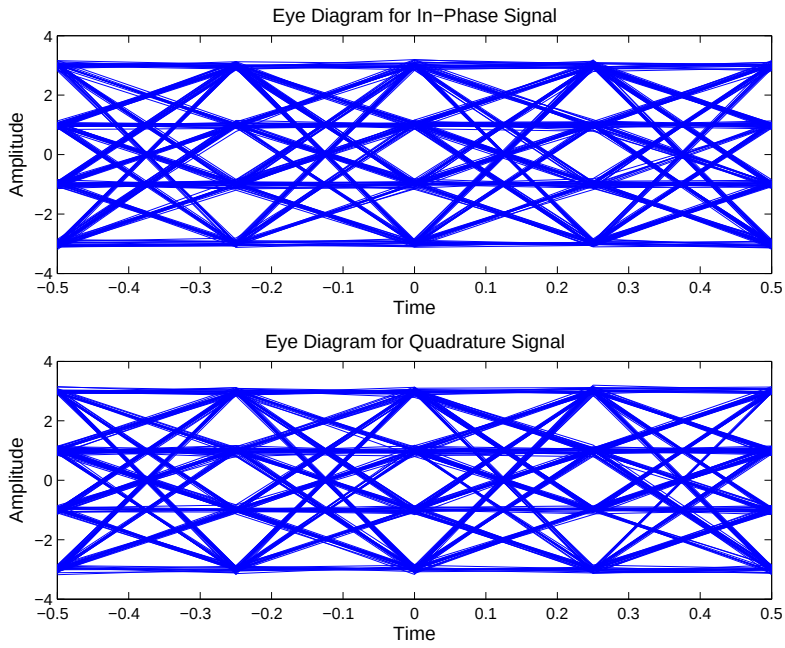

Figure 2.30: Eye-diagram of the signal after convergence (the last 1000 bits) for MCMA-DD algorithm.

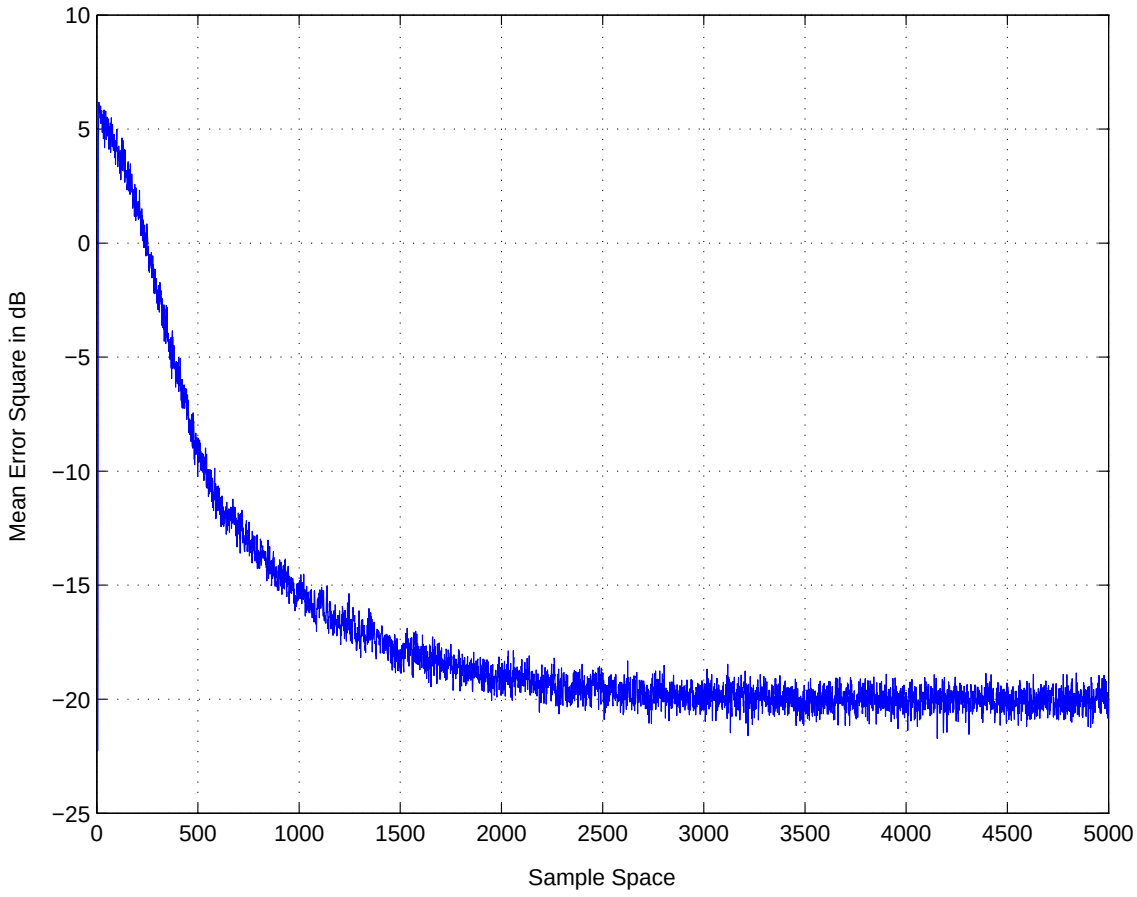

Figure 2.31: The Mean Square Error curve for MCMA-DD algorithm.

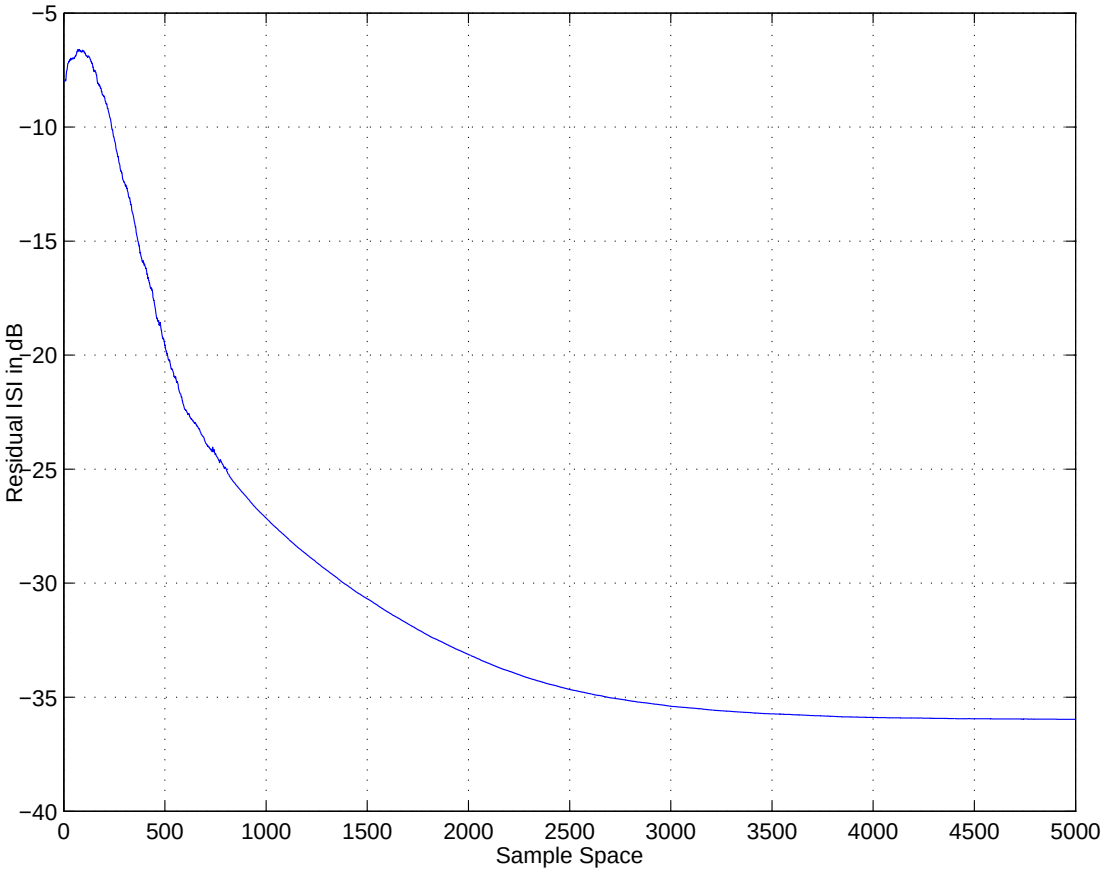

Figure 2.32: The Residual ISI for MCMA-DD algorithm.

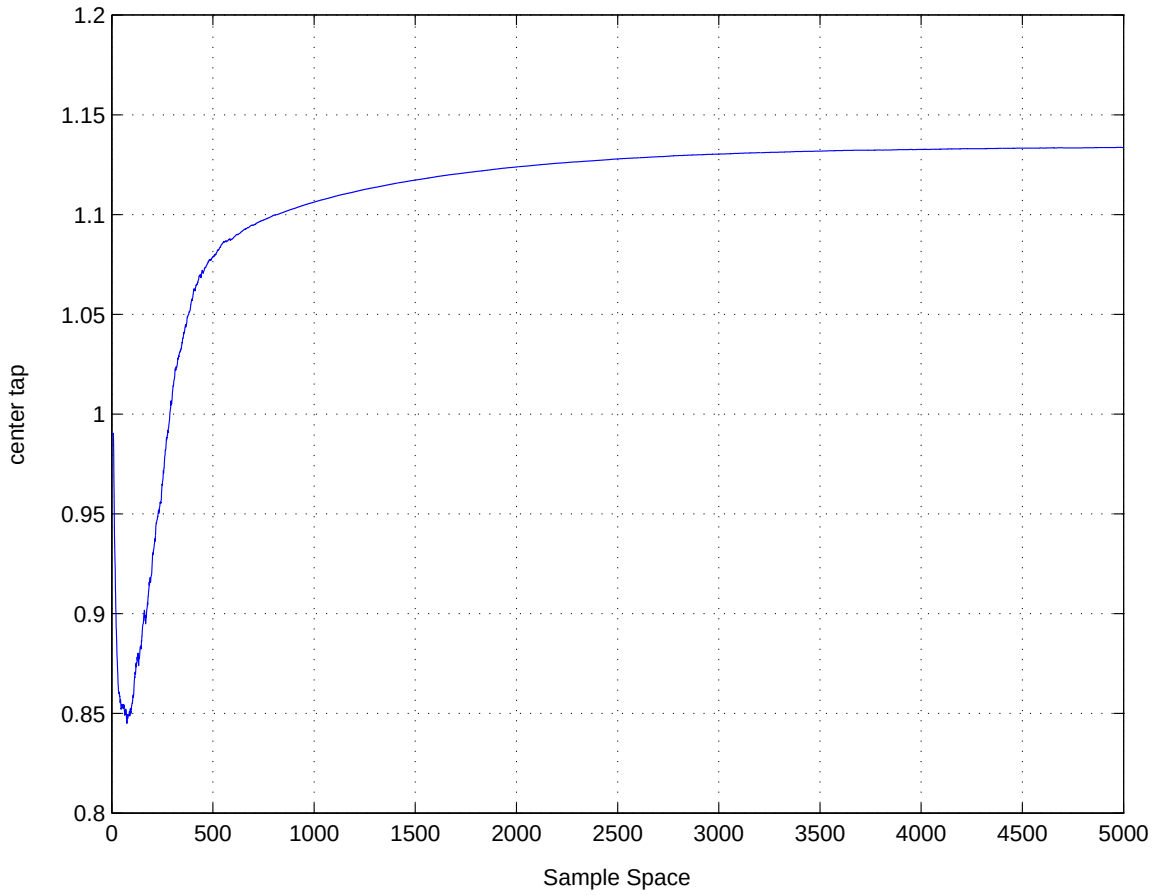

Figure 2.33: Behavior of the center tap of the equalizer for MCMA-DD algorithm.

Table 2.1: Different blind equalization algorithms

Algorithm	Tap Update Function
Sato	$\mathbf{w}(k+1) = \mathbf{w}(k) - [y(k) - R_s \mathtt{sgn}[y(k)]]\mathbf{x}(k)$ $R_s \triangleq \frac{E[a(k)]^2}{E[a(k)]}$
BGR ‡	$\mathbf{w}(k+1) = \mathbf{w}(k) - e_b[y(k)]\mathbf{x}(k)$
Godard †	$\mathbf{w}(k+1) = \mathbf{w}(k) - \mu(\lvert y(k)\rvert^q - R_q)\lvert y(k)\rvert^{q-2}\lvert y(k)\rvert\mathbf{x}^H(k)$ $R_q \triangleq \frac{E\lvert a(k)\rvert^{2q}}{E\lvert a(k)\rvert^q}$
Stop and Go	$\mathbf{w}(k+1) = \mathbf{w}(k) - \mu\psi_1[y(k)]\mathbf{x}(k)$ if $\mathtt{sgn}[\psi_1(y(k))] = \mathtt{sgn}[\psi_2(y(k))]$ $= \mathbf{w}(k)$, if $\mathtt{sgn}[\psi_1(y(k))] \neq \mathtt{sgn}[\psi_2(y(k))]$
NCMA	$\mathbf{w}(k+1) - \mathbf{w}(k) = \mu\frac{\mathtt{sgn}[y^*(k)] - y^*(k)}{\lvert\lvert\mathbf{x}(k)\rvert\rvert^2}\mathbf{x}(k)$
MCMA	$\mathbf{w}(k+1 = \mathbf{w}(k) - \mu e(k)\mathbf{x}^*(k)$ $e_{2R}(k) = y_R(k)(y_R^2(k) - R_{2R})$ $e_{2I}(k) = y_I(k)(y_I^2(k) - R_{2I})$

†CMA is a special case of Godard Algorithm at $q = 2$.
‡For the case of BGR algorithms refer Section 2.2.2

Chapter 3

Derivation of the Proposed Algorithm

3.1 Principle of Minimal Disturbance

"In the light of new input data, the parameters of an adaptive system should only be disturbed in a minimal fashion."

In terms of an adaptive filter the statement can be modified as *"from one iteration to the next, the weight vector of the adaptive filter should be changed in a minimal manner, subject to a constraint imposed on the updated filter's output."* [9]

The normalized LMS [21] uses this principle to combat the gradient noise amplification problem in LMS, which takes place when the inputs to the equalizer are large. In particular the adjustment applied to the tap-weight vector at iteration

$(k+1)$ is normalized with respect to the squared euclidean norm of the tap input vector.

3.2 Normalization of Modified Constant Modulus Algorithm(MCMA)

Lin [10] used the constraint optimization technique by utilizing the principle of minimal disturbance to propose a normalized version of MCMA. This algorithm also used the decision directed mode once the outputs were below a specified level. The optimization problem was formulated as follows:

$$\min_{\mathbf{w}(k+1)} \|\mathbf{w}(k+1)-\mathbf{w}(k)\|^2 \qquad \text{subject to} \begin{cases} s_R(k)[s_R^2(k)-R_R^2]=0, \\ \\ s_I(k)[s_I^2(k)-R_I^2]=0 \end{cases} \tag{3.1}$$

Hence the minimization problem can be formulated as follows

$$\min_{\mathbf{w}(k+1)} \left\{ \|\mathbf{w}(k+1)-\mathbf{w}(k)\|^2 + \lambda_1 s_R(k)(s_R^2(k)-R_R^2) + \lambda_2 s_I(k)(s_I^2(k)-R_I^2) \right\} \tag{3.2}$$

where

$$\begin{aligned} s(k) &= \mathbf{w}^H(k+1)\mathbf{x}(k) \\ &= R_R \mathtt{sgn}[y_R(k)] + jR_I \mathtt{sgn}[y_I(k)]. \end{aligned} \tag{3.3}$$

$$R_R^2 \triangleq \frac{E[|s_R(k)|^4]}{E[|s_R(k)|^2]} \qquad \text{and} \qquad R_I^2 \triangleq \frac{E[|s_I(k)|^4]}{E[|s_I(k)|^2]}. \tag{3.4}$$

The method of Lagrange multipliers was used to solve the above constrained problem and the update equation was obtained as

$$\mathbf{w}(k+1) = \mathbf{w}(k) - \frac{\mu}{\| \mathbf{x}(k) \|^2}\mathbf{x}(k)[e_R(k) + je_I(k)]^* \tag{3.5}$$

where

$$e_R(k) = \begin{cases} y_R(k) - dec[y_R(k)] & \text{if } y(k) \subseteq C_R \\ y_R(k) - R_R\mathtt{sgn}[y_R(k)] & \text{if } y(k) \nsubseteq C_R, \end{cases} \tag{3.6}$$

and

$$e_I(k) = \begin{cases} y_I(k) - dec[y_I(k)] & \text{if } y(k) \subseteq C_I \\ y_I(k) - R_I\mathtt{sgn}[y_I(k)] & \text{if } y(k) \nsubseteq C_I. \end{cases} \tag{3.7}$$

where C_I and C_R are the confidence zones as assumed in the case of MCMA-DD (Figure 2.28 and Figure 2.27). The algorithm in the blind mode updates the tap weight vector in such a way that the value $\mathbf{w}(k+1)$ computed at $(k+1)$ exhibits a minimum change in euclidean norm with respect to the known value $\mathbf{w}(k)$ at time k.

The scheme proposed by Lin [10] was able to accomplish blind equalization and carrier phase recovery simultaneously by taking the advantage of the principle of minimal disturbance since it introduces a normalization factor in the weight update equation. It was able to exploit the time varying step-size parameter to handle the nonstability and gradient noise amplification problem. It was also able to handle small carrier phase offsets in a better way than MCMA algorithm.

3.3 Generalization of Lin's Scheme

The cost function as given by Lin [10] can be modified by utilizing the behavior of the past inputs and adding multiple constraints [11]. Thus the new constrained problem can be formulated in the floowing manner

Find $\mathbf{w}(k+1)$ so as to minimize Euclidean norm of the change in the estimate given by

$$\begin{aligned}
&\|\mathbf{w}(k+1)-\mathbf{w}(k)\| \qquad \text{subject to the following constraints} \\
&s_R(k)(s_R^2(k)-R_R^2)=0 \qquad \text{and} \qquad s_I(k)(s_I^2(k)-R_I^2)=0 \\
&s_R(k-1)(s_R^2(k-1)-R_R^2)=0 \qquad \text{and} \qquad s_I(k-1)(s_I^2(k-1)-R_I^2)=0 \\
&\qquad\qquad\qquad\qquad . \\
&\qquad\qquad\qquad\qquad . \\
&\qquad\qquad\qquad\qquad . \\
&s_R(k-m+1)(s_R^2(k-m+1)-R_R^2)=0 \qquad \text{and} \qquad s_I(k-m+1)(s_I^2(k-m+1)-R_I^2)=0
\end{aligned} \tag{3.8}$$

Hence the following extended optimization problem can be established for m constraints:

$$\min_{\mathbf{w}(k+1)} \left\{ \begin{aligned} &\|\mathbf{w}(k+1)-\mathbf{w}(k)\|^2 \\ &\qquad + \sum_{i=1}^{m} \lambda_{1i} s_R(k-i+1)(s_R^2(k-i+1)-R_R^2) \\ &\qquad + \sum_{i=1}^{m} \lambda_{2k} s_I(k-i+1)(s_I^2(k-i+1)-R_I^2) \end{aligned} \right\} \tag{3.9}$$

where R_R and R_I are same as in the equation (3.4), λ_{1i}, λ_{2i} where $i\epsilon\{1, 2, \ldots, m\}$, are the Lagrange multipliers. The a priori output $s(k)$ can be set in the following way.

$$\begin{aligned} s(k) &= s_R(k) + js_I(k) \\ &= \mathbf{w}_{apriori}^H \mathbf{x}(k) \end{aligned} \tag{3.10}$$

where $\mathbf{w}_{apriori} = \mathbf{w}(k+1)$. The a priori output $s(k)$ can be assumed in similar way as was assumed in [20]:

$$s(k) = R_R \mathtt{sgn}[y_R(k)] + jR_I \mathtt{sgn}[y_I(k)] \tag{3.11}$$

By using the method of Lagrange multipliers, equation (3.9) can be solved and the tap update recursion relation can be obtained. For simplicity reasons, the algorithm is initially derived for $m = 2$, i.e, the minimization problem contains only four constraints, then it is extended for m constraints. Doing so, the minimization problem can be written as:

$$\min_{\mathbf{w}(k+1)} \left\{ \begin{array}{l} \|\mathbf{w}(k+1) - \mathbf{w}(k)\|^2 \\ \qquad + \lambda_{11} s_R^2(k)[s_R(k) - R_R^2] + \lambda_{12} s_I(k)[s_I^2(k) - R_I^2] \\ \qquad + \lambda_{21} s_R(k)[s_R^2(k-1) - R_R^2] + \lambda_{22} s_I(k-1)[s_I^2(k-1) - R_I^2] \end{array} \right\} \tag{3.12}$$

where

$$s(k) = \mathbf{w}^H(k+1)\mathbf{x}(k) \tag{3.13}$$

$$= s_R(k) + js_I(k) \tag{3.14}$$

and

$$s(k-1) = \mathbf{w}^H(k+1)\mathbf{x}(k-1) \tag{3.15}$$

$$= s_R(k-1) + js_I(k-1) \tag{3.16}$$

In the ensuing analysis, the following notations are considered

$$w_l(k) = a_l(k) + jb_l(k), \quad \text{and} \quad x(k) = u(k) + jv(k). \tag{3.17}$$

Therefore, the squared norm of the difference $\|\mathbf{w}(k+1) - \mathbf{w}(k)\|^2$ in the tap-weight vector $\mathbf{w}(k+1)$ can be expressed as

$$\|\mathbf{w}(k+1) - \mathbf{w}(k)\|^2 = \sum_{l=0}^{N-1}([a_l(k+1) - a_l(k)]^2 + [b_l(k+1) - b_l(k)]^2) \tag{3.18}$$

A real-valued cost function $J(k)$ for the constrained optimization problem can be then formulated by combining the equation (3.12) and (3.18).

$$\begin{aligned} J(k) = \sum_{l=0}^{N-1}&([a_l(k+1) - a_l(k)]^2 + [b_l(k+1) - b_l(k)]^2) \\ &+ \lambda_{11}s_R^2(k)[s_R(k) - R_R^2] + \lambda_{12}s_I(k)[s_I^2(k) - R_I^2] \\ &+ \lambda_{21}s_R(k)[s_R^2(k-1) - R_R^2] + \lambda_{22}s_I(k-1)[s_I^2(k-1) - R_I^2] \end{aligned} \tag{3.19}$$

To find the optimal values of $a_l(k+1)$ and $b_l(k+1)$ the above given cost function $J(k)$ is differentiated with respect to these parameters and the results are set to zero. i.e,

$$\frac{\partial J(k)}{\partial a_l(k+1)} = 0 \quad \text{and} \quad \frac{\partial J(k)}{\partial b_l(k+1)} = 0 \tag{3.20}$$

which yield the following equations respectively,

$$\begin{aligned} 2[a_l(k+1) - a_l(k)] + \lambda_{11}[s_R^2(k) - R_R^2]u(k) + 2\lambda_{11}s_R^2(k)u(k) \\ + \lambda_{12}[s_I^2(k) - R_I^2]v(k) + 2\lambda_{12}s_I(k)v(k) \\ + \lambda_{21}[s_R^2(k-1) - R_R^2]u(k-1) + 2\lambda_{21}s_R(k-1)u(k-1) \\ + \lambda_{22}[s_I^2(k-1) - R_I^2]v(k-1) + 2\lambda_{22}s_I(k-1)v(k-1) = 0 \end{aligned} \tag{3.21}$$

$$\begin{aligned} 2[b_l(k+1) - b_l(k)] + \lambda_{11}[s_R^2(k) - R_R^2]v(k) + 2\lambda_{11}s_R(k)v(k) \\ - \lambda_{12}[s_I^2(k) - R_I^2]u(k) - 2\lambda_{21}s_I(k)u(k) \\ + \lambda_{21}[s_R^2(k-1) - R_R^2]v(k-1) + 2\lambda_{21}s_R(k-1)v(k-1) \\ - \lambda_{22}[s_I^2(k-1) - R_I^2]u(k-1) - 2\lambda_{22}s_I(k-1)u(k-1) = 0 \end{aligned} \tag{3.22}$$

Since the method of Lagrange multipliers is used, the minimization problem defined in (3.12) is also partially differentiable with respect to the Lagrange multipliers. Doing so, the following values are obtained after the partial derivative of the mini-

mization problem is set to zero:

$$\begin{aligned} s_R^2(k) &= R_R^2, \\ s_I^2(k) &= R_I^2, \\ s_R^2(k-1) &= R_R^2, \\ s_{2I}^2(k-1) &= R_I^2. \end{aligned} \tag{3.23}$$

Adding the equations (3.21) and (3.22), and using the equation (3.23), the following equation is obtained:

$$\begin{aligned} w_l(k+1) - w_l(k) + \lambda_{11} R_R[u(k) - jv(k)] + \lambda_{12} R_I[v(k) + ju(k)] + \\ \lambda_{21} R_R[u(k-1) - jv(k-1)] + \lambda_{22} R_I[v(k-1) + ju(k-1)] = 0 \end{aligned} \tag{3.24}$$

Rearranging the above equation to the following form we have from equation (3.24)

$$w_l(k+1) - w_l(k) - [\lambda_{11} - j\lambda_{21}][u(k) + jv(k)] - [\lambda_{12} - j\lambda_{22}][u(k-1) + jv(k-1)] = 0 \tag{3.25}$$

In the vector form, equation (3.25) can be written as:

$$\mathbf{w}(k+1) = \mathbf{w}(k) + \lambda_a \mathbf{x}(k) + \lambda_b \mathbf{x}(k-1) \tag{3.26}$$

where

$$\lambda_a = R_R \lambda_{11} - j R_I \lambda_{12} \tag{3.27}$$

$$\lambda_b = R_R \lambda_{21} - j R_I \lambda_{22} \tag{3.28}$$

Equation (3.25) can also be written in matrix form as

$$\mathbf{w}(k+1) = \mathbf{w}(k) + \begin{bmatrix} \mathbf{x}(k) & \mathbf{x}(k-1) \end{bmatrix} \begin{bmatrix} \lambda_a \\ \\ \lambda_b \end{bmatrix} \tag{3.29}$$

where

$$\mathbf{x}(k) = \begin{bmatrix} x(k) & x(k-1) & x(k-2)..... & x(k-M) \end{bmatrix}^T \tag{3.30}$$

$$\mathbf{x}(k-1) = \begin{bmatrix} x(k-1) & x(k-2) & x(k-3)..... & x(k-M-1) \end{bmatrix}^T \tag{3.31}$$

Equation (3.29) can also be written as

$$\mathbf{w}(k+1) = \mathbf{w}(k) + \mathbf{X}\Lambda \tag{3.32}$$

where

$$\Lambda = \begin{bmatrix} \lambda_a \\ \\ \lambda_b \end{bmatrix} \tag{3.33}$$

$$\mathbf{X} = \begin{bmatrix} \mathbf{x}(k) & \mathbf{x}(k-1) \end{bmatrix} \tag{3.34}$$

Multiplying both the sides of equation (3.32) by X^H we have the value of λ as

$$\Lambda = [\mathbf{X}^H\mathbf{X}]^{-1}[\mathbf{X}^H\mathbf{w}(k+1) - \mathbf{X}^H\mathbf{w}(k)] \tag{3.35}$$

or

$$\Lambda = \Omega^{-1}[\mathbf{s}^H - \mathbf{y}^H] \tag{3.36}$$

where

$$\Omega = \mathbf{X}^H \mathbf{X} \tag{3.37}$$

$$\mathbf{s} = \begin{bmatrix} \mathbf{w}^H(k+1)\mathbf{x}(k) & \mathbf{w}^H(k+1)\mathbf{x}(k-1)] \end{bmatrix} \tag{3.38}$$

$$\mathbf{y} = \begin{bmatrix} \mathbf{w}^H(k)\mathbf{x}(k) & \mathbf{w}^H(k)\mathbf{x}(k-1) \end{bmatrix} \tag{3.39}$$

Substituting the value of Λ in equation (3.32) we have

$$\boxed{\mathbf{w}(k+1) = \mathbf{w}(k) + X\Omega^{-1}[\mathbf{s}^H - \mathbf{y}^H]} \tag{3.40}$$

where

$$\mathbf{s} = \begin{bmatrix} s(k) & s(k-1) & .... & s(k-i+1) \end{bmatrix}$$

$$\mathbf{y} = \begin{bmatrix} y(k) & y(k-1) & .... & y(k-i+1) \end{bmatrix}$$

$$\mathbf{X} = \begin{bmatrix} \mathbf{x}(k) & \mathbf{x}(k-1) & .... & \mathbf{x}(k-i+1) \end{bmatrix}$$

$$\Omega = \mathbf{X}^H \mathbf{X}$$

$$y(k) = \mathbf{w}^H(k)\mathbf{x}(k)$$

$$s(k) = \mathbf{w}^H(k+1)\mathbf{x}(k)$$

3.3.1 Decision Directed Mode

Lin [10] incorporated the decision directed mode in his algorithm in order to obtain better convergence rates and lower steady state errors. The above derived algorithm can also be switched into the decision directed mode once the error drops below a

particular threshold value. The threshold value can be chosen as shown in the Figures 2.28 and 2.27 which was taken from the previous work of Kil [30]

Equation (3.40) can be modified by replacing the difference of the vectors **s** and **y** by a single vector **E**:

$$\mathbf{w}(k+1) = \mathbf{w}(k) + \mu_{LR}\mathbf{X}\Omega^{-1}\mathbf{E}^{H} \tag{3.41}$$

where μ_{LR} is the learning rate used to control the convergence speed. For the case of two constraints **E** can be written as:

$$\mathbf{E} = \begin{bmatrix} E_1 & E_2 & .... & E_i \end{bmatrix} \tag{3.42}$$

where

$$\begin{aligned} E_1 =& R_R\mathtt{sgn}[y_R(k)] + jR_I\mathtt{sgn}[y_I(k)] - y(k) \\ E_2 =& R_R\mathtt{sgn}[y_R(k-1)] + jR_I\mathtt{sgn}[y_I(k-1)] - y(k-1) \\ & ... \\ & ... \\ E_i =& R_R\mathtt{sgn}[y_R(k-i+1)] + jR_I\mathtt{sgn}[y_I(k-i+1)] - y(k-i+1) \end{aligned} \tag{3.43}$$

Once the equalizer output $y(k)$ reaches the boundary levels as specified in Figure 3.1, the algorithm can be switched in the decision directed mode. Thus the values of $E_1, E_2, ...E_i$ can be changed according to the following equation:

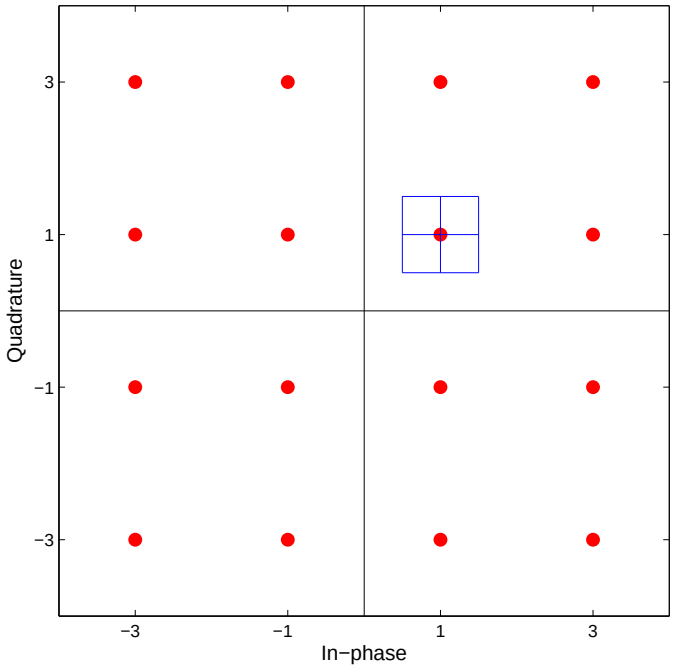

Figure 3.1: Decision boundaries for a 16-QAM constellation

$$E_i = \begin{cases} R_R\mathtt{sgn}[y_R k - i + 1)] + jR_I\mathtt{sgn}[y_I(k - i + 1)] - y(k - i + 1), \forall\ y(k - i + 1) \nsubseteq C \\ \\ R_R\mathtt{sgn}[y_R(k - i + 1)] + jR_I\mathtt{sgn}[y_I(k - i + 1)] - \hat{A}, \forall\ y(k - i + 1) \subseteq C \end{cases} \tag{3.44}$$

Where $\hat{A}$ is a set desired output as shown in the Figure 3.1. Another good aspect of this algorithm is the smooth shift from the blind mode to the decision directed mode according to the magnitude of the equalizer output error without any specific detection mechanism, because the algorithm can cluster the output signal at the

right positions . Hence the equalization of the derived technique both in the blind mode and decision directed mode operates with the same stability as the normalized least mean square algorithm which can also be treated as a least squares solution [9]. The main difference between the new scheme and the one proposed by Lin [10] with respect to the decision directed mode is that, in the new scheme unless and until both the real and the imaginary parts of the output signal are inside the bounded box simultaneously as shown in Figure 3.1, the algorithm doesn't shift to the decision directed mode, whereas in case of the Lin's algorithm the decision directed mode is applied to the real and the imaginary parts independently. Applying the decision directed mode in a way as used in the newly derived algorithm, gives more scope for the algorithm and it performs in a better fashion when dealing with the signal infected by phase offset.

The complexity of the newly derived algorithm is compared with that of other blind equalization algorithms based on CMA in the Table. The complexity was calculated for each iteration of window update. N represents the number of window taps used in the equalizer

3.4 Summary

This chapter in briefly deals with the derivation of the new scheme using Lagrange multipliers optimization technique. The newly derived scheme can be said as an

Algorithm	Addition	Multiplication
Sato	2N	2N+2
Godard	2N	2N+1
NCMA	2N	2N+2
MCMA	2N	2N+8
New scheme with Single Constraint	2N+1	2N+3
New scheme with Double Constraints	2(2N+1)	4N+6
New scheme with Triple Constraints	3(2N+1)	6N+8
New scheme with m Constraints	m(2N+1)	m(2N+2)+2

Table 3.1: Complexity comparison table of different algorithms

extension of the algorithm as derived by Lin [10] using the idea as given by Tanrikulu [28]. It is expected that the new algorithm will perform better than Lin's algorithm. The constraints added to this algorithm are meant for this purpose. The performance analysis of this algorithm for both $T-$spaced and $T/2-$ spaced equalizers will be detailed in Chapter 4 and Chapter 5 with the help of simulation results. Finally, the computational complexity among other well established blind equalization algorithms is detailed Table 3.1

Chapter 4

Simulations for Baud Spaced Equalizer

The above derived algorithm is simulated under various scenarios and conditions. All the results are plotted for 100 Monte Carlo iterations. The signal constellation used is as shown in Figure 2.3. For each scenario the input and the output constellation are plotted along with the eye diagrams. In order to investigate the convergence rate and the steady state error the residual ISI and the MSE are also plotted for single, double and triple constraints. Single, double and triple constraints corresponds to $i = 1, 2, 3$ in the equation 3.9. The residual ISI is calculated using the formula as given in equation (2.12)

4.1 Real Channel

The simplest of all scenarios is the performance under the real channel. The channel chosen is as shown in Figure 2.2. The variance of noise is assumed to be 0.01. An equalizer with 9 taps is used. It is found that the mean square error converges at approximately -22 dB. However, it is observed that no matter how many constraints are added the convergence rate of the learning curve remained almost the same. Similar is the case with residual ISI (from Figure 4.5 and Figure 4.6).Only the learning curve for algorithm with double constraints is plotted as the curve is almost the same for different constraints.Since the center tap of the equalizer is assumed to be equal to 1, its behavior is also plotted inorder to confirm the convergence rate.

4.2 Complex Channel-I

The complex channel is selected from the paper by Picchi and Prati [1] (as shown in the Figure 4.8 and Figure 4.9). It is found out by simulation that the mean square error converges approximately at -20 dB and the ISI around -36 dB. Since the center tap of the equalizer is assumed to be equal to 1, its behavior is also plotted in order to confirm the convergence rate, the behavior of the center tap is plotted in Figure 4.2.

As is evident from the Figures 4.16 and 4.17 the equalizer for single constraint

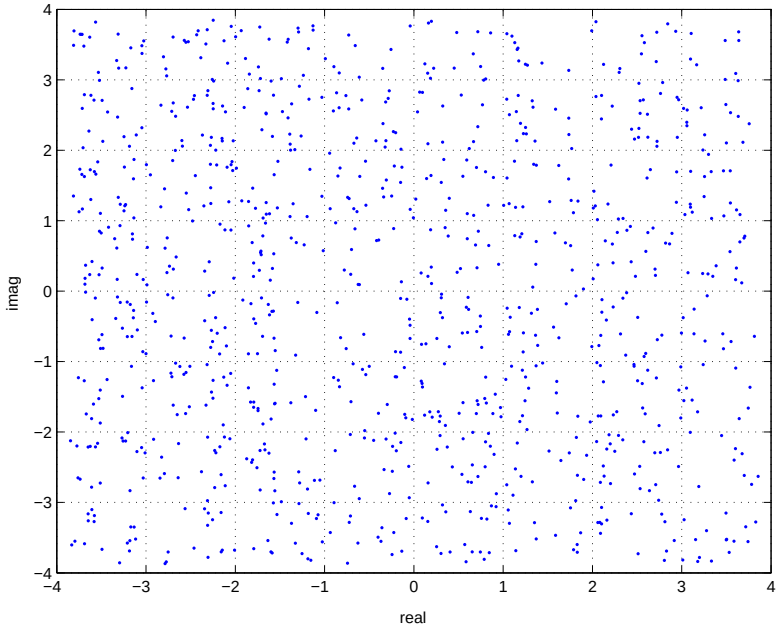

Figure 4.1: Constellation of 16-QAM signal before convergence when passed through real channel (last 1000 samples).

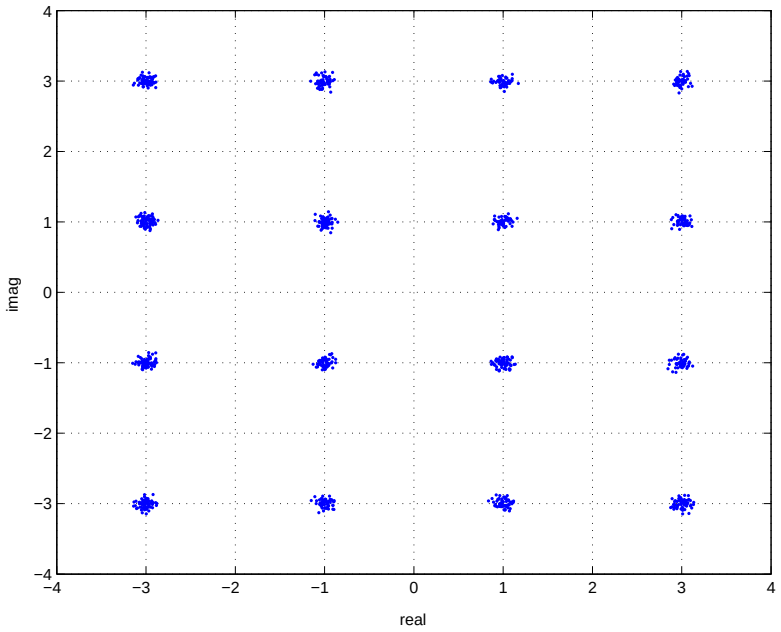

Figure 4.2: Constellation of 16-QAM signal after convergence when passed through real channel (last 1000 samples).

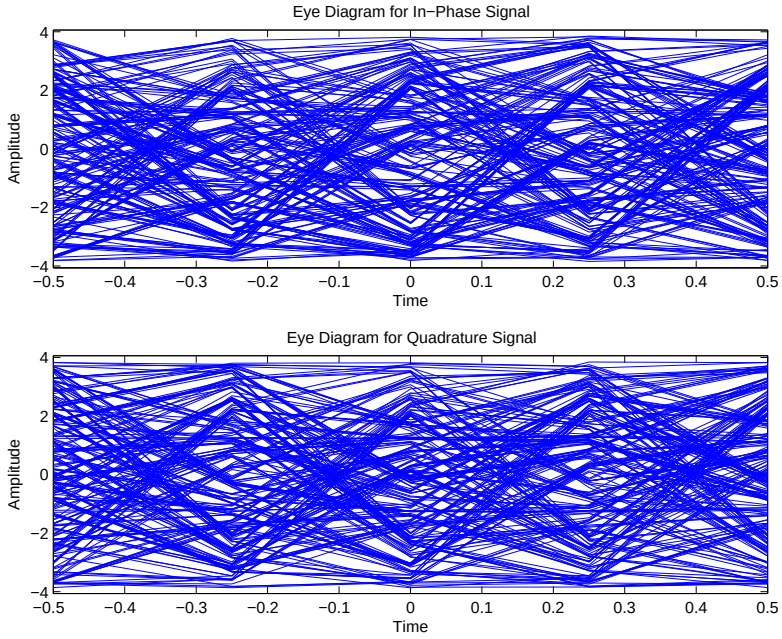

Figure 4.3: Eye diagram of 16-QAM signal before convergence when passed through real channel (last 1000 samples).

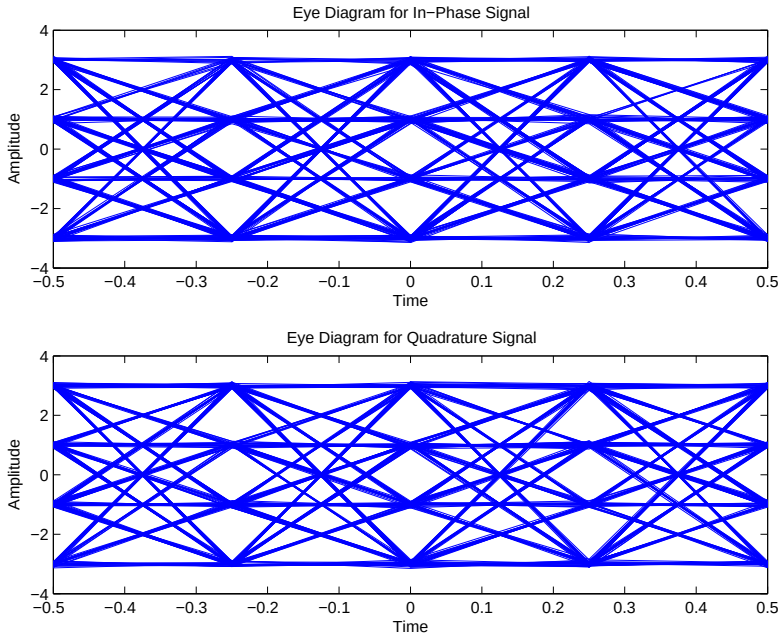

Figure 4.4: Eye diagram of 16-QAM signal after convergence when passed through real channel (last 1000 samples).

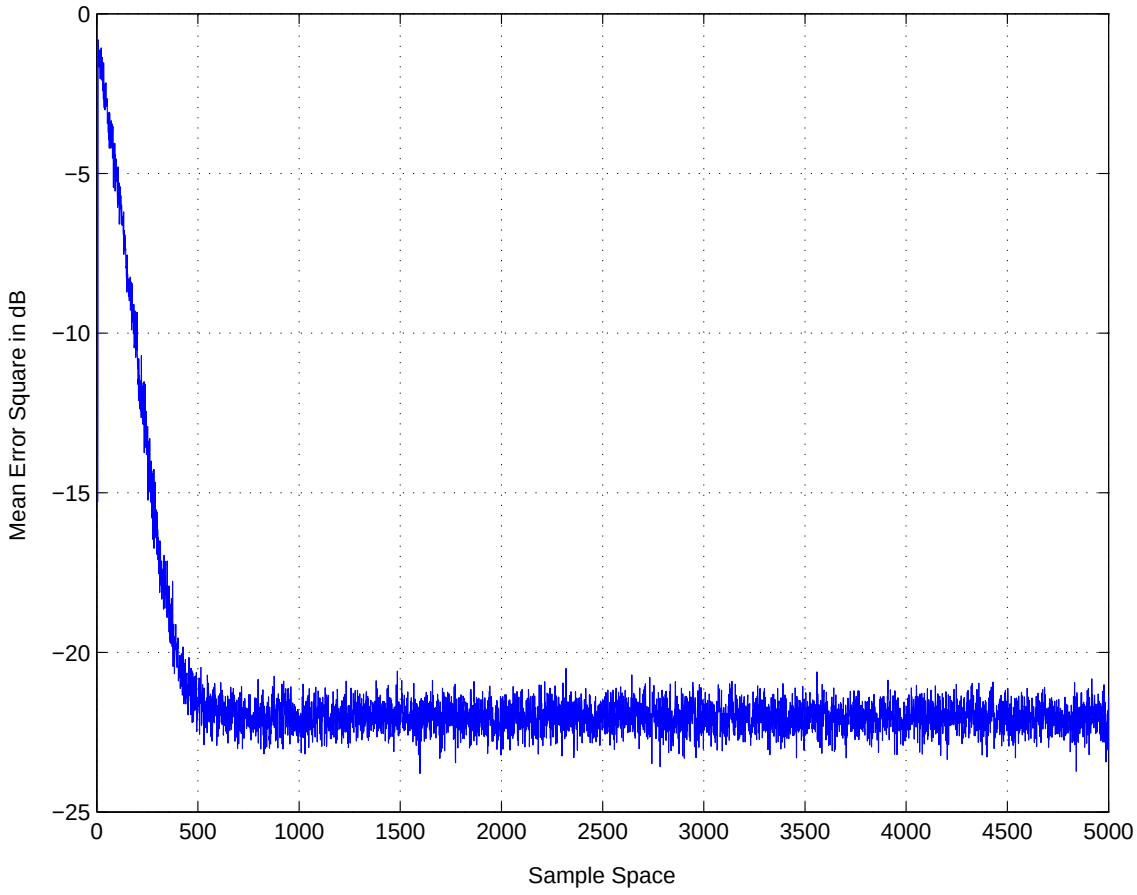

Figure 4.5: MSE curve for the signal passing through real channel and the algorithm using double constraints.

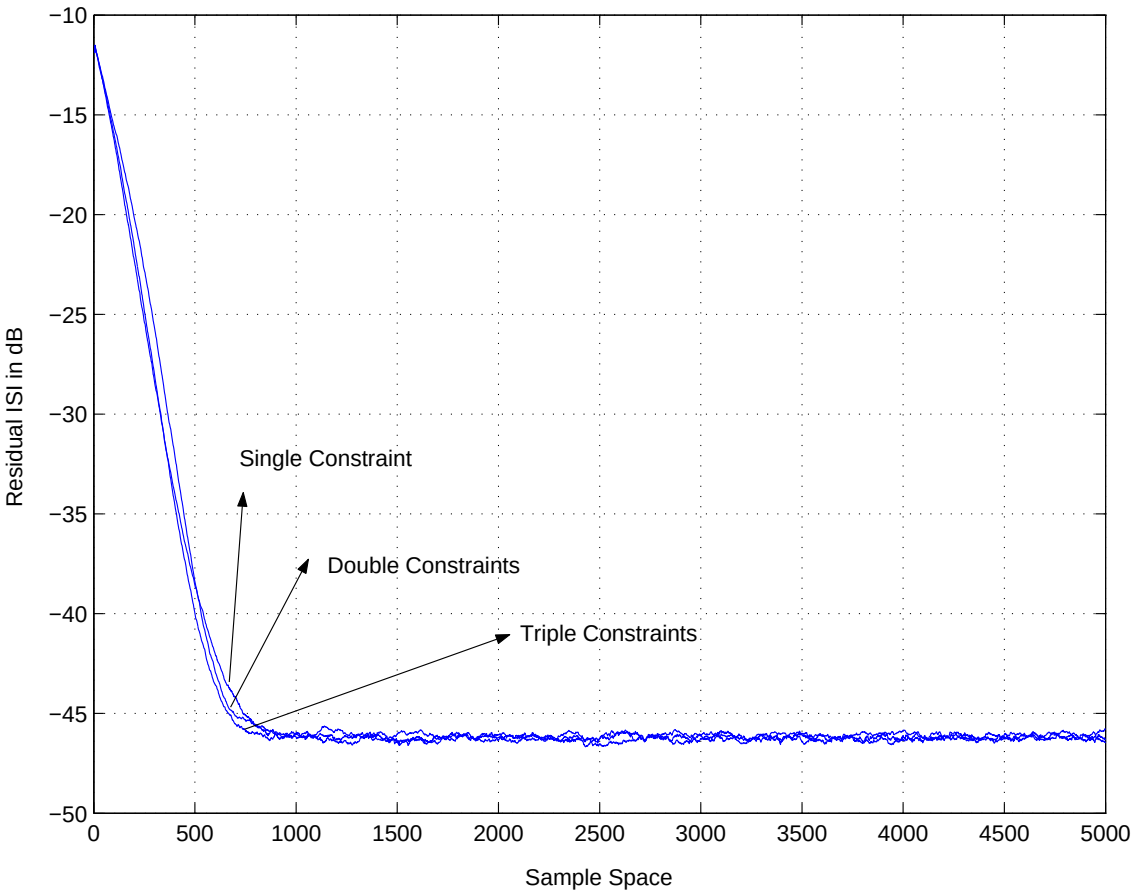

Figure 4.6: Residual ISI for single,double and triple constraints for real channel.

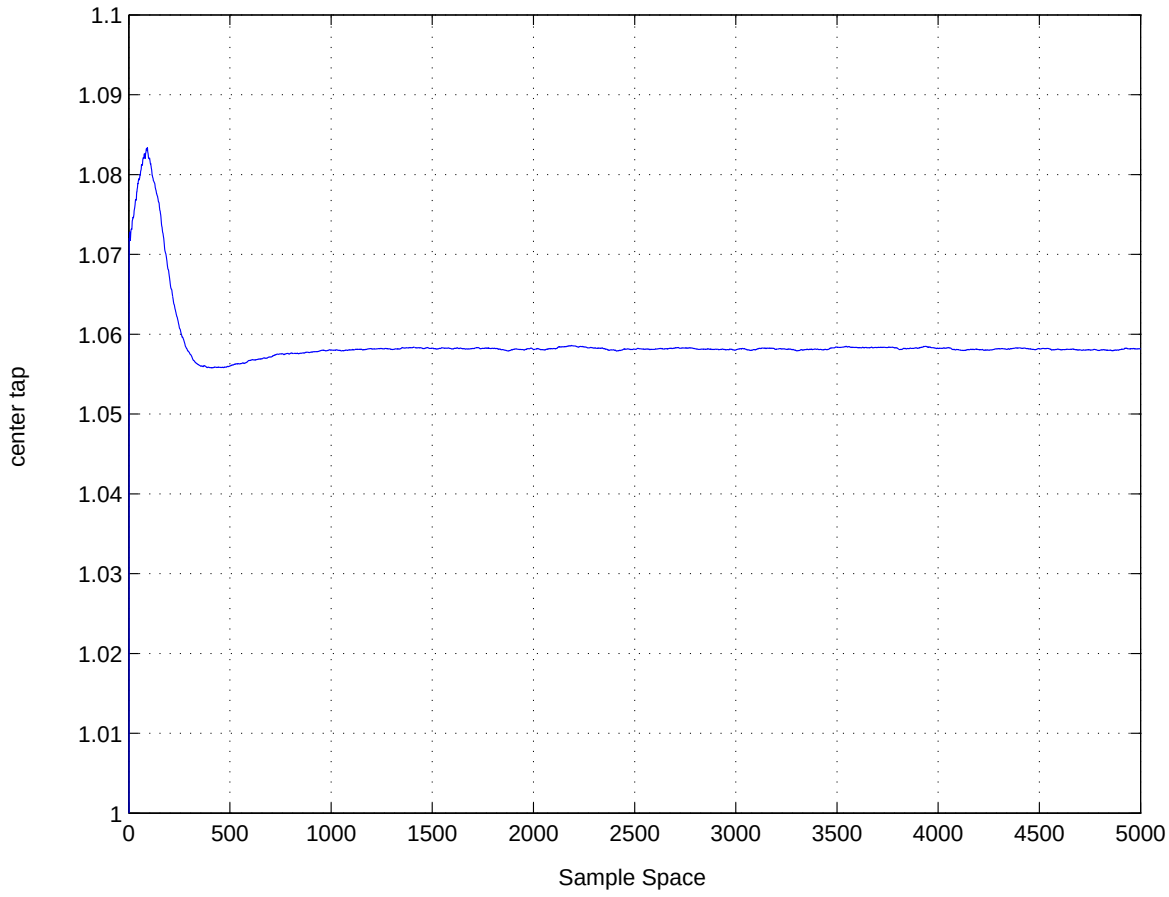

Figure 4.7: Behaviour of the center tap of the equalizer for the real channel (double constraints).

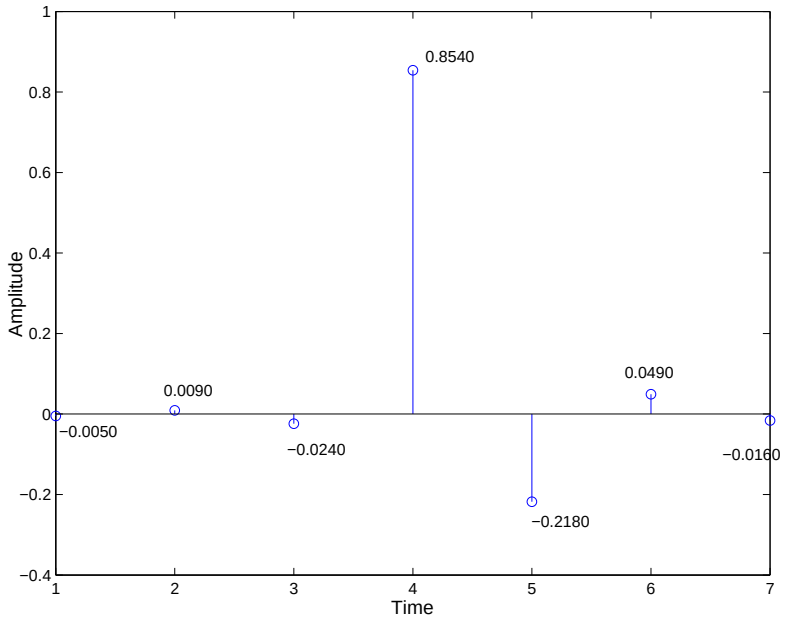

Figure 4.8: Real part of the complex channel.

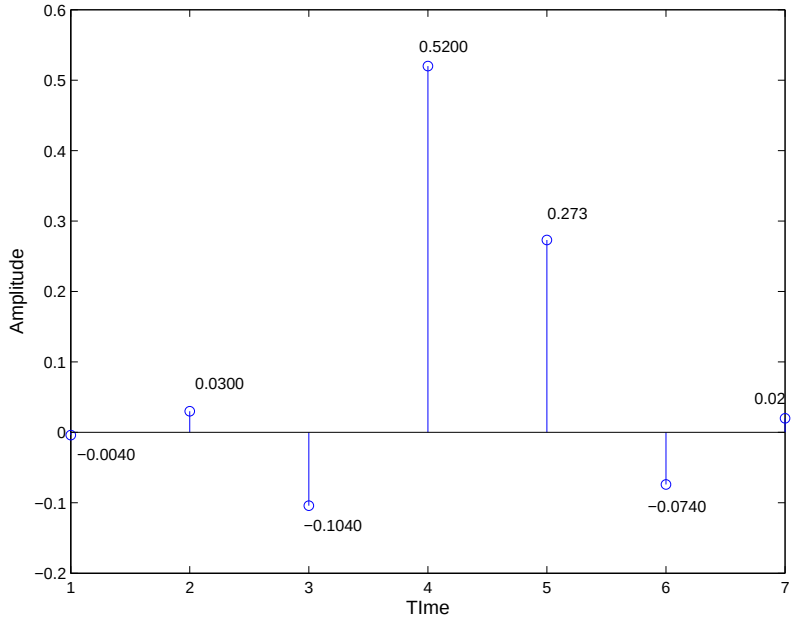

Figure 4.9: Imaginary part of the complex channel.

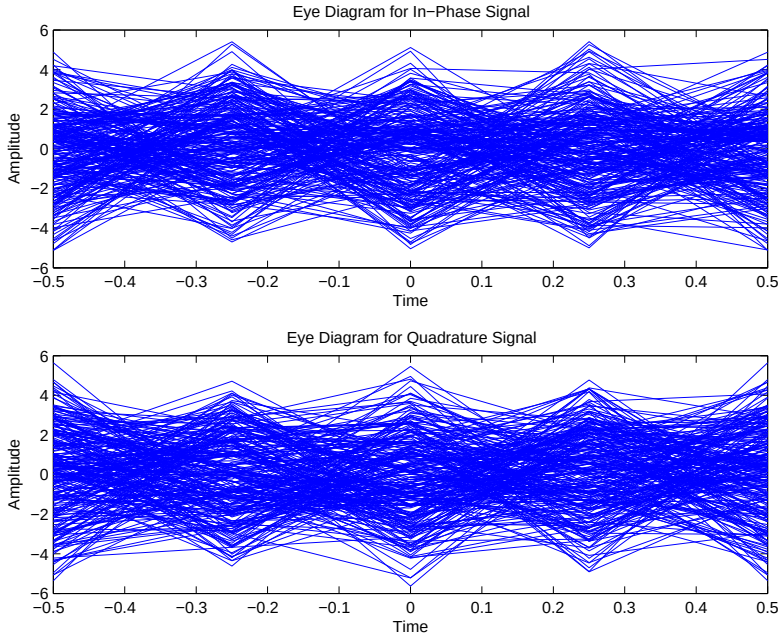

Figure 4.10: Eye diagram of 16-QAM signal before convergence when passed through complex channel-I as given in [1] (last 1000 samples).

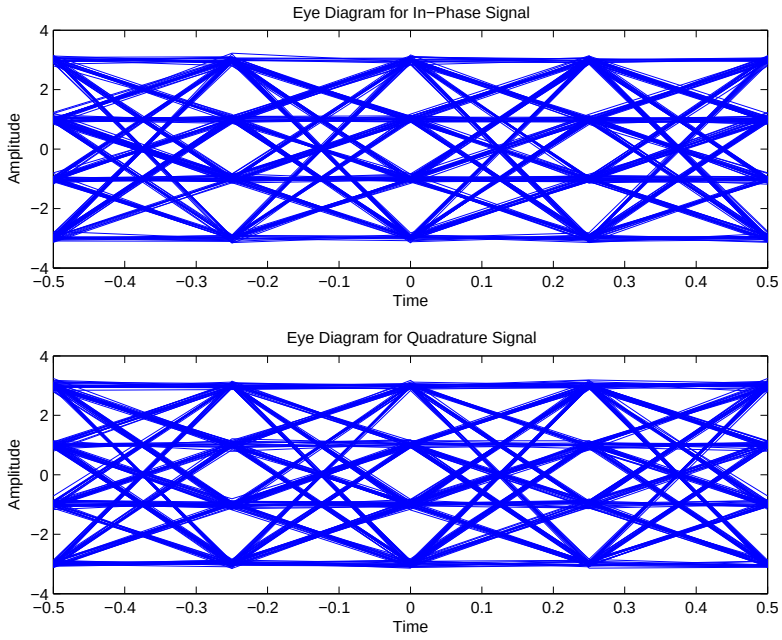

Figure 4.11: Eye diagram of 16-QAM signal after convergence when passed through complex channel-I as given in [1] (last 1000 samples).

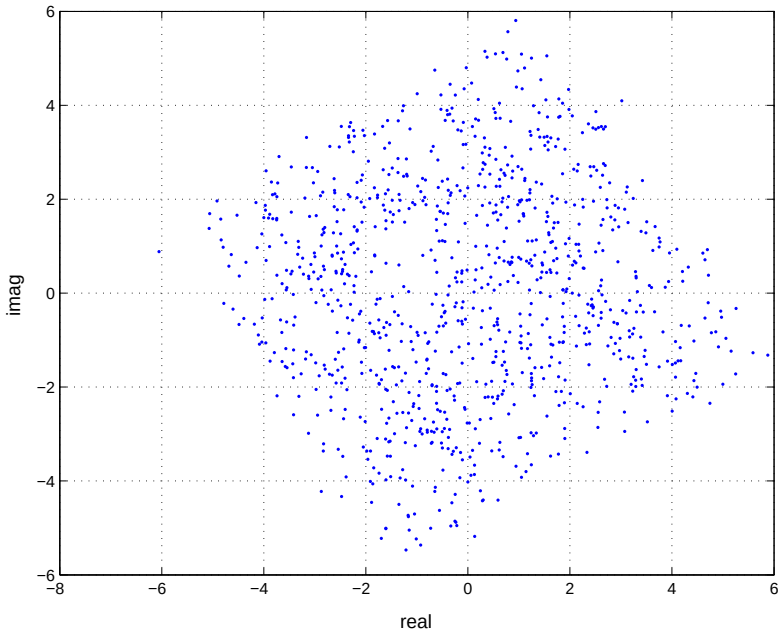

Figure 4.12: Constellation of 16-QAM signal before equalization when passed through complex channel-I as given in [1] (last 1000 samples).

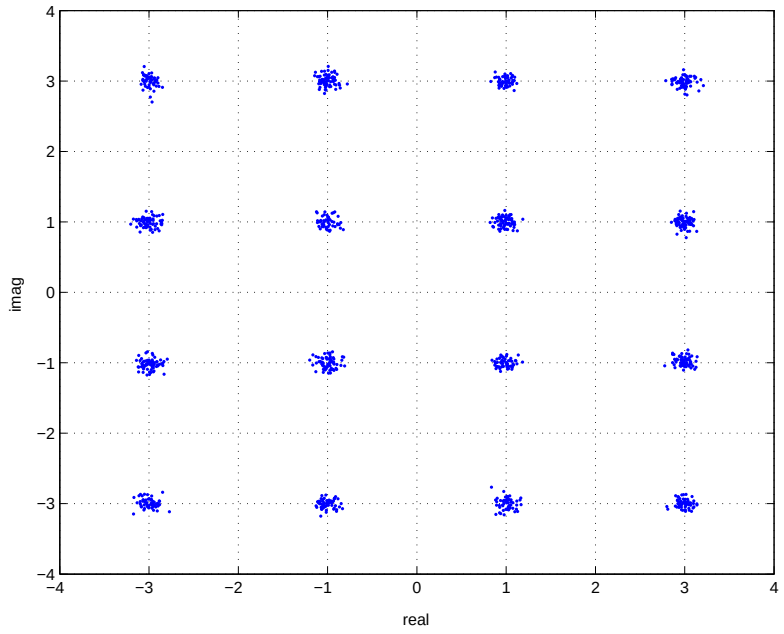

Figure 4.13: Constellation of 16-QAM signal after equalization when passed through complex channel-I as given in [1] (last 1000 samples) for single constraint.

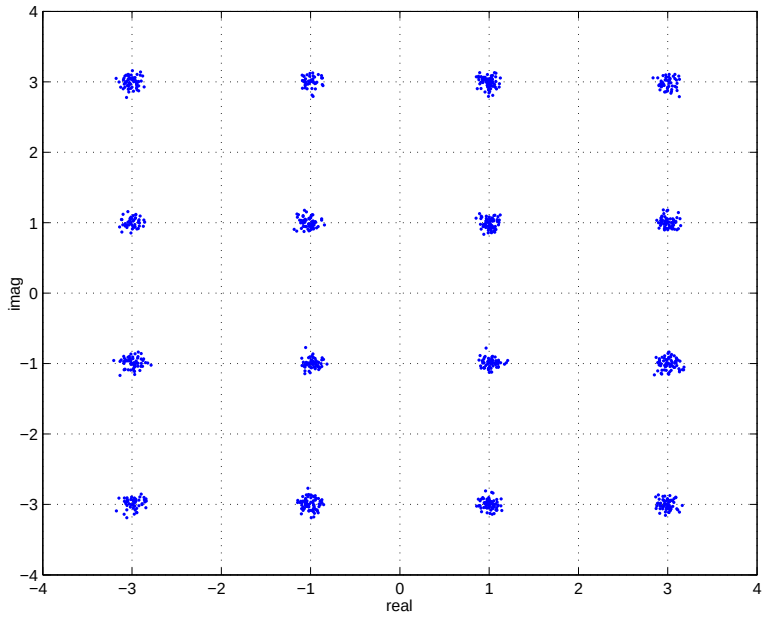

Figure 4.14: Constellation of 16-QAM signal after equalization when passed through complex channel-I as given in [1] (last 1000 samples) for double constraints.

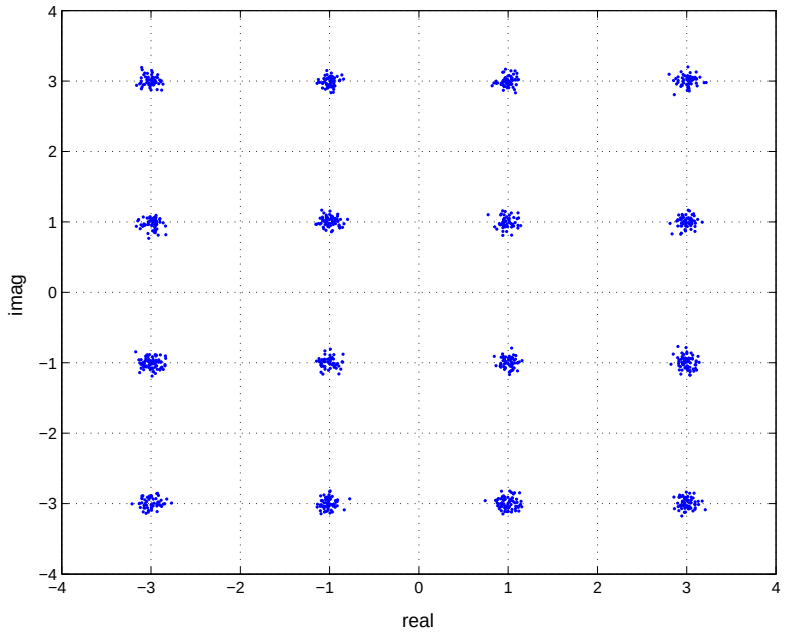

Figure 4.15: Constellation of 16-QAM signal after equalization when passed through complex channel-I as given in [1] (last 1000 samples) for triple constraints.

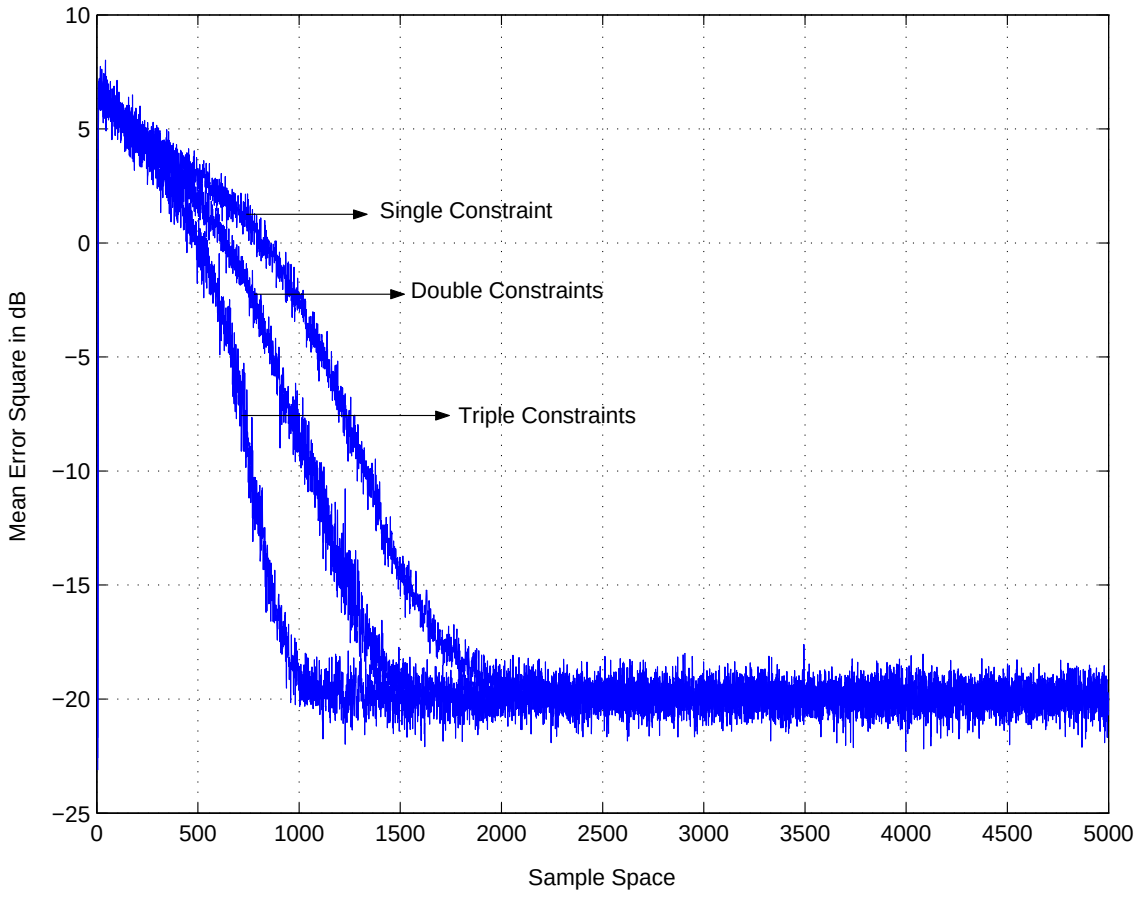

Figure 4.16: Comparison of the convergence rate for different constraints on complex channel-I as given in [1] using the MSE.

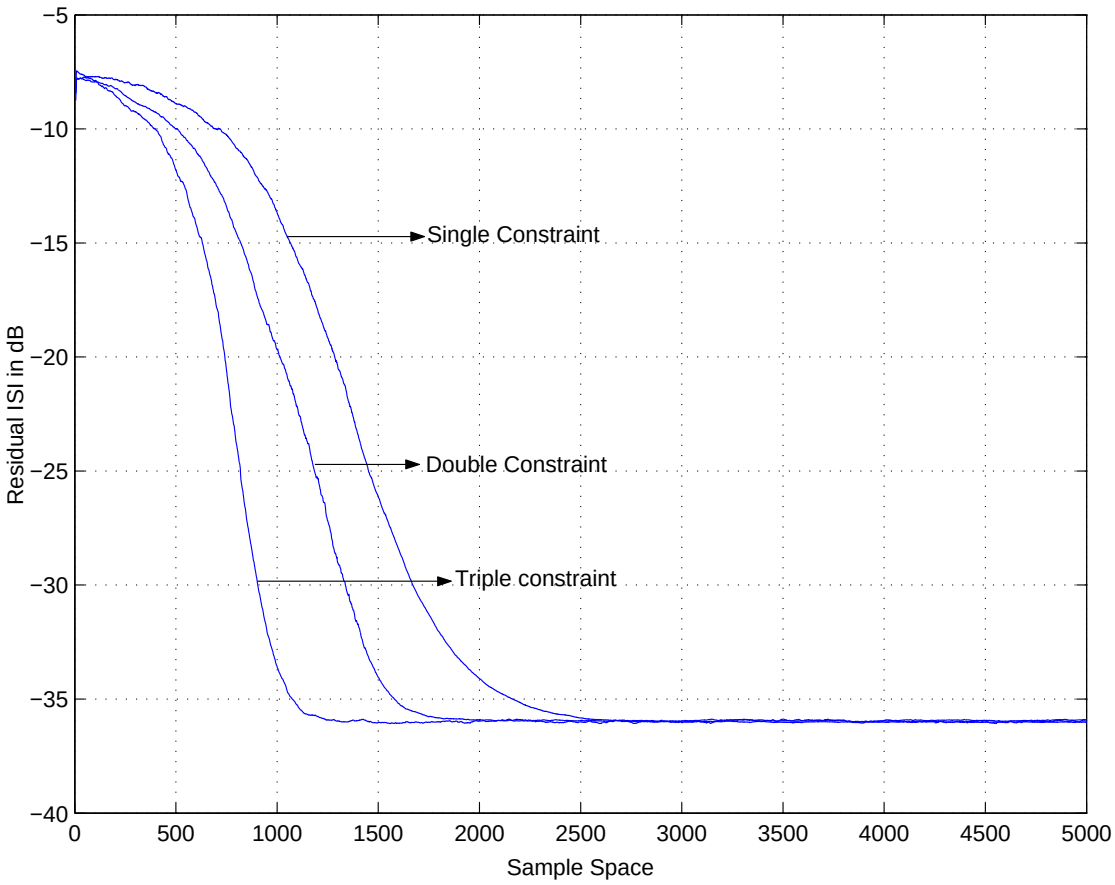

Figure 4.17: Comparison of the convergence rate for different constraints on complex channel-I as given in [1] using the Residual ISI.

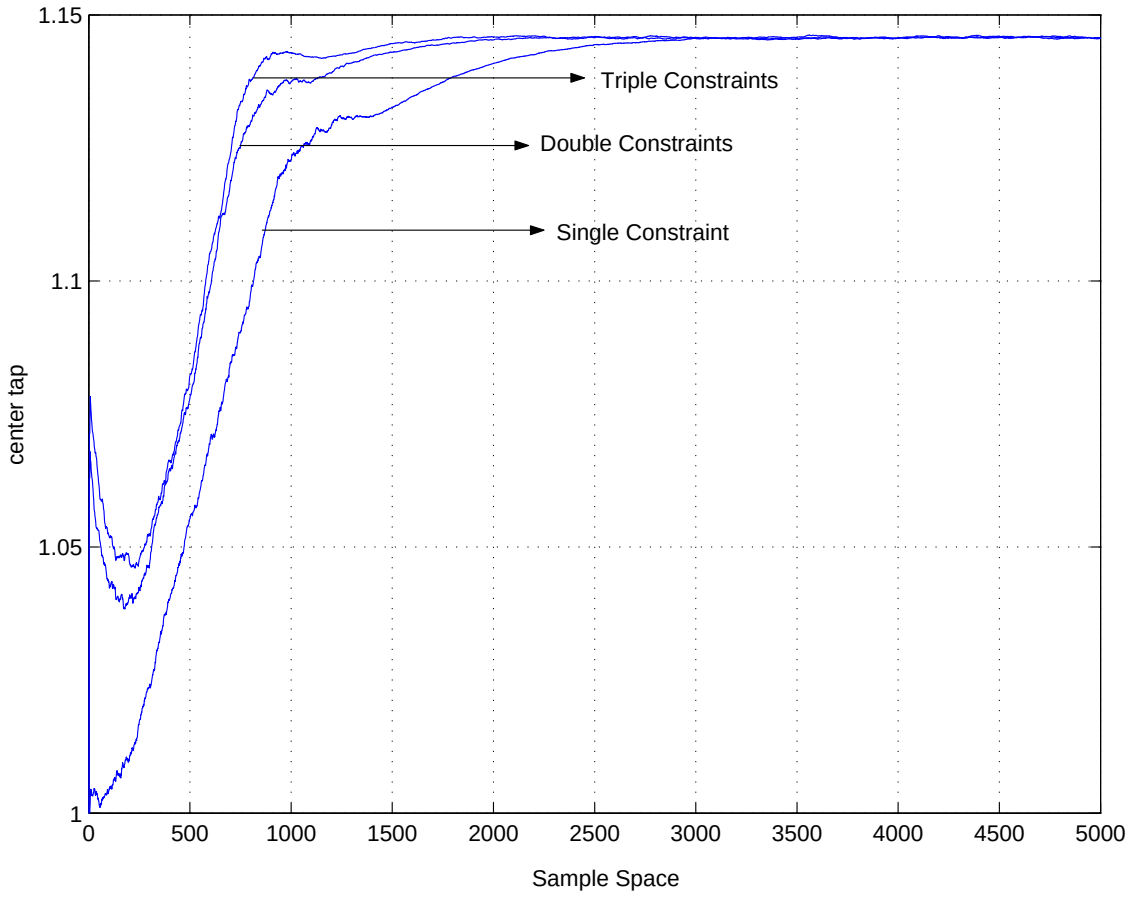

Figure 4.18: Comparison of the convergence rate for different constraints on complex channel-I as given in [1] using the absolute value of the center tap.

converged around 2500 symbols where as for double and triple constraints converged around 1700 and 1100 respectively which corroborates the fact as stated by Tanrikulu [11] that as the number of constraints increased according to the equation (3.9) the rate of convergence also increased.

4.3 Complex Channel-II

The impulse response of the channel-II is tabulated in Table 4.1 which is taken from paper by Chen [31]. A 25 tap equalizer is used instead of 9 because of the large number of channel taps.

It is found out by simulation that the mean square error converged approximately at -20 dB and the Residual-ISI around -32 dB. As can be seen from the Figures 4.25 and 4.26 the equalizer with single constraint converges at 9000 symbols whereas the equalizer with double and triple constraints converges at 6500 and 5000 symbols respectively. Thus it can be said that for severe channels it is more effective to increase the number of constraints in the cost function than to the less severe channels. The severity of the channel can be analyzed from constellation of the signal before equalization . From Figures 4.12 and 4.21 it can be concluded that the complex channel II is more severe than complex channel I. Since the center tap of the equalizer is assumed to be equal to 1, its behavior is also plotted in order to confirm the convergence rate (from Figure 4.27).

Table 4.1: Channel II Impulse Response

Tap No.	Real	Imaginary
0	0.0145	0.0006
1	0.0750	0.0176
2	0.3951	0.0033
3	0.7491	0.1718
4	0.1951	0.0972
5	-0.2856	0.1896
6	0.0575	0.2096
7	0.0655	0.1139
8	-0.0825	0.0424
9	0.0623	0.0085
10	-0.0438	0.0034
11	0.0294	0.0049
12	-0.0181	0.0032
13	0.0091	0.0003
14	-0.0038	0.0023
15	0.0019	0.0027
16	-0.0018	0.0014
17	0.0006	0.0003
18	0.0005	0.0000
19	-0.0008	0.0001
20	0.0000	0.0002
21	0.0001	0.0006

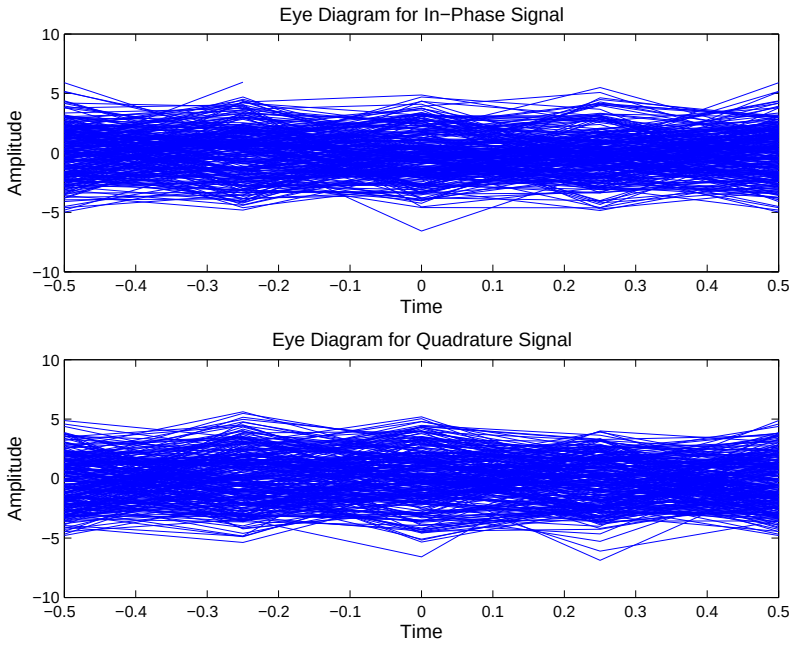

Figure 4.19: Eye diagram of 16-QAM signal before convergence when passed through complex channel-II as given in Table 4.1 (last 1000 samples).

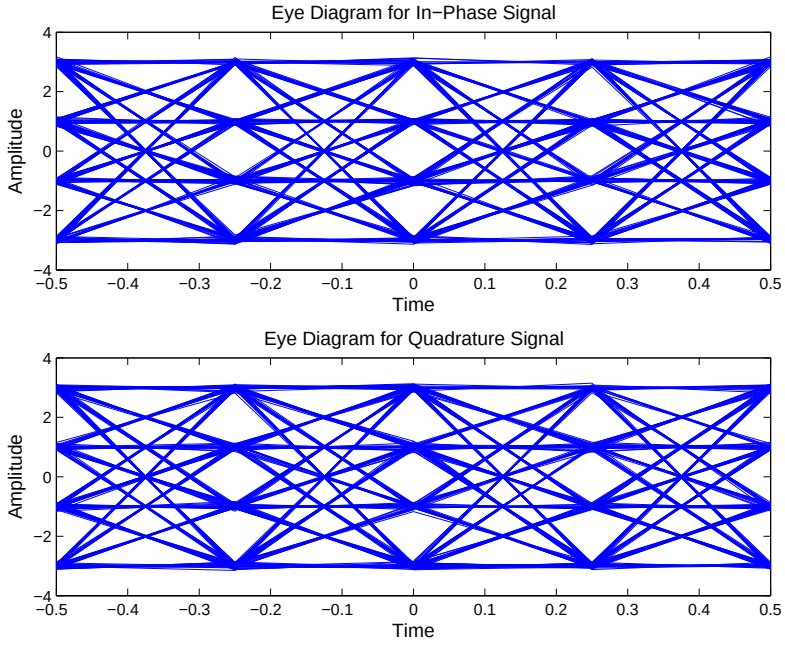

Figure 4.20: Eye diagram of 16-QAM signal after convergence when passed through complex channel-II as given in Table 4.1 (last 1000 samples).

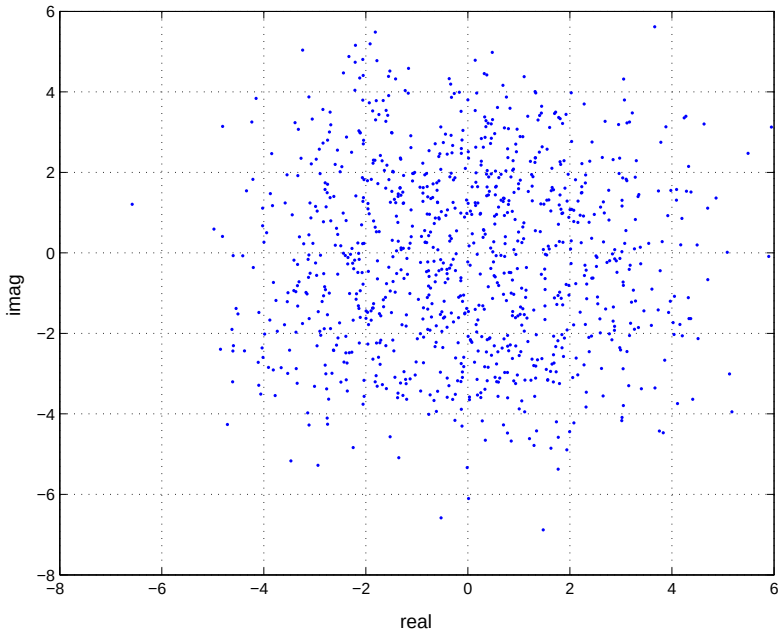

Figure 4.21: Constellation of 16-QAM signal before equalization when passed through complex channel-II as given in Table 4.1 (last 1000 samples).

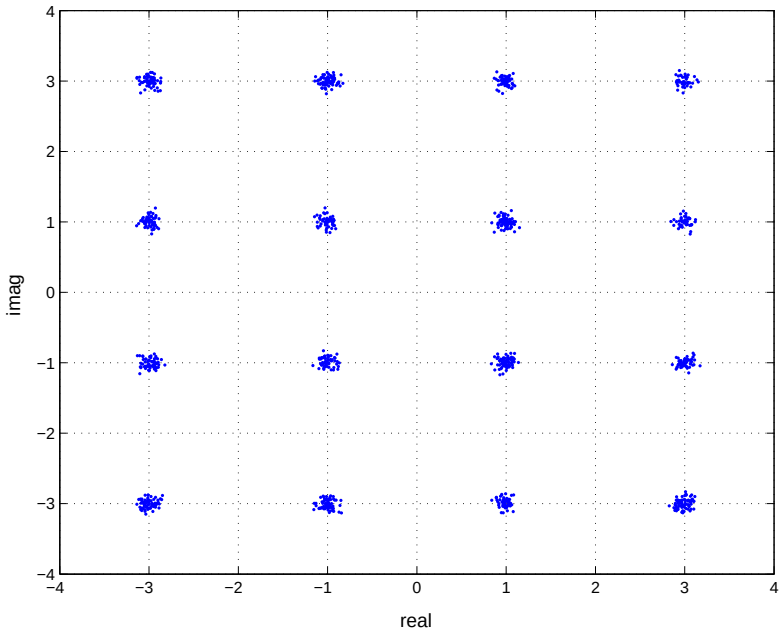

Figure 4.22: Constellation of 16-QAM signal after equalization when passed through complex channel-II as given in Table 4.1 (last 1000 samples) for single constraint.

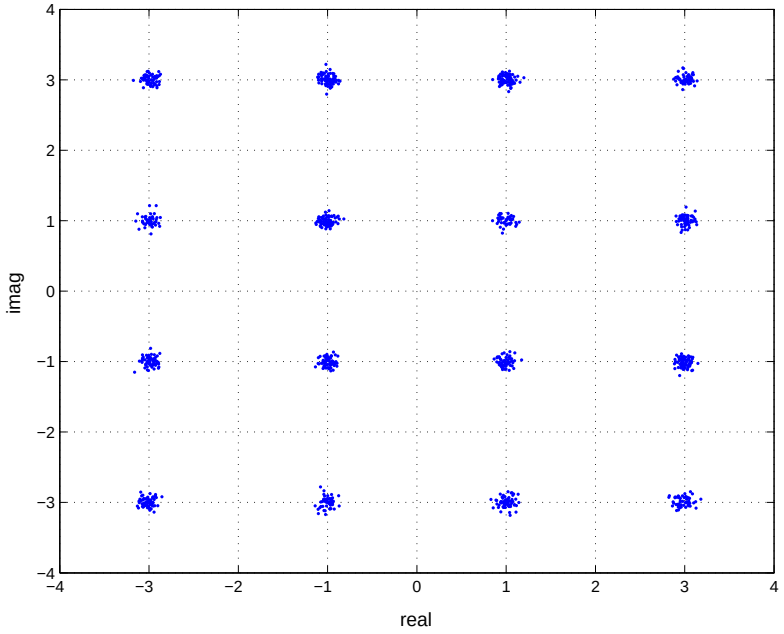

Figure 4.23: Constellation of 16-QAM signal after equalization when passed through complex channel-II as given in Table 4.1 (last 1000 samples) for double constraints.

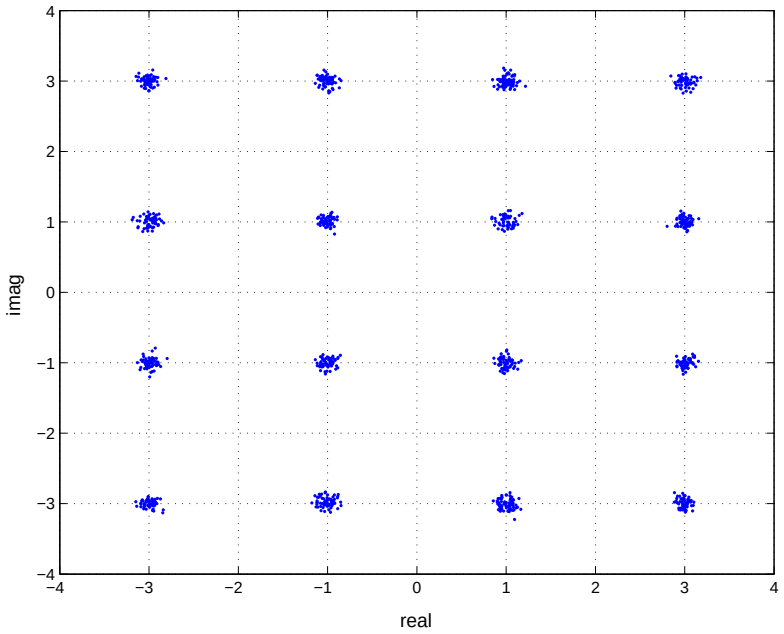

Figure 4.24: Constellation of 16-QAM signal after equalization when passed through complex channel-II as given in Table 4.1 (last 1000 samples) for triple constraints.

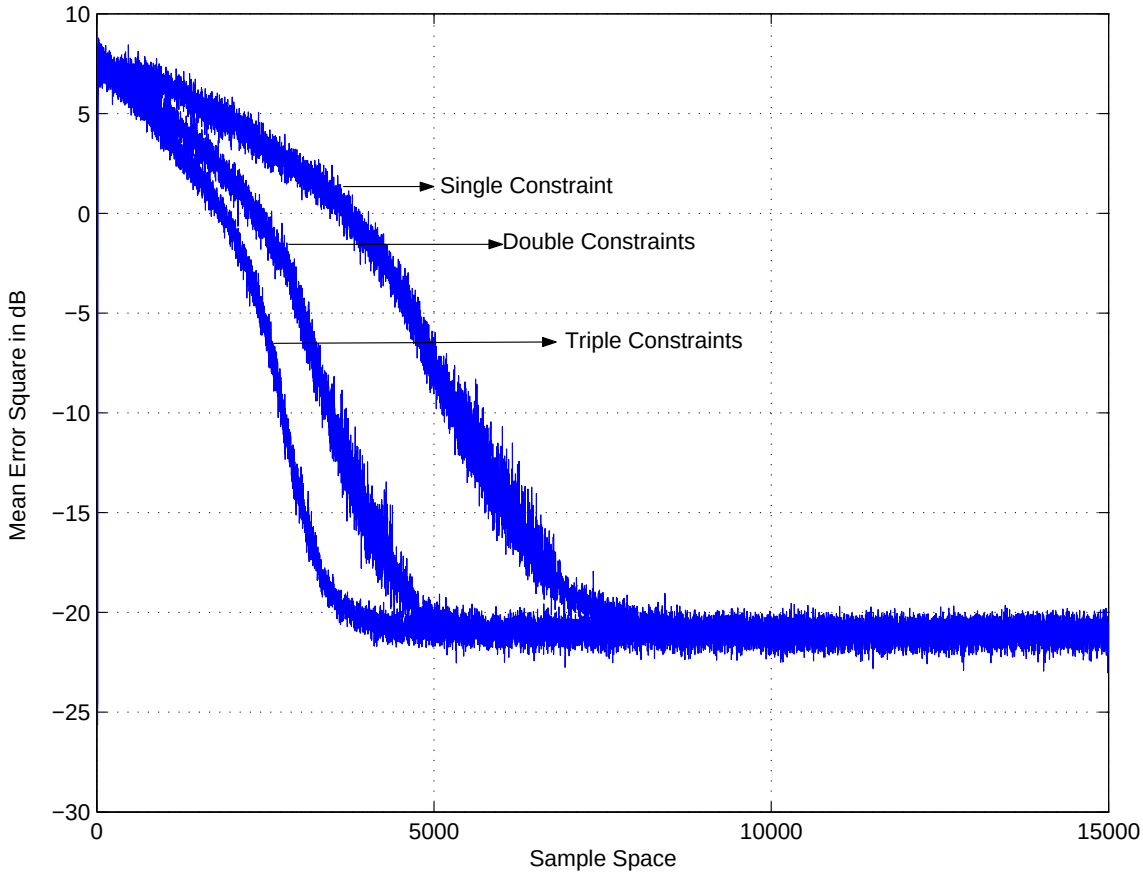

Figure 4.25: Comparison of the convergence rate for different constraints on complex channel-II as given in Table 4.1 using the MSE.

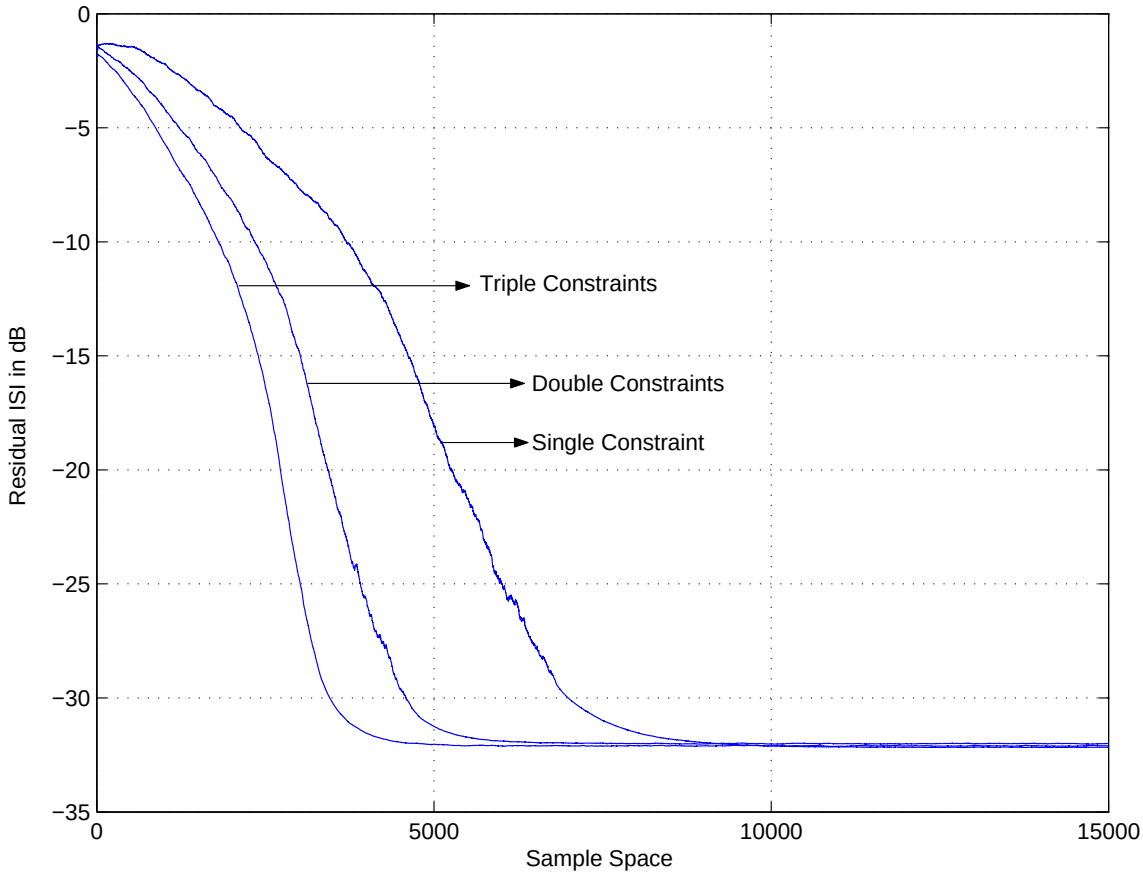

Figure 4.26: Comparison of the convergence rate for different constraints on complex channel-II as given in Table 4.1 using the Residual ISI.

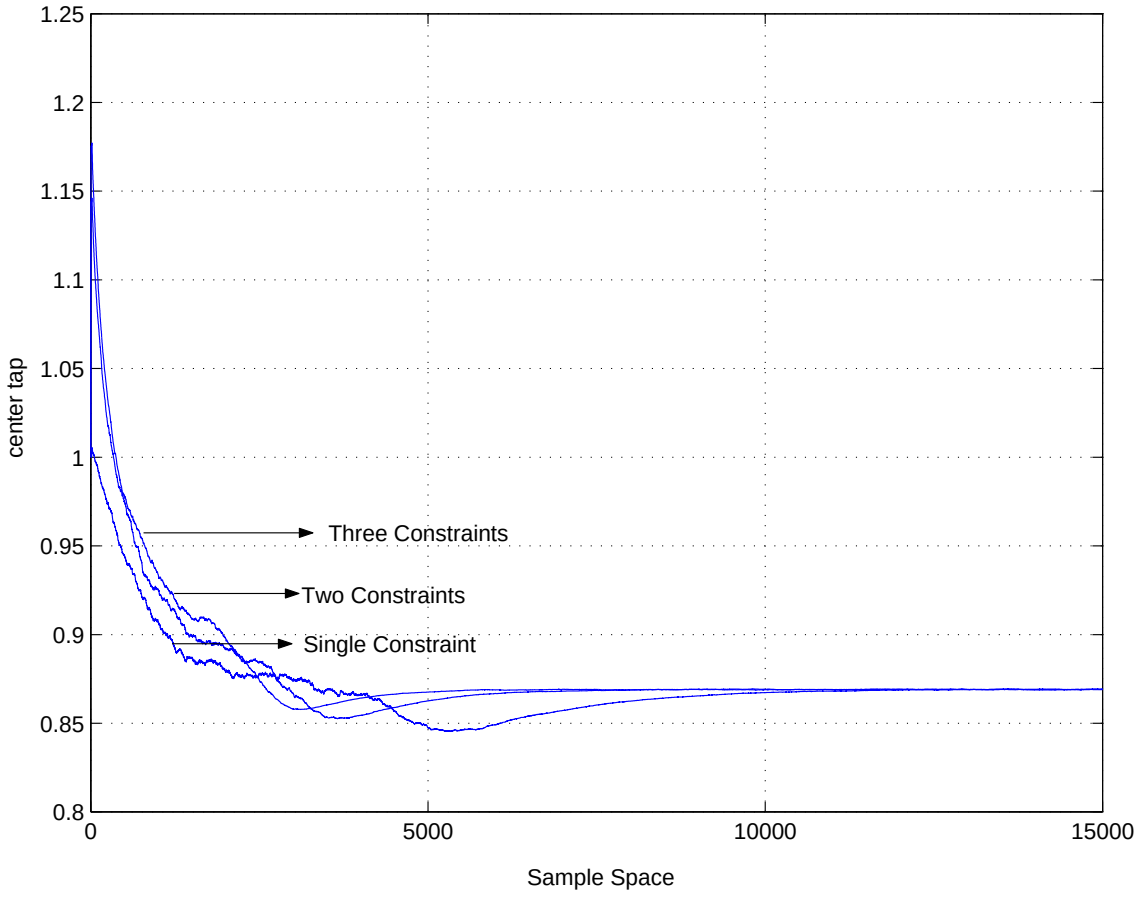

Figure 4.27: Comparison of the convergence rate for different constraints on complex channel-II as given in Table 4.1 using the center tap of the equalizer.

4.4 Simulation without the aid of decision directed mode

The following results are obtained after the decision directed algorithm is removed from the new scheme. Although the performance for increased number of constraints is almost constant, a slight improvement in the steady state error is observed. The algorithm for triple constraints converges for 3500 symbols with a steady state residual ISI of -25 dB and for the single constraint converges around 5000 symbols with a steady state residual ISI of -24.5 dB (from Figure 4.32). In the case of MSE the algorithm converges around -14 dB (as shown in the Figure 4.31). Hence it can be concluded from these results that applying multiple constraints for the newly derived scheme, in certain cases does not necessarily increases the convergence rate.

The dispersion constant used in this scenario for simulation is varied i.e , the dispersion constants as given by Sato [6], Godard [14] and Yang *et.al.* [32] are used. For the case of CMA, i.e., when $q = 2$ in equation (2.20) the dispersion constant for the Godard's algorithm equals to that of the Multi Modulus Algorithm (MMA) as given by Yang *et.al.* As can be seen from the Figures 4.28, 4.29, 4.49 and Figures 4.34, 4.35, 4.36 better results are obtained for the dispersion constant as given by Sato (from equation (2.10)). The above fact can also be corroborated by observing the MSE curves for both the situations (from Figures 4.31 and 4.37). Hence it can be said that the newly derived scheme bear the characteristics of reduced constel-

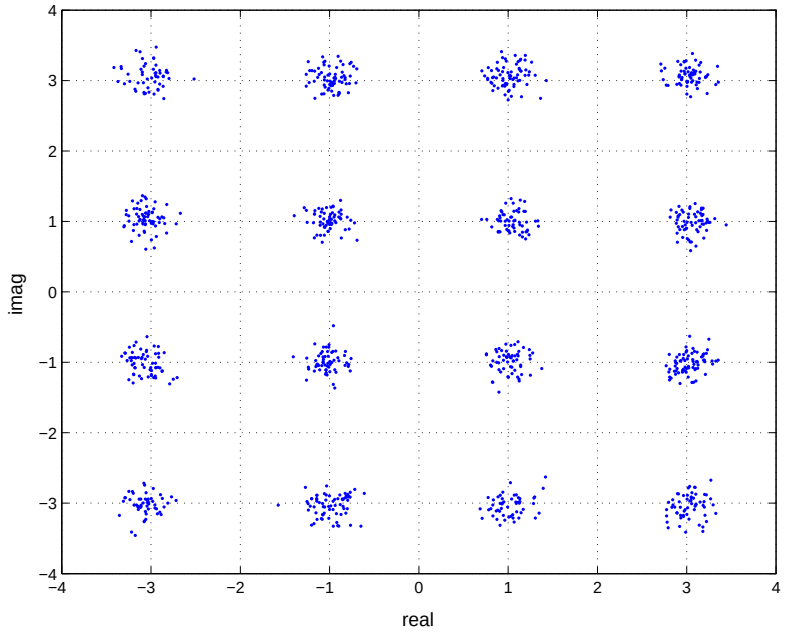

Figure 4.28: Constellation of 16-QAM signal after equalization when passed through complex channel-I (last 1000 samples) for single constraint without the aid of decision directed mode with dispersion constant as given by Sato (equation (2.10)).

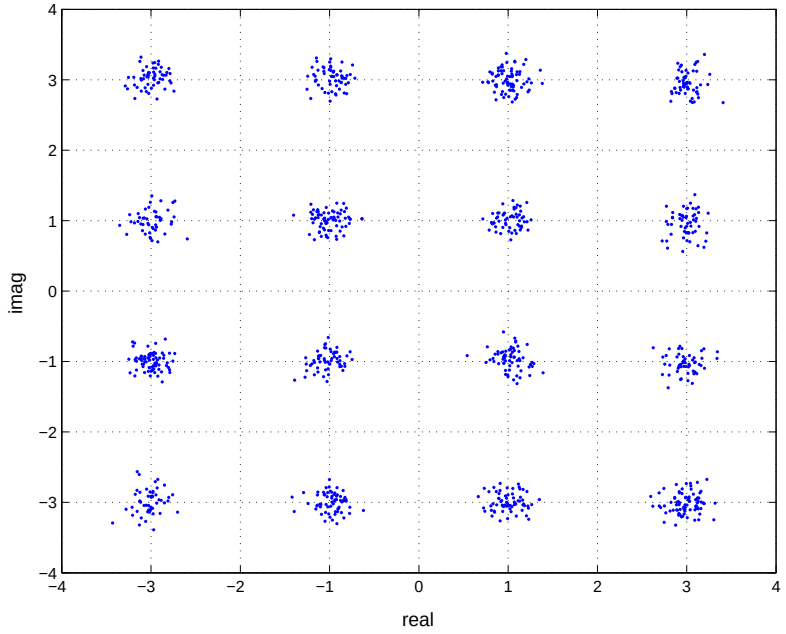

Figure 4.29: Constellation of 16-QAM signal after equalization when passed through complex channel-I (last 1000 samples) for double constraints without the aid of decision directed mode with dispersion constant as given by Sato (equation (2.10)).

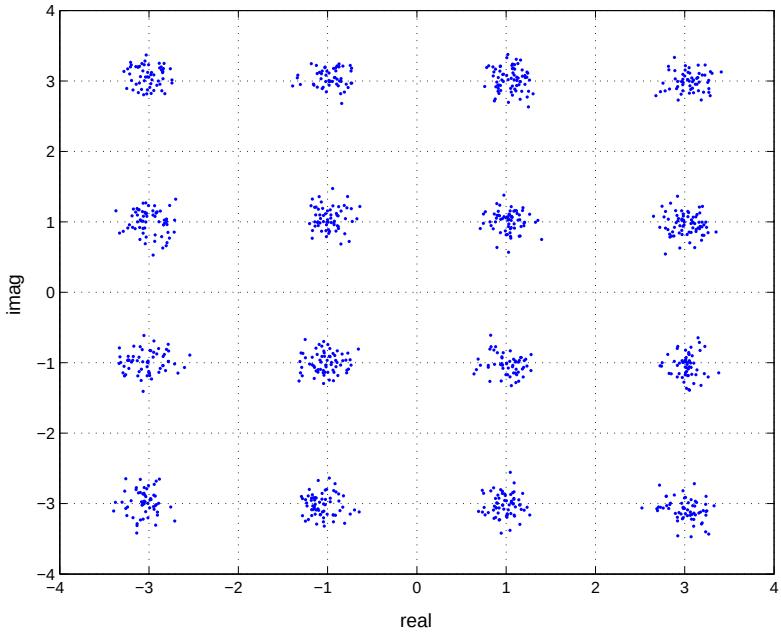

Figure 4.30: Constellation of 16-QAM signal after equalization when passed through complex channel-I (last 1000 samples) for triple constraints without the aid of decision directed mode with dispersion constant as given by Sato (equation (2.10)).

lation algorithm (RCA) [32] rather than the CMA. RCA uses the fixed dispersion constant as specified by Sato [6]. But according to Yang *et.al.*, performance wise, CMA and multi-modulus algorithm (MMA) are better than RCA. Hence the newly proposed scheme without the aid of the decision directed mode performs poorly when compared to its peers like the MCMA which has its traits in CMA. The above statement can be proved by observing the MSE curves for the newly derived scheme without the aid of the decision directed mode (Figure 4.31) and MCMA (Figure 2.24). Since the center tap of the equalizer is assumed to be equal to 1, its behavior is also plotted inorder to confirm the convergence rate (from Figure 4.33 and Figure 4.39).

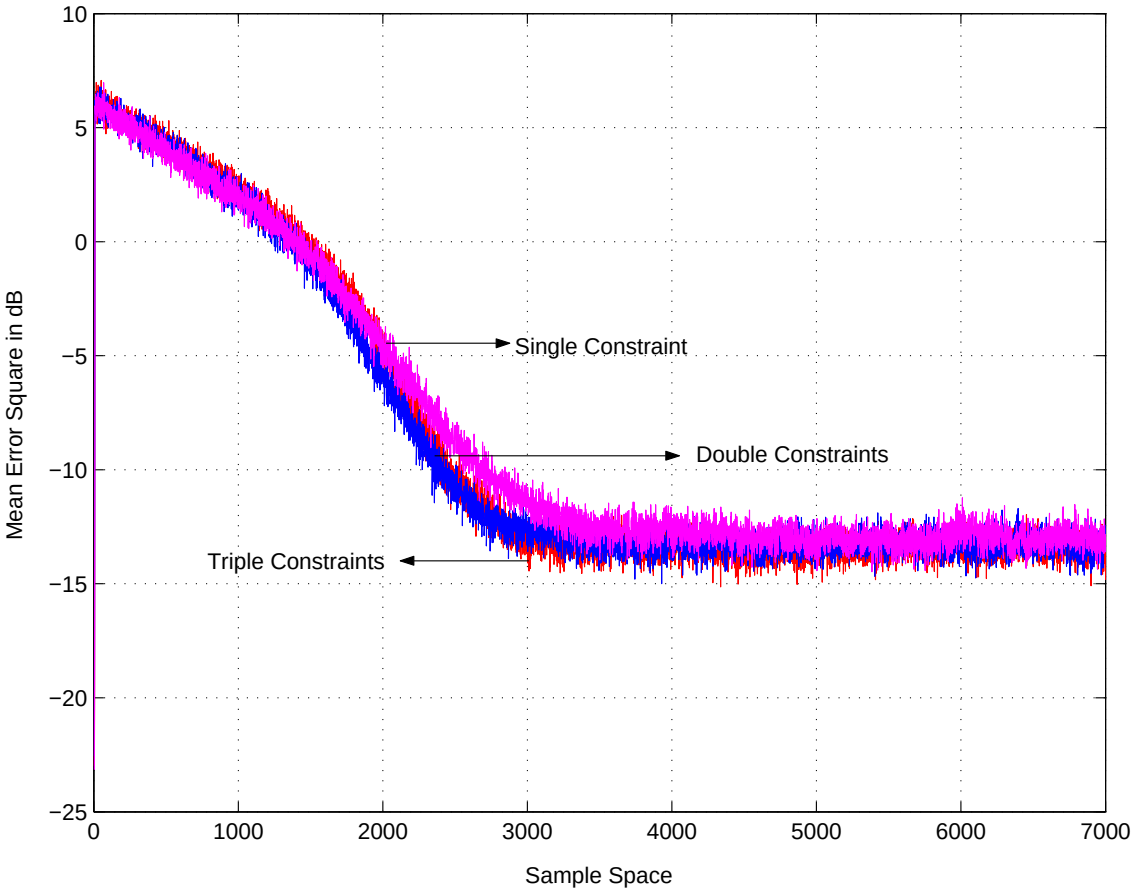

Figure 4.31: Comparison of the convergence rate for different constraints on complex channel-I as given in Figures 4.8 and 4.9 without DD mode with dispersion constant as given by Sato (equation (2.10)) using the MSE .

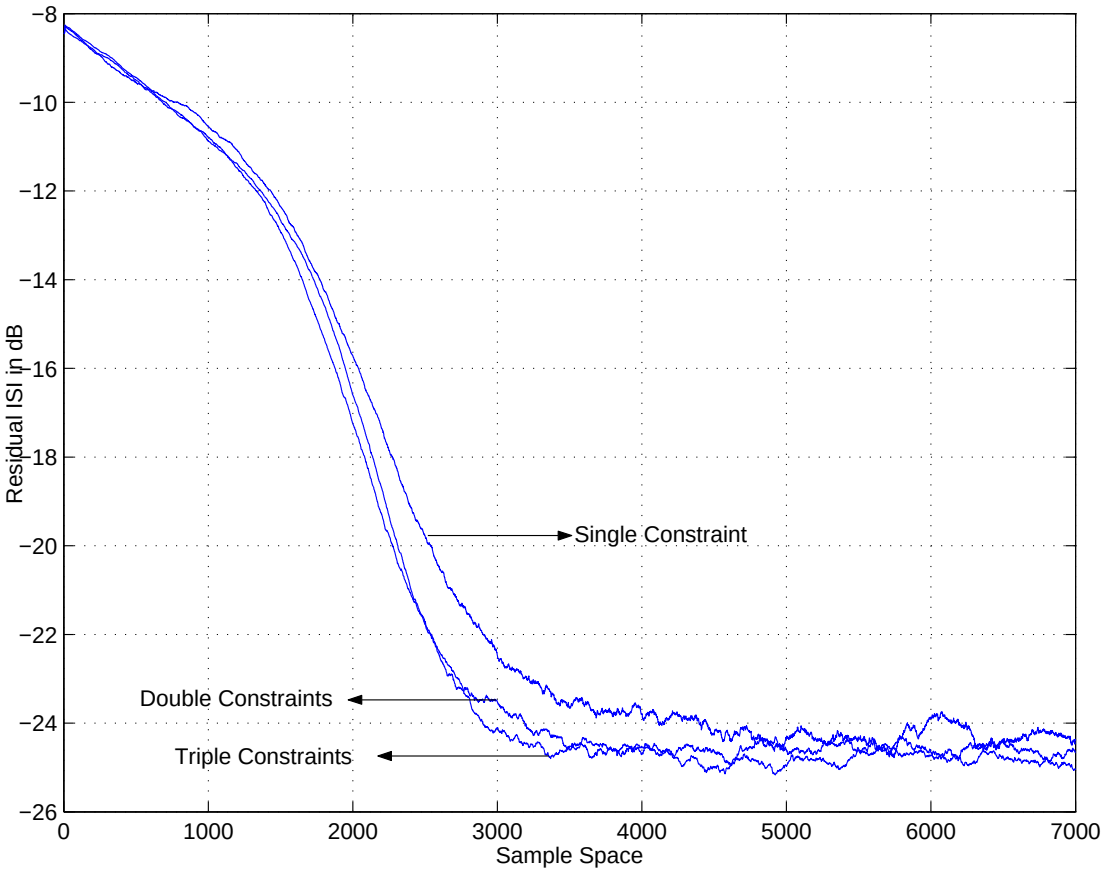

Figure 4.32: Comparison of the convergence rate for different constraints on complex channel-I as given in Figures 4.8 and 4.9 without DD mode with dispersion constant as given by Sato (equation (2.10)) using the Residual ISI .

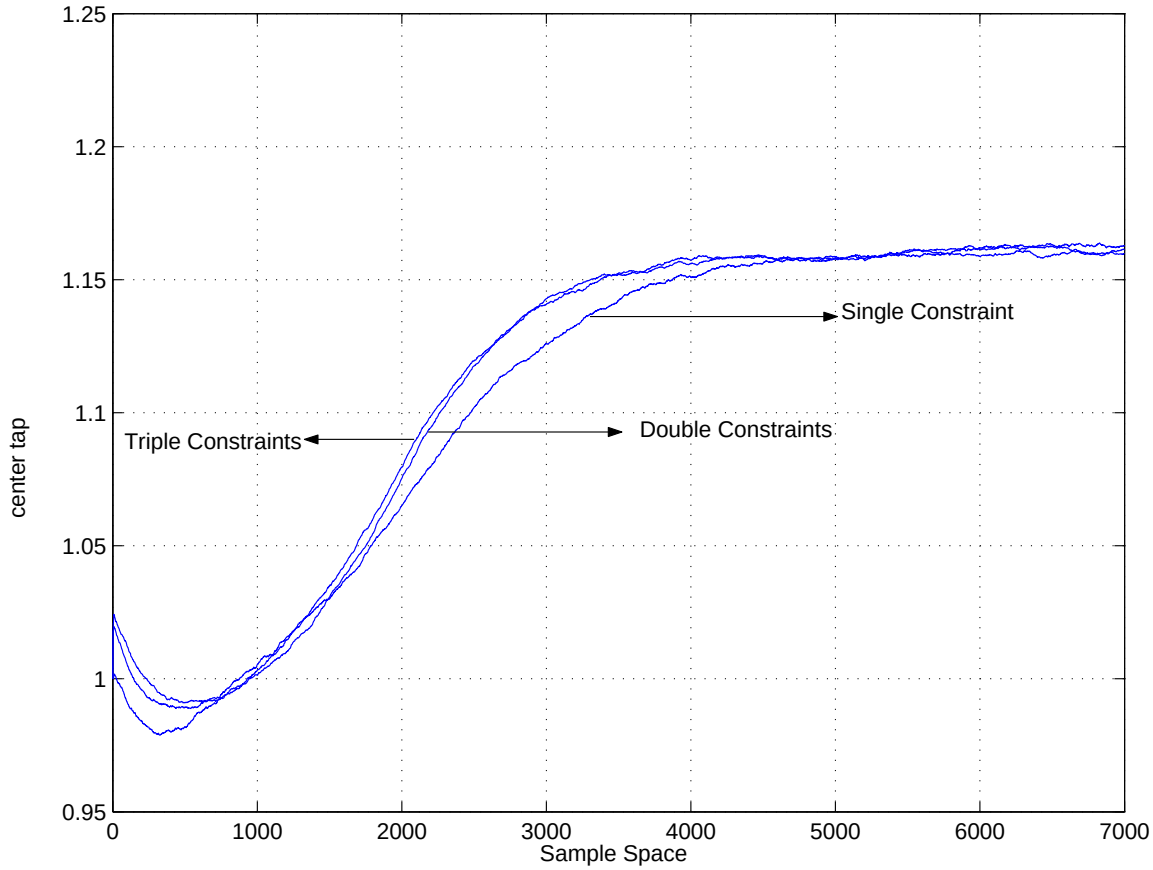

Figure 4.33: Comparison of the convergence rate for different constraints on complex channel-I as given in Figures 4.8 and 4.9 using the center tap of the equalizer without DD mode with dispersion constant as given by Sato (equation (2.10)).

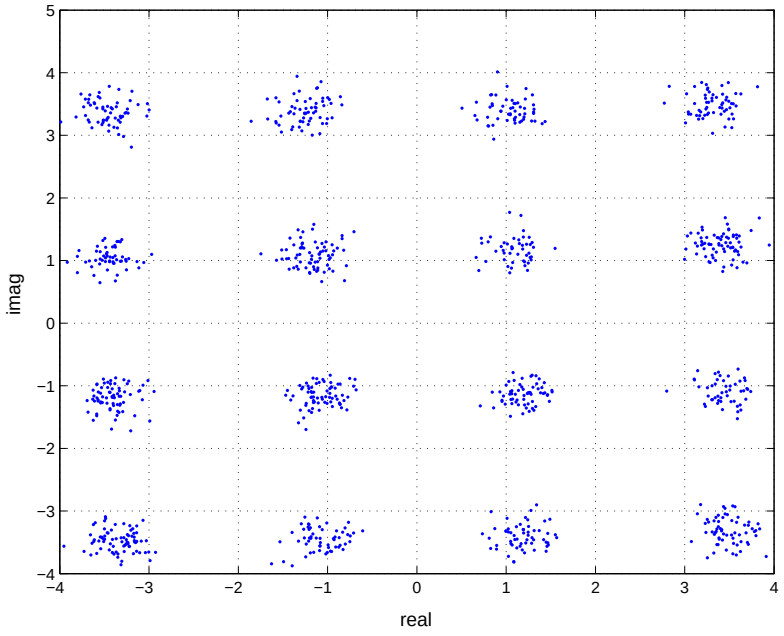

Figure 4.34: Constellation of 16-QAM signal after equalization when passed through complex channel-I (last 1000 samples) for single constraint without the aid of decision directed mode with dispersion constant as given by Godard (equation (2.20)).

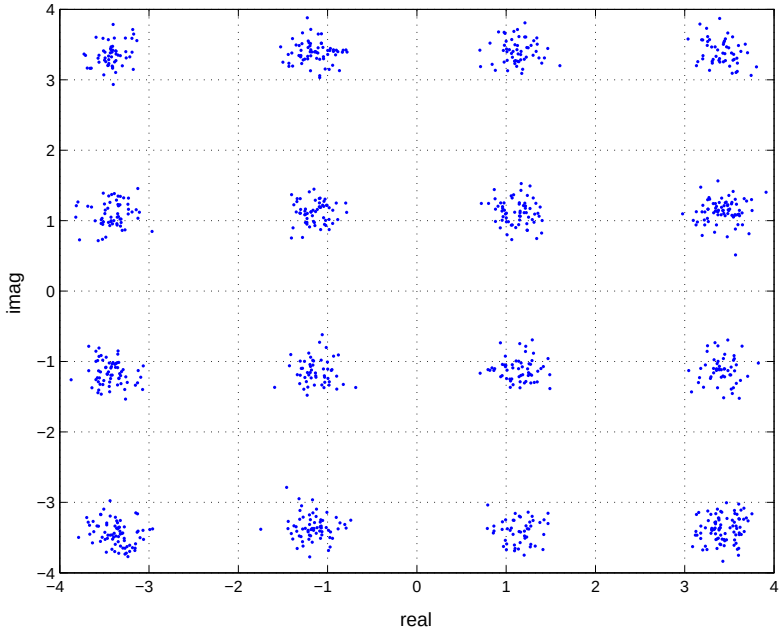

Figure 4.35: Constellation of 16-QAM signal after equalization when passed through complex channel-I (last 1000 samples) for double constraints without the aid of decision directed mode with dispersion constant as given by Godard (equation (2.20)).

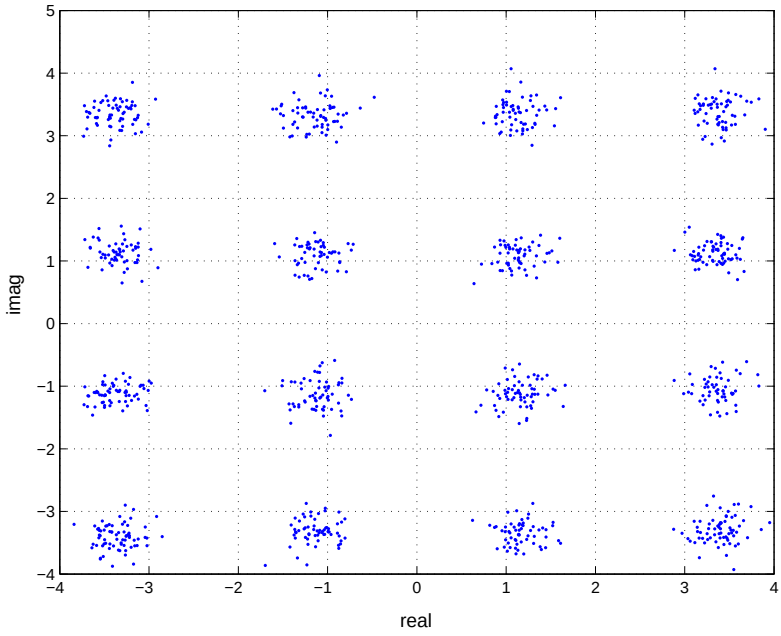

Figure 4.36: Constellation of 16-QAM signal after equalization when passed through complex channel-I (last 1000 samples) for triple constraints without the aid of decision directed mode with dispersion constant as given by Godard (equation (2.20)).

When the dispersion constant is varied and the DD mode is used, it is observed that the results remained the same. Hence it can be concluded that RCA exhibits a smooth shift from the blind mode to the decision directed mode and if a decision directed mode is used, variation in the dispersion constant as specified by Sato [6] or Godard[14] or Yang *et.al* [32] does not have any impact on the equalizer output.

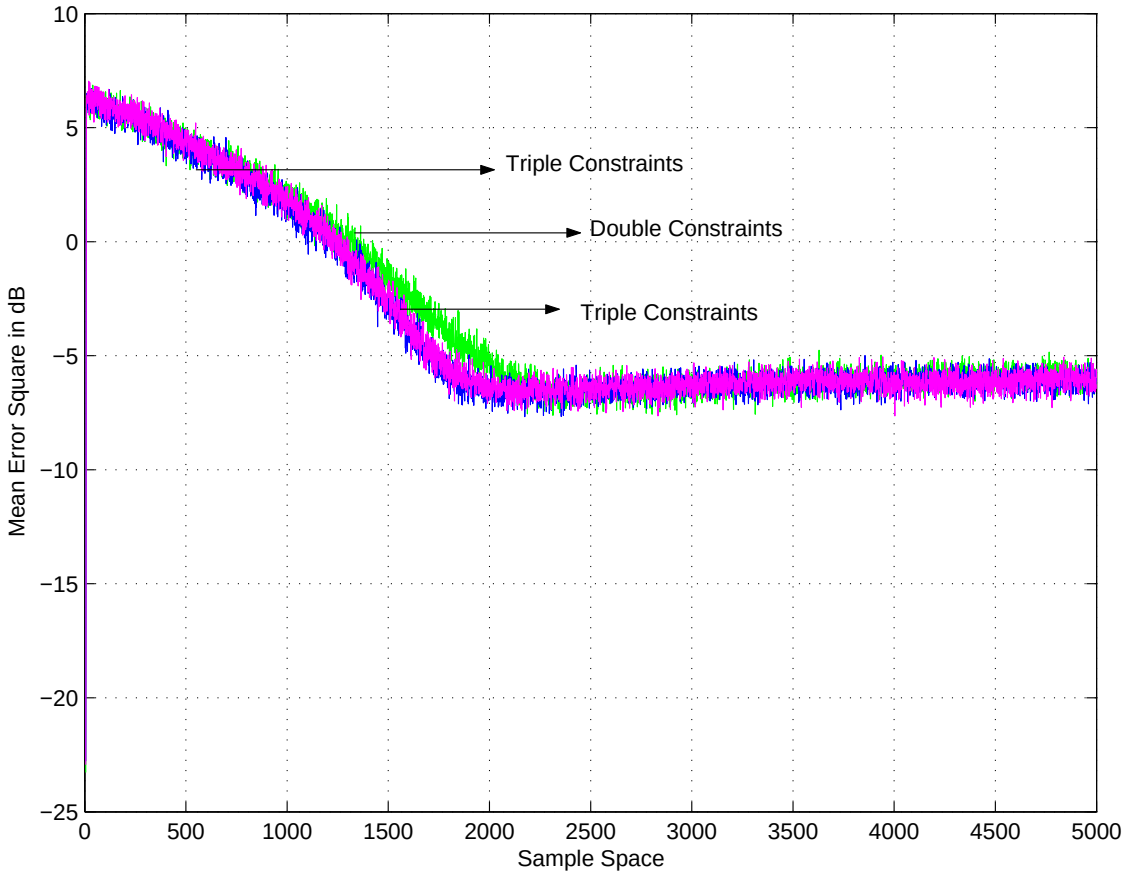

Figure 4.37: Comparison of the convergence rate for different constraints on complex channel-I as given in Figures 4.8 and 4.9 without DD mode with the dispersion constant as given by Godard (equation (2.20)) using the MSE.

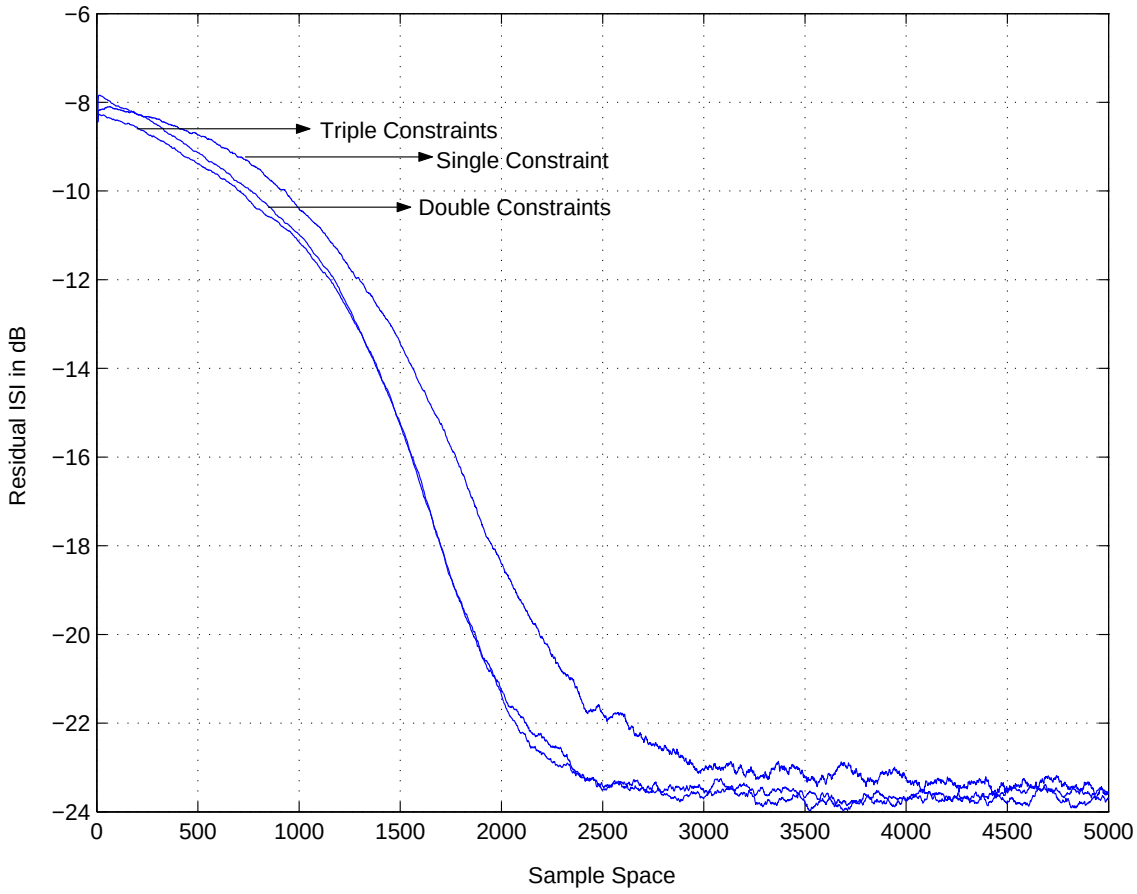

Figure 4.38: Comparison of the convergence rate for different constraints on complex channel-I as given in Figures 4.8 and 4.9 without DD mode with the dispersion constant as given by Godard (equation (2.20)) using the Residual ISI .

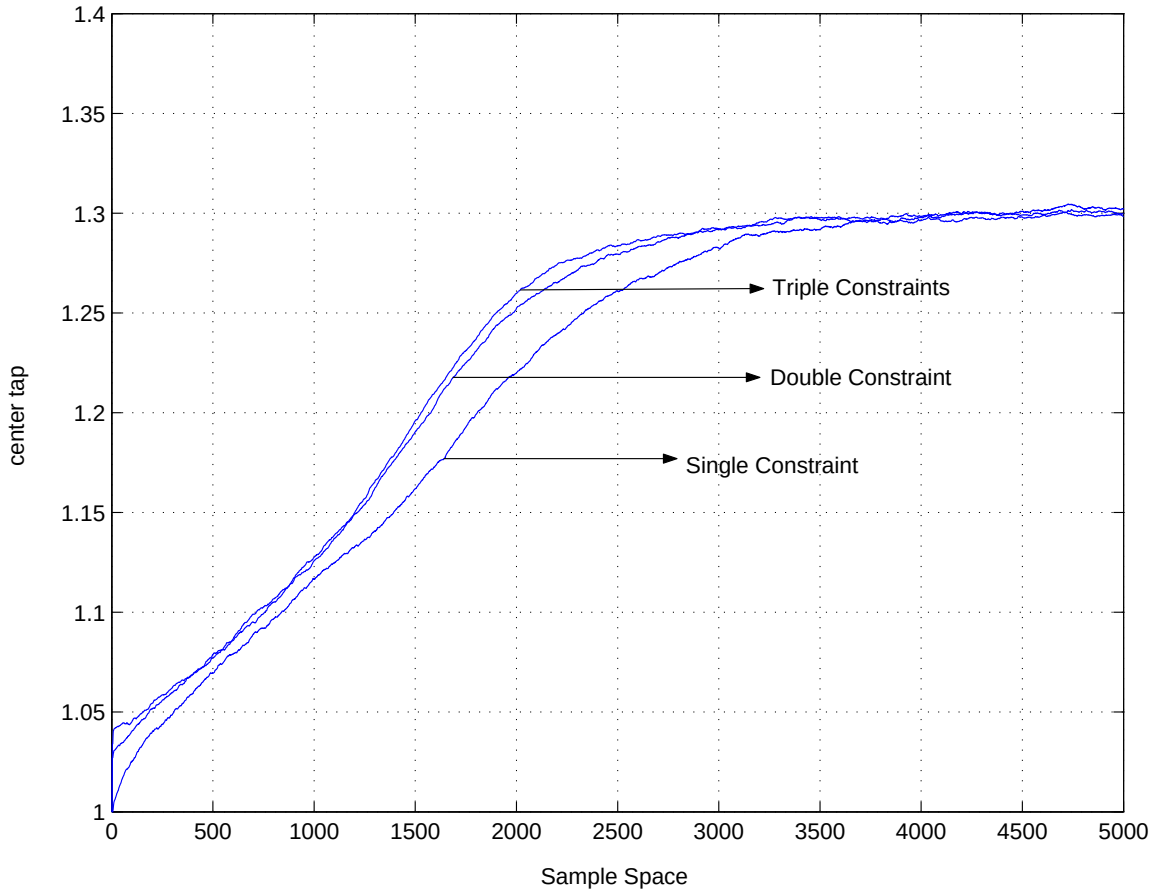

Figure 4.39: Comparison of the convergence rate for different constraints on complex channel-I as given in Figures 4.8 and 4.9 without DD mode with the dispersion constant as given by Godard (equation (2.20)) using the center tap of the equalizer.

4.5 Simulation at a SNR = 20dB

The following results are obtained after the SNR of the signal is reduced from 30 dB to 20 dB for a channel depicted in Figures 4.9 and 4.8. It is observed that the algorithm behaved in the same manner as in the previous scenarios excepting that the error floor is raised above. The MSE is observed to converge at a steady state value of -11 dB as shown in the Figure 4.43 and the ISI is observed to converge at a steady state value of -31 dB as shown in the Figure 4.44. The algorithm for single constraint is observed to converge at 2300 symbols where as for double and triple constraints converge below 1500 symbols. The constellation diagrams of the signals after equalization for single, double and triple constraints are also plotted in Figures 4.40, 4.41 and 4.42. Since the center tap of the equalizer is assumed to be equal to 1, its behavior is also plotted inorder to confirm the convergence rate in Figure 4.45

4.6 Simulation when the signal is affected by phase offset

In order to introduce a phase offset in the signal, the signal is multiplied by an exponential term as given in the equation below

$$x(k) = \sum_{i=0}^{L-1} h(k)a(k-i)e^{j\phi(k)} + \omega(k) \tag{4.1}$$

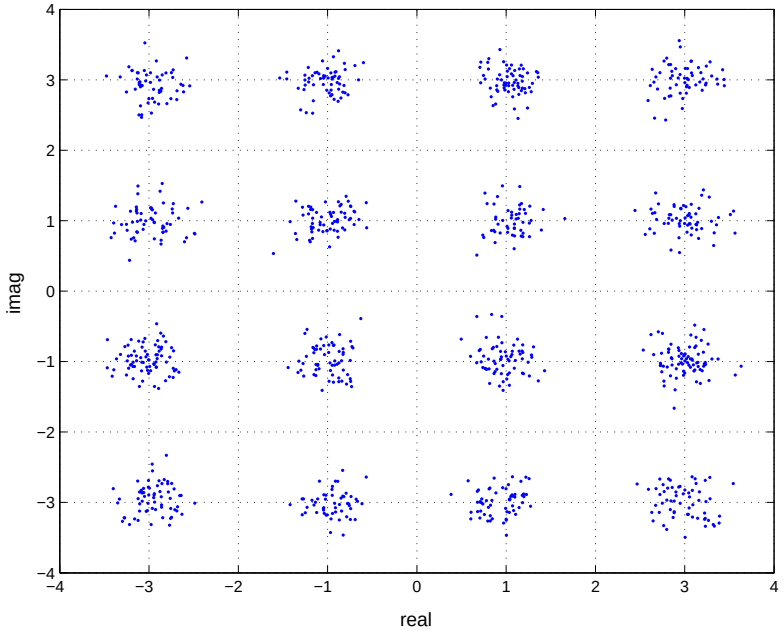

Figure 4.40: Constellation of 16-QAM signal after equalization when passed through complex channel-I (last 1000 samples) for single constraint when SNR = 20dB.

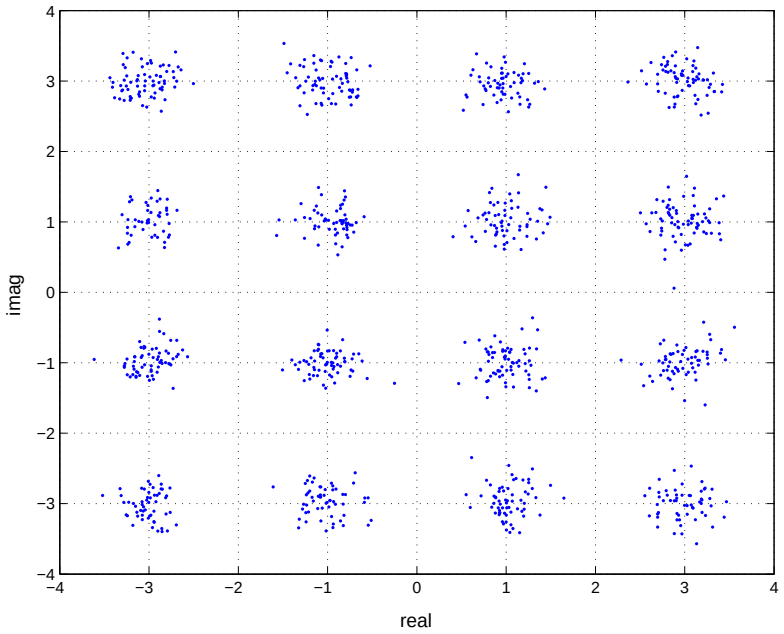

Figure 4.41: Constellation of 16-QAM signal after equalization when passed through complex channel-I (last 1000 samples) for double constraints when SNR = 20dB.

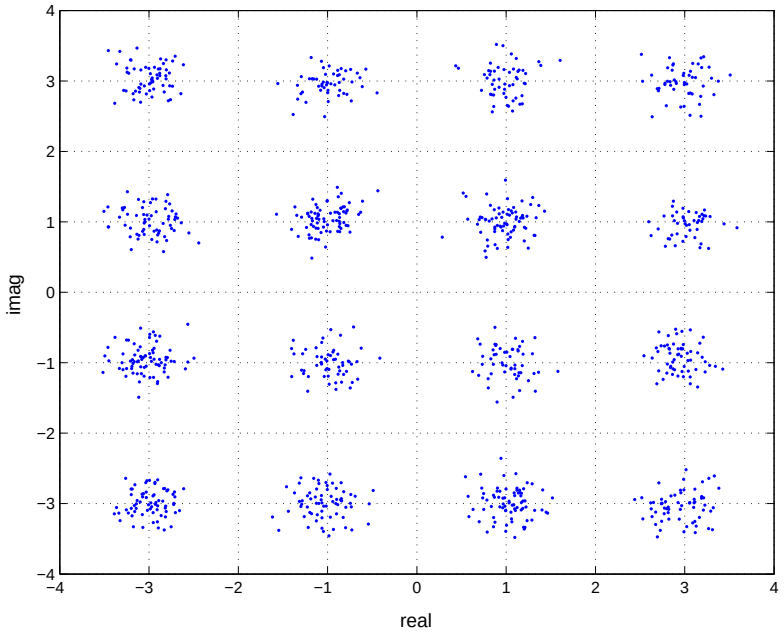

Figure 4.42: Constellation of 16-QAM signal after equalization when passed through complex channel-I (last 1000 samples) for triple constraints when SNR = 20dB.

where $h(i), i = 0, 1, \ldots L-1$ are the complex channel tap weights, L is the length of the channel response, $a(k)$ are the complex data symbols, k is the time index, $e^{j\phi(k)}$ is caused by a carrier phase error given by $\phi(k) = 2\pi\Delta f/R$ where R is the dispersion constant used and Δf in the frequency shift. The value of $\Delta f/R$ is chosen to be equal to 10^{-5}.

The simulation is done using a complex channel I [1]. The phase offset caused by the channel can be clearly observed by comparing the Figures 4.12 and 4.46. The algorithm converges with single constraint on 2700 symbols, with double constraints on 2300 and symbols with triple constraints on 1700. Also the constellation diagrams of the signals after the convergence are plotted in Figures 4.47, 4.48 and 4.47. In

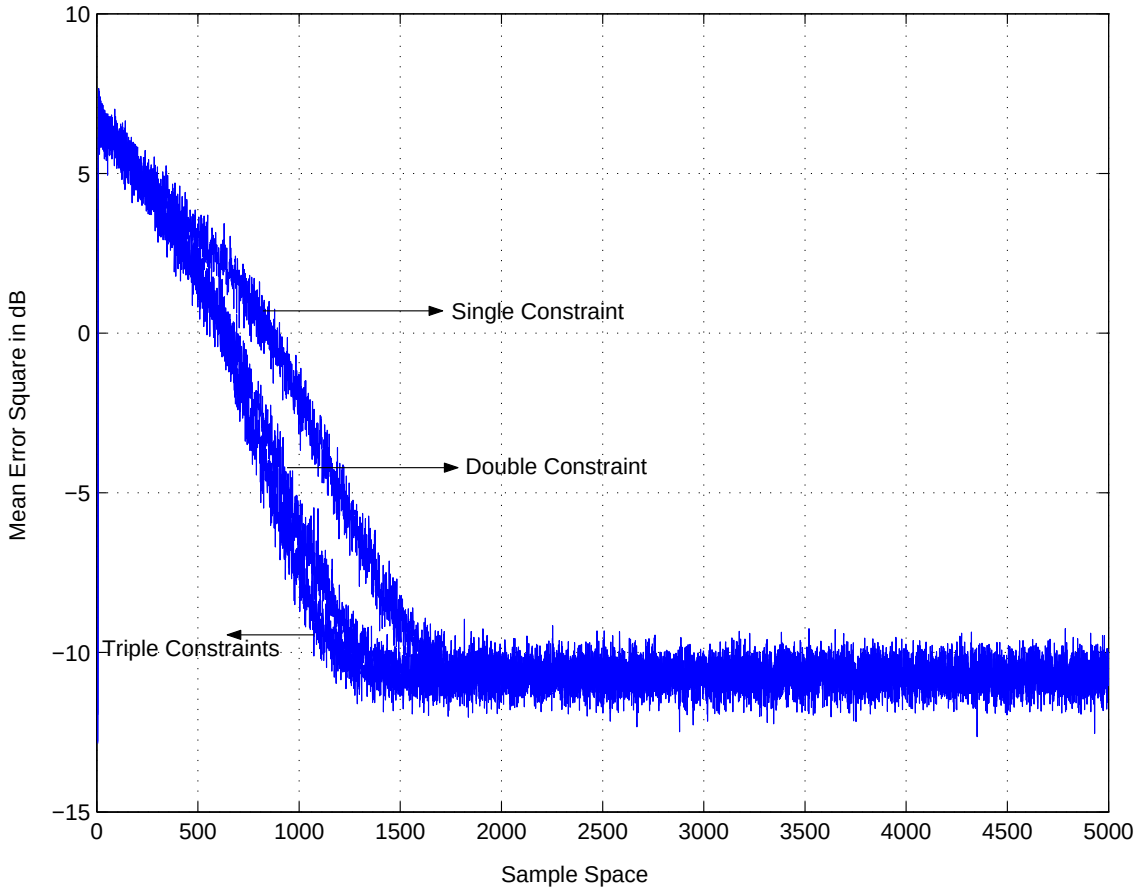

Figure 4.43: Comparison of the convergence rate for different constraints on complex channel-I as given in Figures 4.8 and 4.9 using the MSE with $SNR = 20$dB.

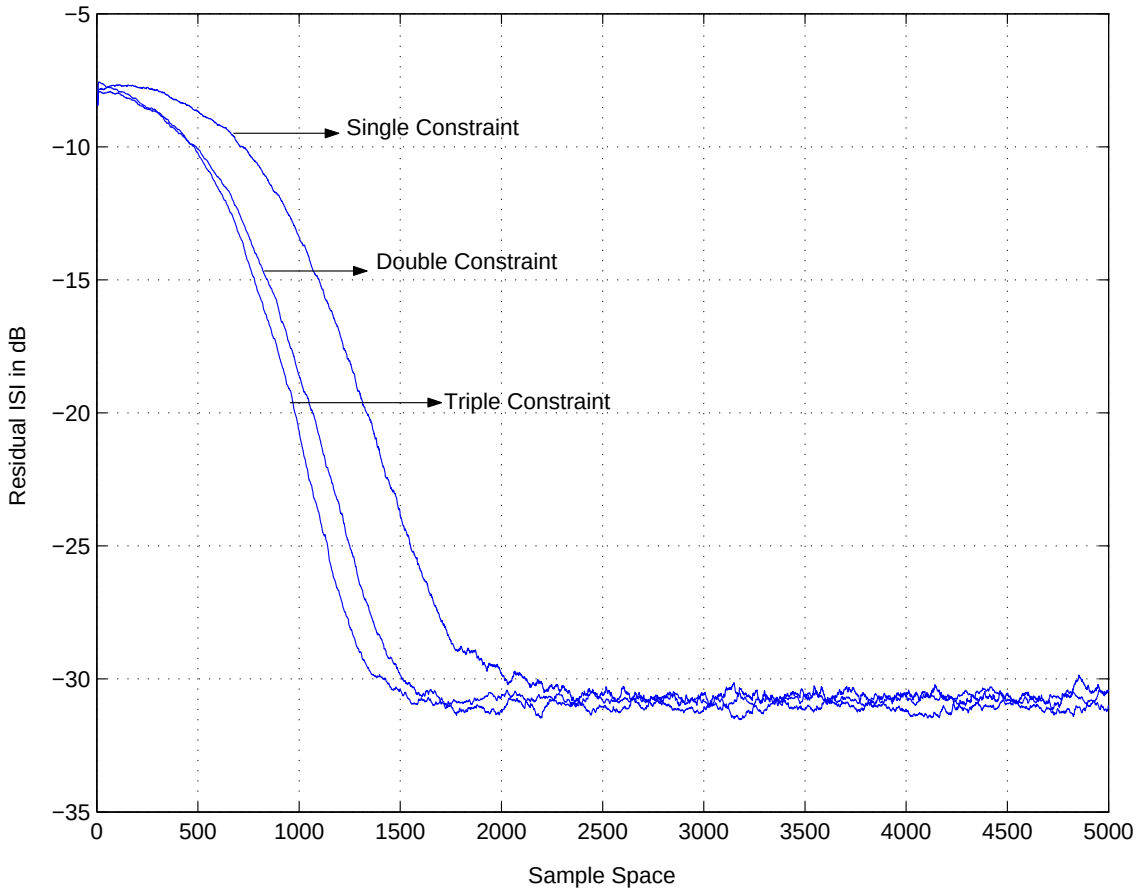

Figure 4.44: Comparison of the convergence rate for different constraints on complex channel-I as given in Figures 4.8 and 4.9 using the Residual ISI with $SNR = 20$dB.

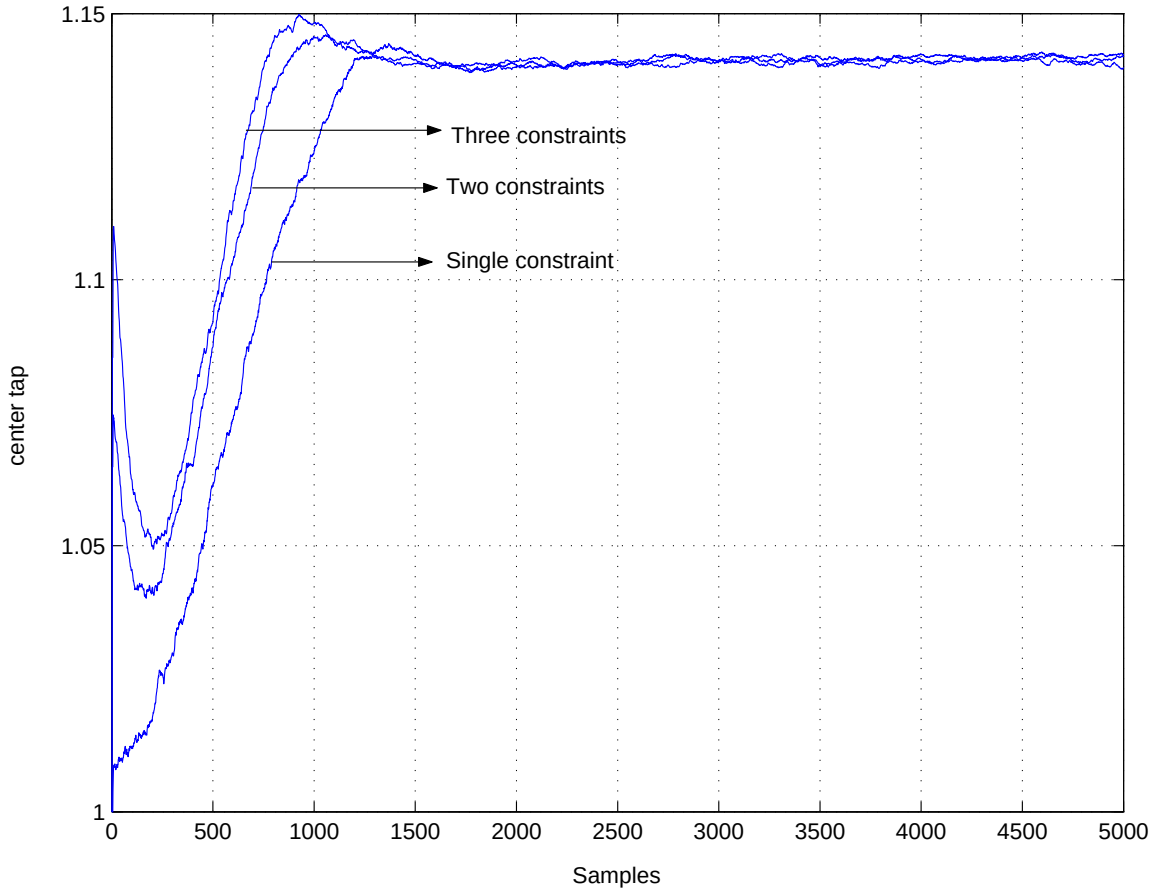

Figure 4.45: Comparison of the convergence rate for different constraints on complex channel-I as given in Figures 4.8 and 4.9 using the center tap of the equalizer with $SNR = 20$dB.

order to confirm the convergence rate the residual ISI and the center tap behavior is also plotted as shown in the Figure 4.52. Hence it can be concluded that the newly derived scheme can handle small phase offsets introduced in the channel apart from small phase jitters.

4.7 Summary

The main aim of this chapter is to illustrate the point that as the number of constraints in the newly derived scheme are increased the faster convergence rate is observed using simulations. The new scheme is tested on three different channels. In case of real channel the convergence rate remained constant no matter how many constraints are increased. In the other two complex channels a mark difference is observed in the convergence rates. Simulations are also done for signals with low signal to noise ratio , the equalizer without the aid of the decision directed mode and for signals infected by phase offsets. All of them corroborated that any increment in the number of constraints caused the convergence rate to improve

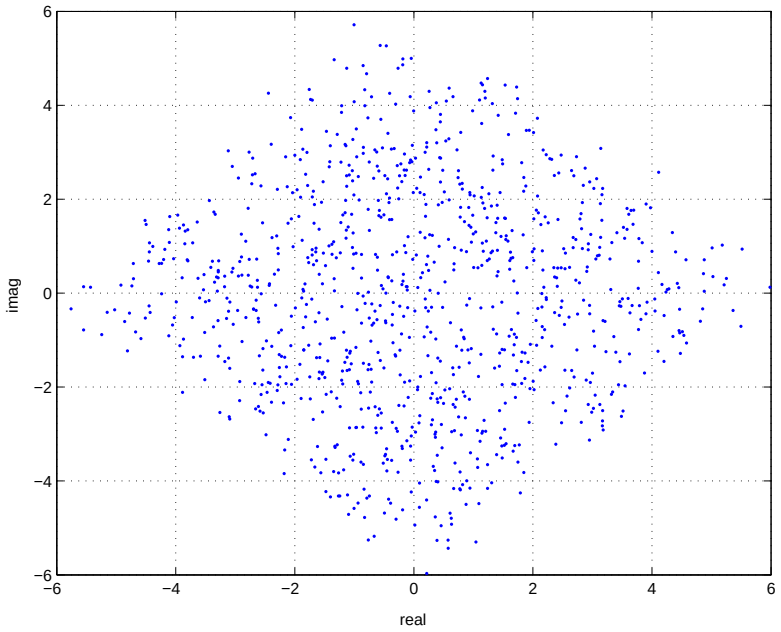

Figure 4.46: Constellation of 16-QAM signal before equalization when passed through complex channel-I (last 1000 samples) affected by phase offset .

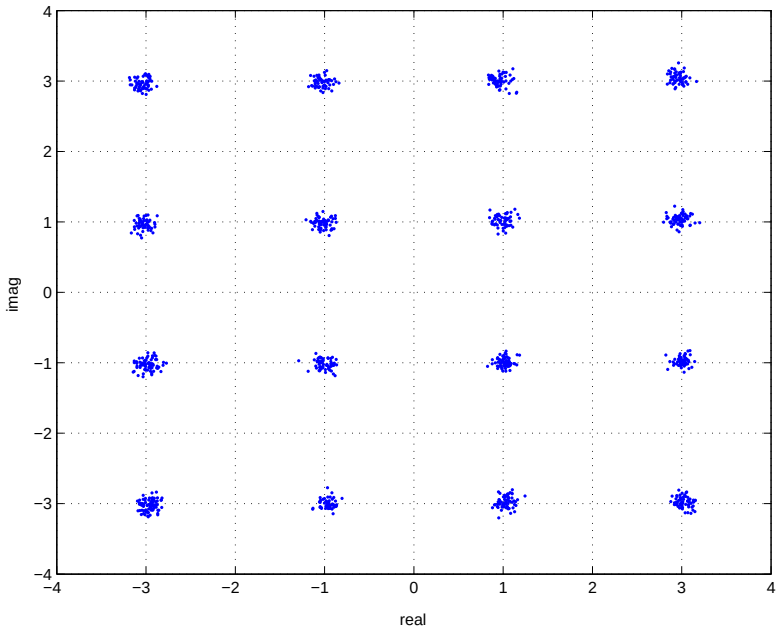

Figure 4.47: Constellation of 16-QAM signal after equalization when passed through complex channel-I (last 1000 samples) affected by phase offset for a single constraint.

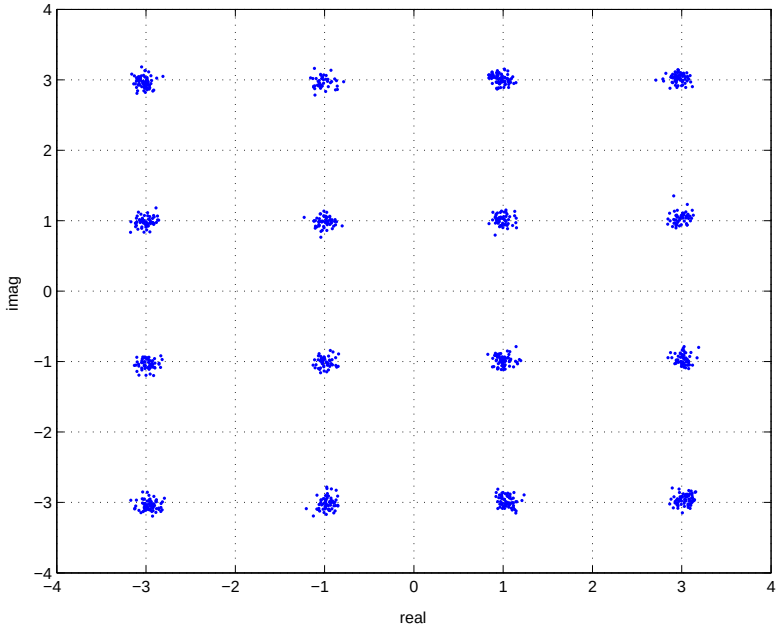

Figure 4.48: Constellation of 16-QAM signal after equalization when passed through complex channel-I (last 1000 samples) affected by phase offset for double constraints.

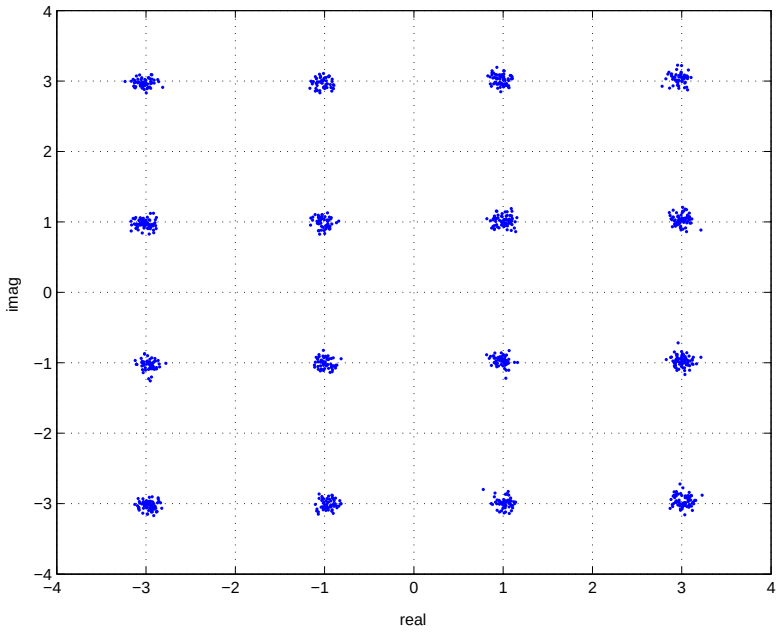

Figure 4.49: Constellation of 16-QAM signal after equalization when passed through complex channel-I (last 1000 samples) affected by phase offset for triple constraints.

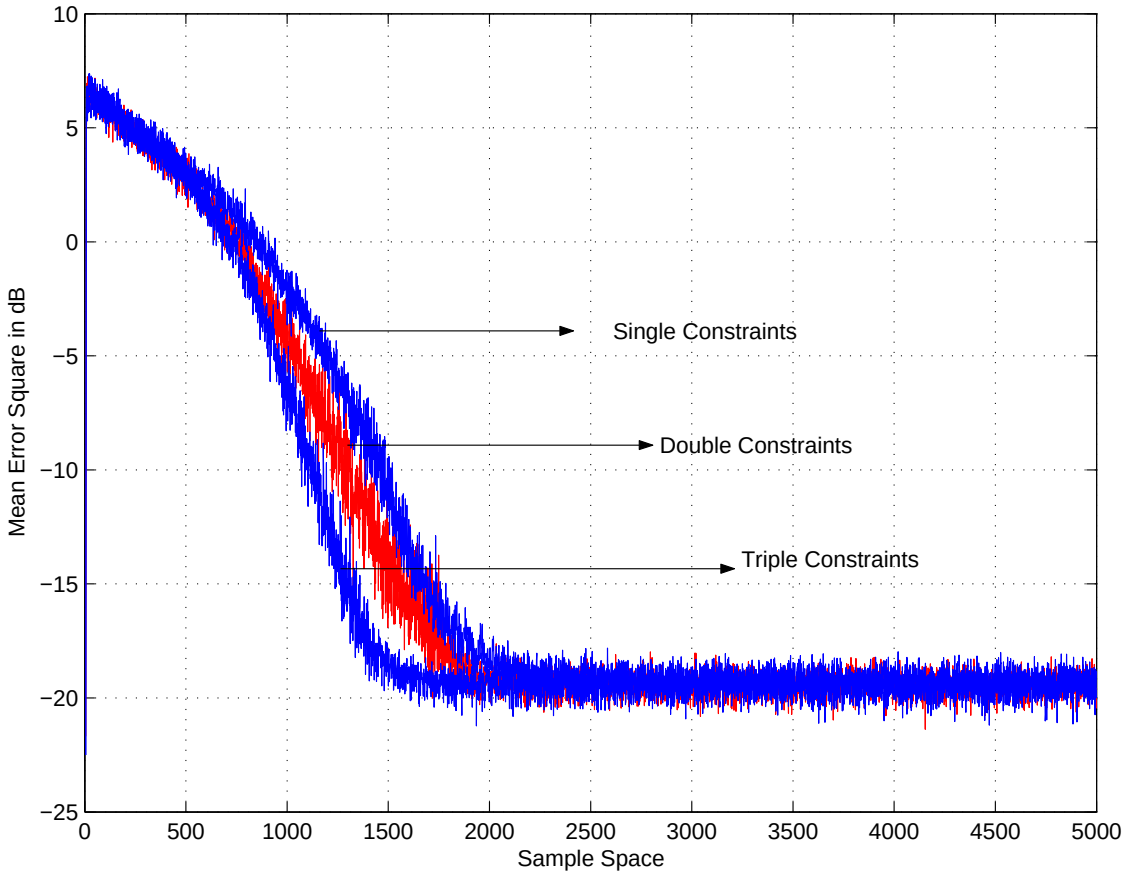

Figure 4.50: Comparison of the convergence rate for different constraints on complex channel-I as given in Figures 4.8 and 4.9 affected by phase offset, using the MSE.

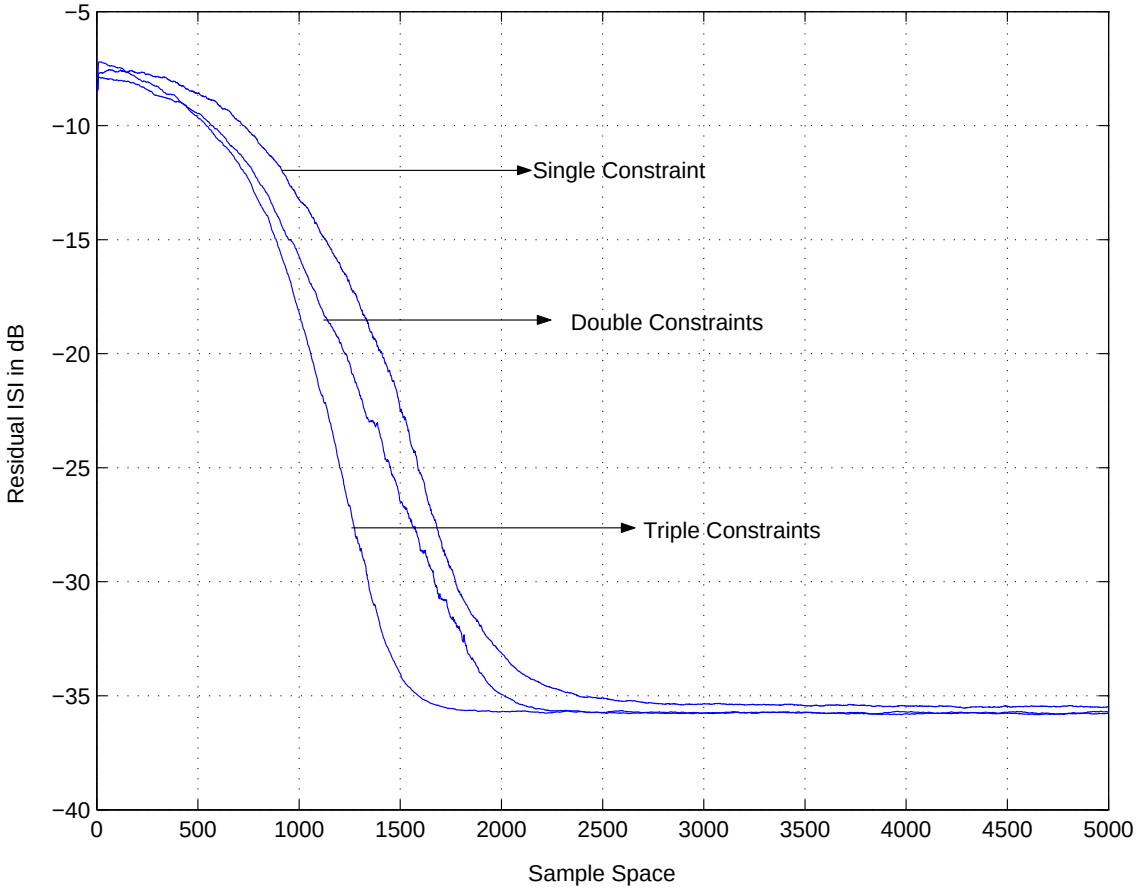

Figure 4.51: Comparison of the convergence rate for different constraints on complex channel-I as given in Figures 4.8 and 4.9 affected by phase offset using the Residual ISI .

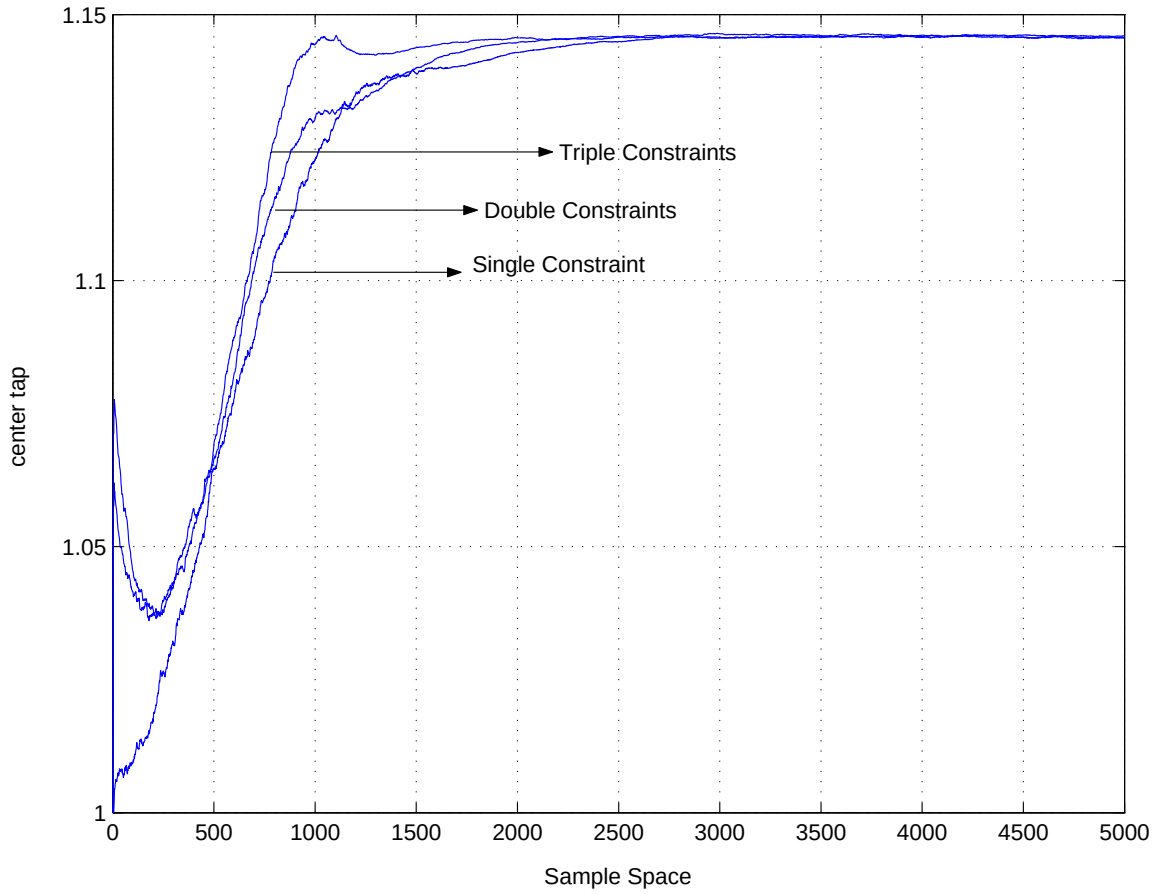

Figure 4.52: Comparison of the convergence rate for different constraints on complex channel-I as given in Figures 4.8 and 4.9 affected by phase offset using the center tap of the equalizer.

Chapter 5

Simulations for Fractionally Spaced Equalizer

Fractionally spaced equalizers are those which use a fraction of symbol duration spacing between the different window taps of an equalizer filter (as shown in Figure 5.1).

The CMA and its variants were primarily designed for linear equalization using the baud spaced FIR equalizer. However, because of baud spacing the CMA and its variants suffered from two main disadvantages

1. For finitely parameterized equalizers, the Godard algorithm has local minima that do not correspond to acceptable equalizer setting [19]

2. Noise enhancement can be severe for channels with zeros on or near the the

unit circle. Longer equalizer is typically required in order to over come this drawback [33]

In practice, Godard algorithm and its variants are often been implemented as Fractionally Spaced Equalizers (FSE). The main advantages of implementation of FSE are suppression of timing phase sensitivity and noise enhancement [8], apart from convergence to global minima and counteracting the affect of zeros near the unit circle [34].

The fractionally spaced equalizer can be represented as a filter as shown in the Figure 5.1.

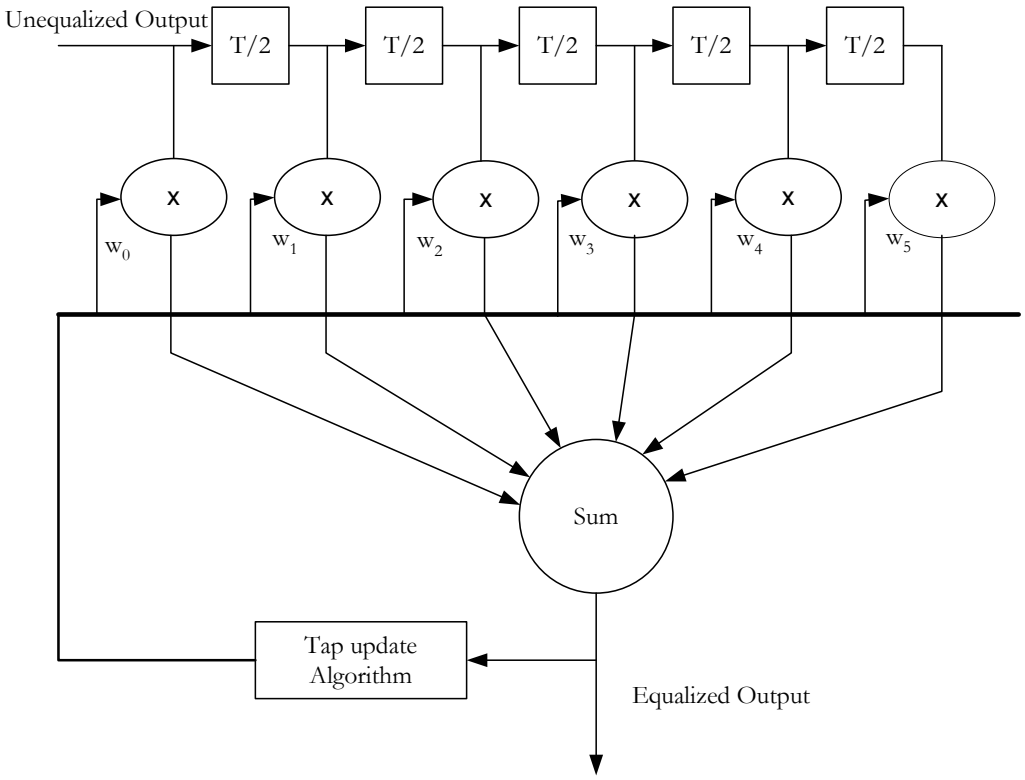

Figure 5.1: Fractionally spaced equalizer as a linear filter

The newly derived algorithm is implemented on a fractionally spaced equalizer for four different scenarios and the results are plotted. The implementation of FSE is done by over sampling the input sequence by a rate 2 just before the signal enters the equalizer.

5.1 Complex Channel-I

The tap space is reduced from baud rate to T/2 and the performance of the algorithm is observed for the complex channel I. It is observed by simulation that the mean square error converges approximately at -22dB (from Figure 5.6), a difference of 2 dB, when compared to the baud spaced scenario. Also it is observed that the difference in the algorithm convergence rate for double and three constraints at $T/2$ is reduced when compared to the difference in the convergence rate for double and three constraints at baud spacing. The signal constellation after convergence is also plotted in Figure 5.3, Figure 5.4 and Figure 5.5 which also proves the improvement in the MSE when compared to that of the baud spacing scenario.

Since the center tap of the equalizer was assumed to be equal to 1, its behaviour was also plotted inorder to confirm the convergence rate (from Figure 5.7)

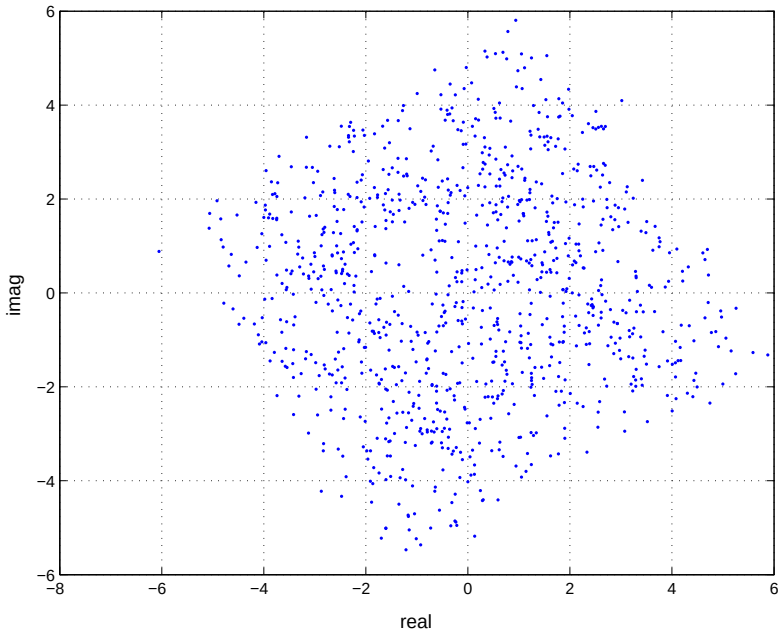

Figure 5.2: Constellation of 16-QAM signal before equalization when passed through complex channel-I as given in [1] (last 1000 samples)

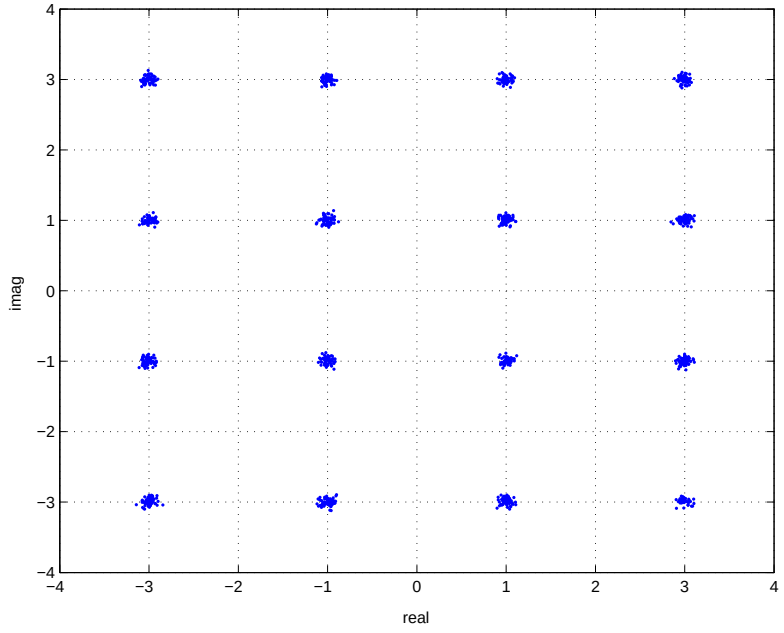

Figure 5.3: Constellation of 16-QAM signal after equalization when passed through complex channel-I as given in [1] (last 1000 samples) for single constraint at $T/2$ spacing

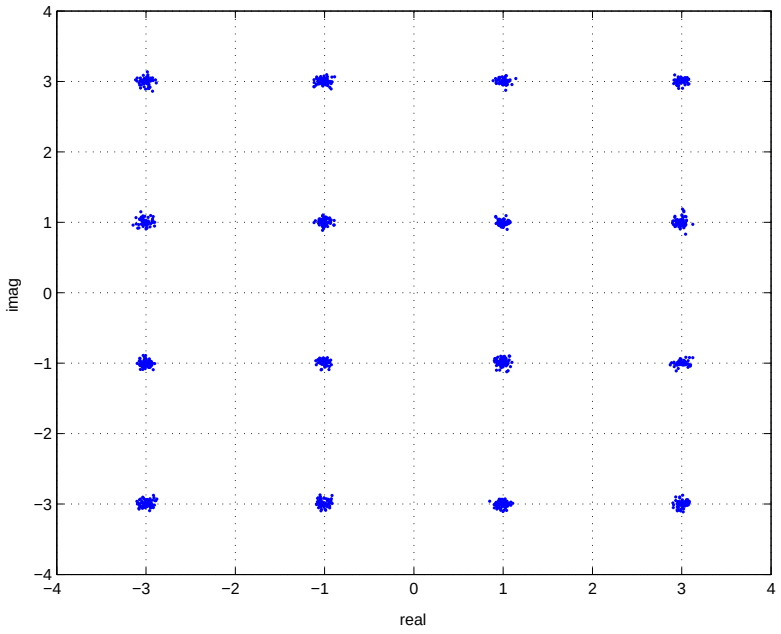

Figure 5.4: Constellation of 16-QAM signal after equalization when passed through complex channel-I as given in [1] (last 1000 samples) for double constraints at $T/2$ spacing

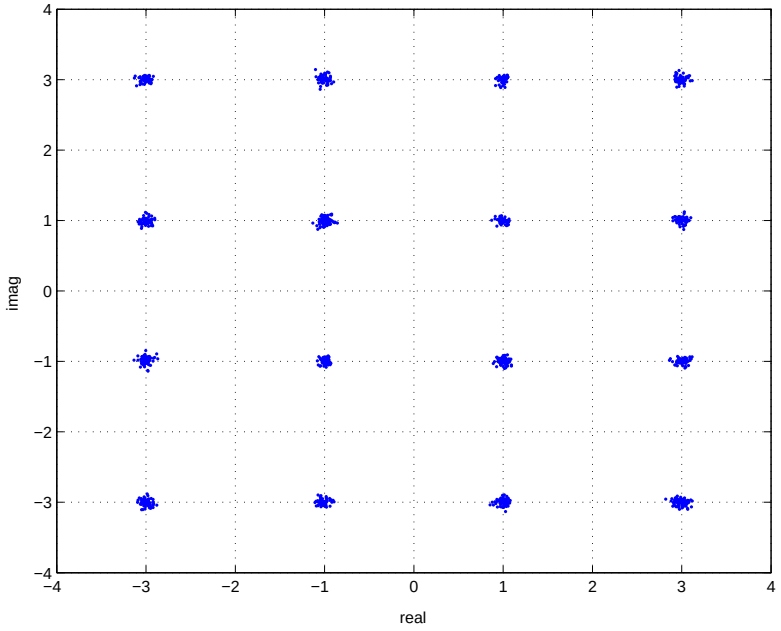

Figure 5.5: Constellation of 16-QAM signal after equalization when passed through complex channel-I as given by [1] (last 1000 samples) for three constraints at $T/2$ spacing

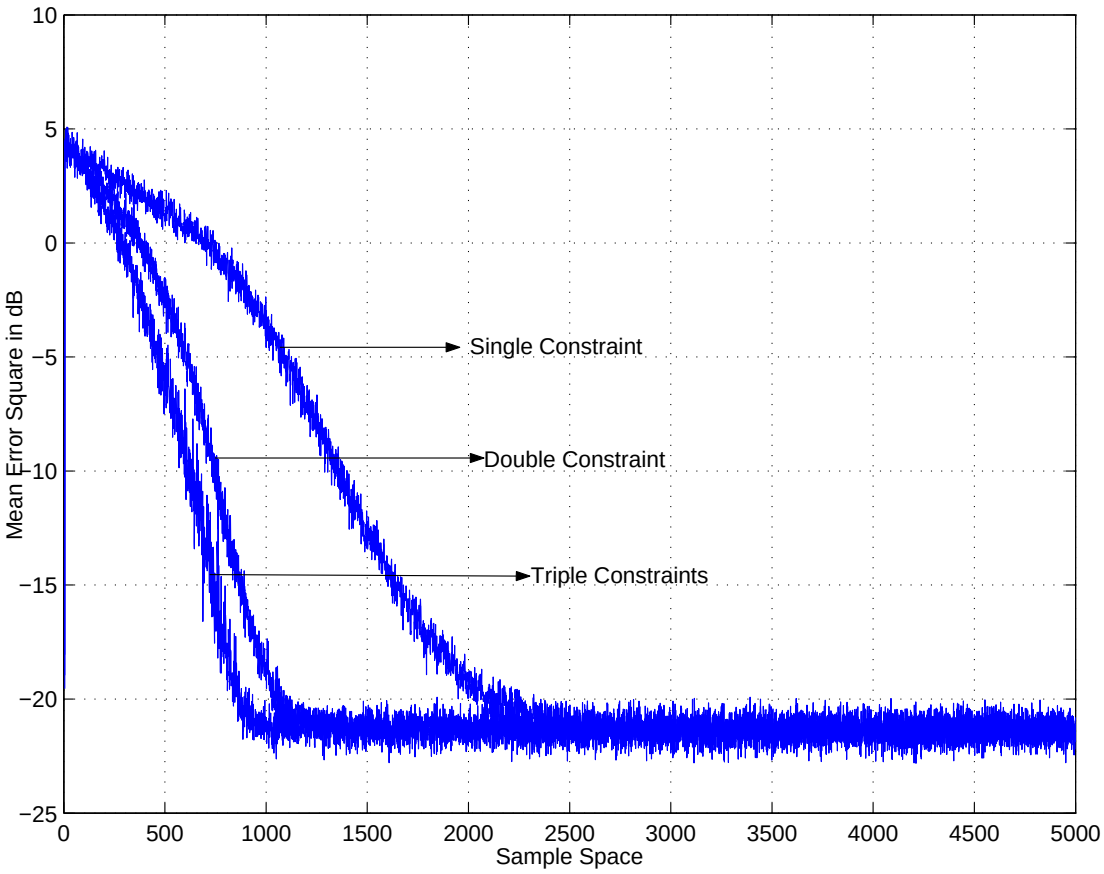

Figure 5.6: Comparison of the convergence rate for different constraints on complex channel-I using the MSE for T/2 spaced equalizer

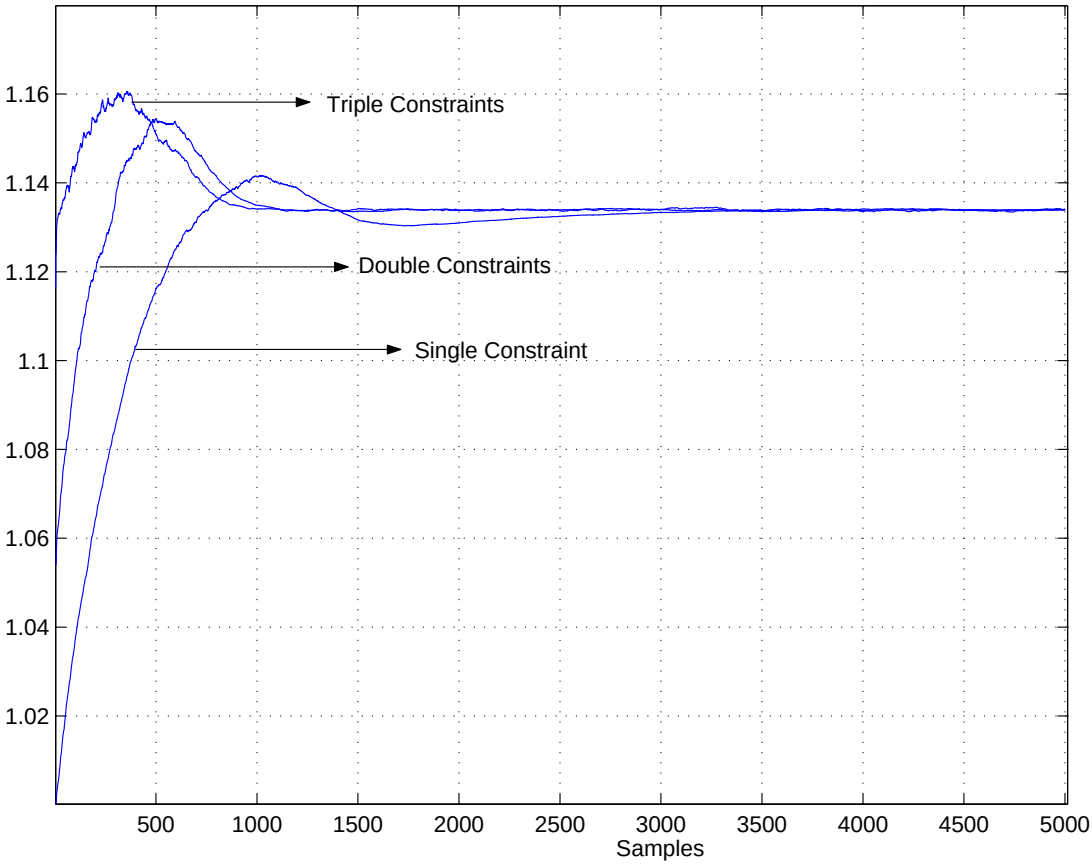

Figure 5.7: Comparison of the convergence rate for different constraints on complex channel-I using the behaviour of the center tap of a T/2 spaced equalizer

5.2 Complex Channel-II

The channel assumed is taken from the paper by Chen [31](Table 4.1). It is evident from Figure 5.11 that the MSE converges around 3000 symbols for single constraint, 2200 symbols for double constraints and 1700 symbols for triple constraints. When these results are compared with those in the baud spaced equalizer, a mark improvement not only in the convergence rate was observed but also in the MSE. The difference in the MSE is observed to be -3 dB. The constellation after convergence are also observed to be more concentrated than their counterparts in the baud spaced scenarios (from Figures 5.8, 5.9 and 5.10). Also the behaviour of the center tap is plotted to prove the convergence rate in Figure 5.12

5.3 Without the aid of decision directed scheme

The algorithm is simulated without the aid of the decision directed scheme as is done in the case of baud spaced. A nominal difference is observed in the rate of convergence for single, double and triple constraints as is seen in the case of baud spaced scenario (as shown in the Figure 5.16) . The steady state MSE is observed to be around -15 dB, a difference 2 dB from its counterpart in baud spaced scenario. The signal constellations after convergence are also plotted in Figures 5.13, 5.14 and 5.15. Since the center tap of the equalizer was assumed to be equal to 1, its behaviour is also plotted in order to confirm the convergence rate in Figure 5.17.

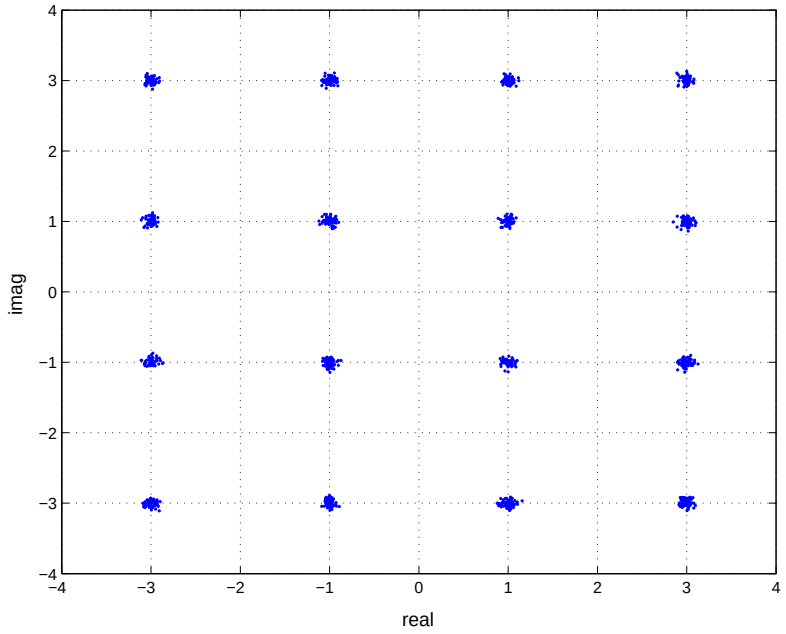

Figure 5.8: Constellation of 16-QAM signal after equalization when passed through complex channel-II as given by Table 4.1 (last 1000 samples) for single constraint at $T/2$ spacing

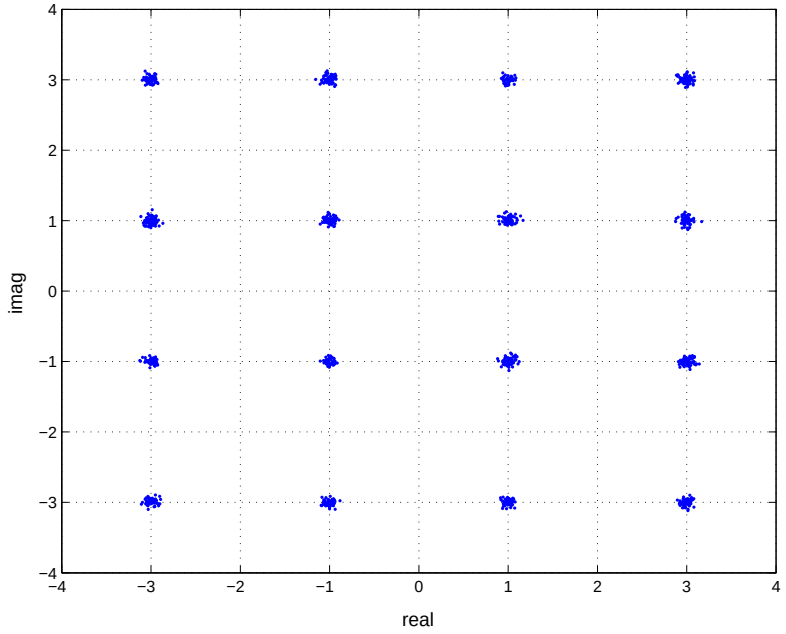

Figure 5.9: Constellation of 16-QAM signal after equalization when passed through complex channel-II as given by Table 4.1 (last 1000 samples) for double constraints at $T/2$ spacing

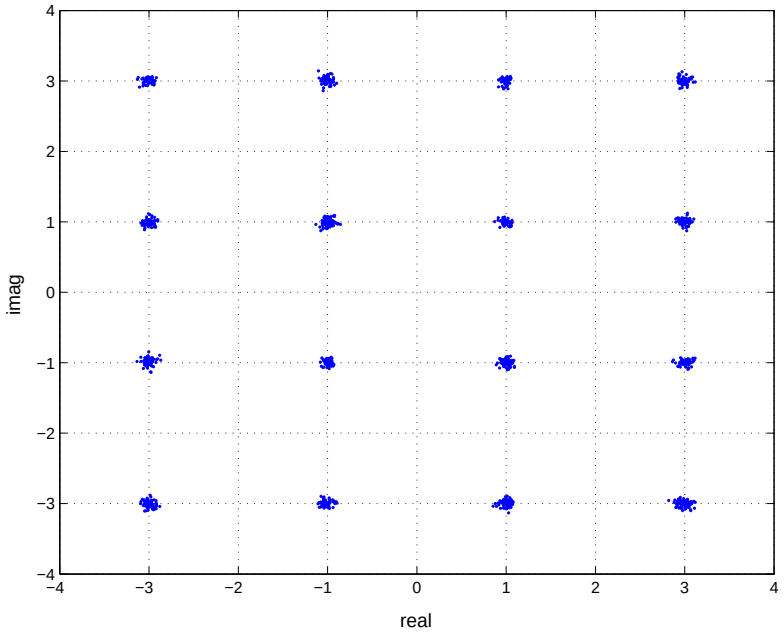

Figure 5.10: Constellation of 16-QAM signal after equalization when passed through complex channel-II as given by Table 4.1 (last 1000 samples) for three constraints at $T/2$ spacing

5.4 Simulation when the signal is effected by the phase offset

Phase offset is introduced in the signal in similar manner as done in the previous case of baud spaced equalizers (Section 4.6). The algorithm for single constraint converges around 2500 symbols. However, for the case of double and three constraints the algorithm converges at almost the same rate of 1000 symbols (as shown in Figure 5.21). In order to confirm the convergence rates the behavior of the absolute value of the center tap is also plotted (as shown in Figure 5.22). These results when are compared with the results of its counterpart in baud spaced equalizer, clearly sug-

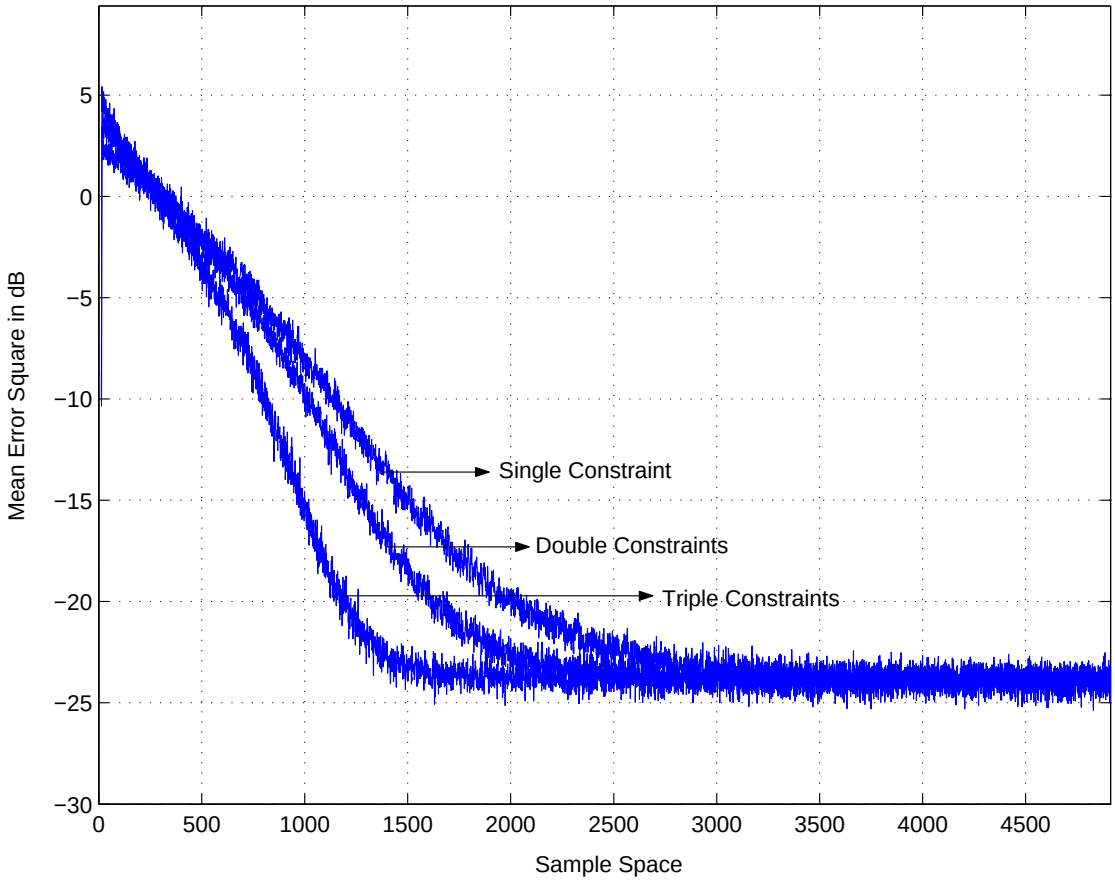

Figure 5.11: Comparison of the convergence rate for different constraints on complex channel-II as given by Table 4.1 using the MSE for T/2 spaced equalizer

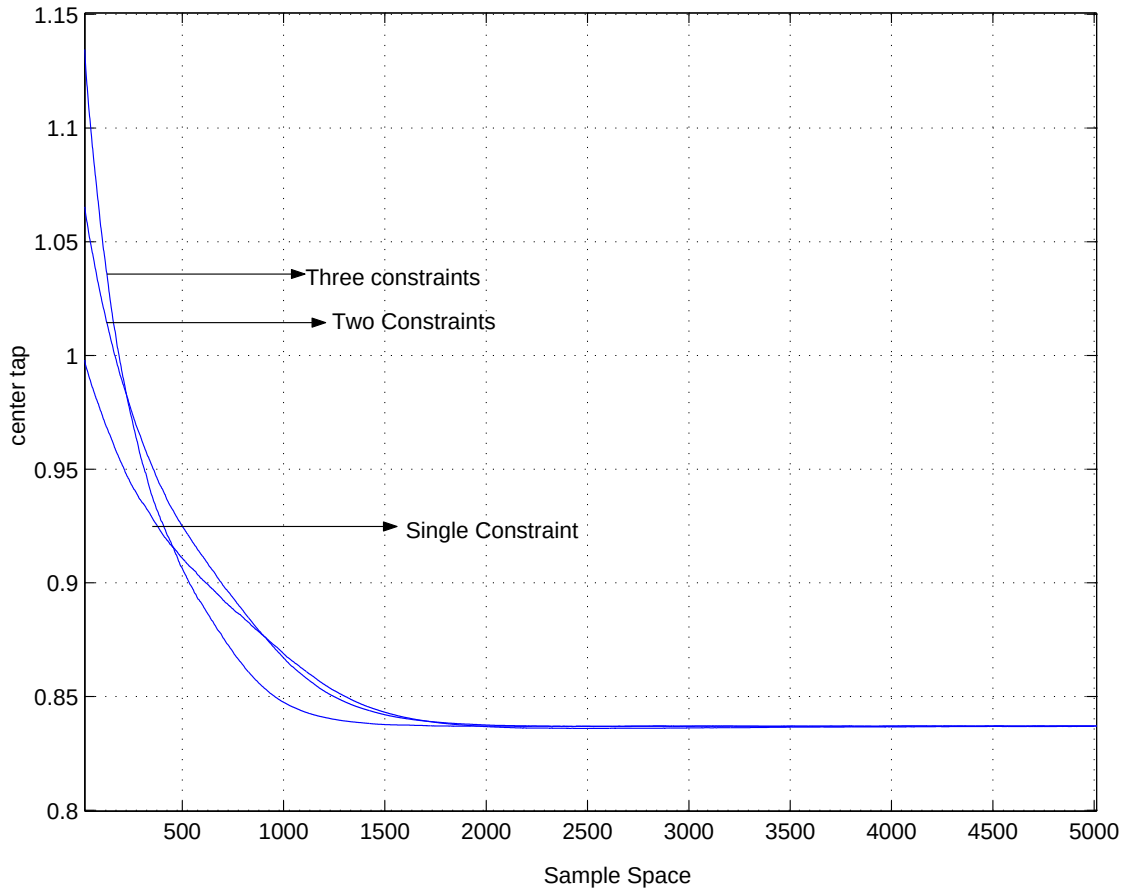

Figure 5.12: Comparison of the convergence rate for different constraints on complex channel-II as given by Table 4.1 using the center tap of the T/2 spaced equalizer

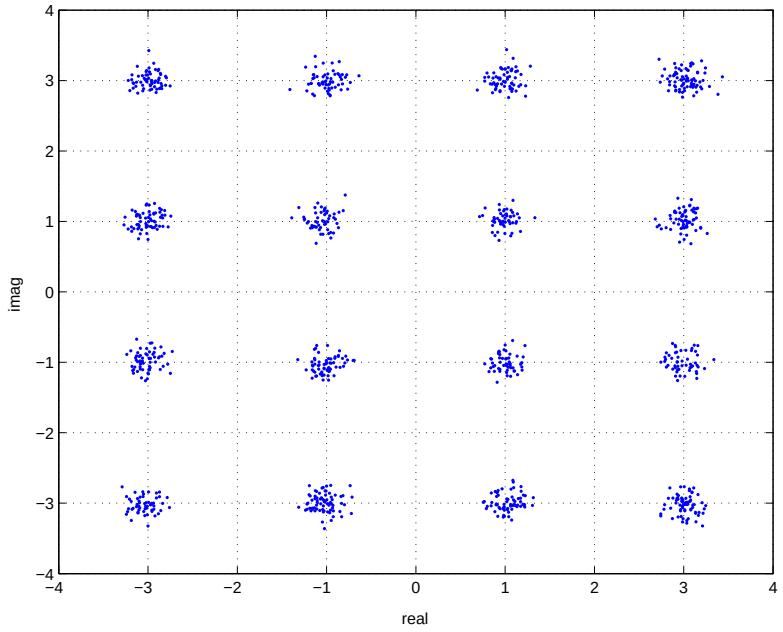

Figure 5.13: Constellation of 16-QAM signal after equalization when passed through complex channel-I as given by Picchi and Pratti [1] (last 1000 samples) for single constraint at $T/2$ spacing without the aid of decision directed mode

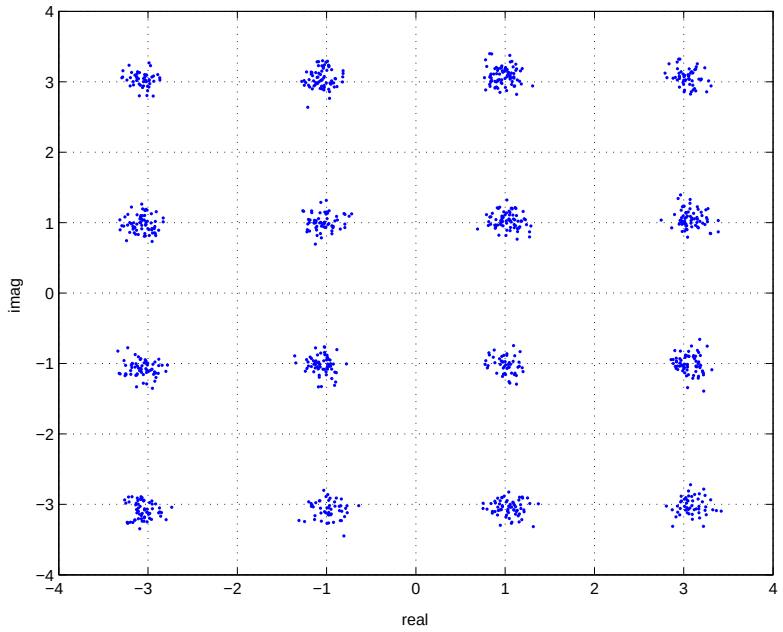

Figure 5.14: Constellation of 16-QAM signal after equalization when passed through complex channel-I as given by Picchi and Pratti [1] (last 1000 samples) for double constraints at $T/2$ spacing without the aid of decision directed mode

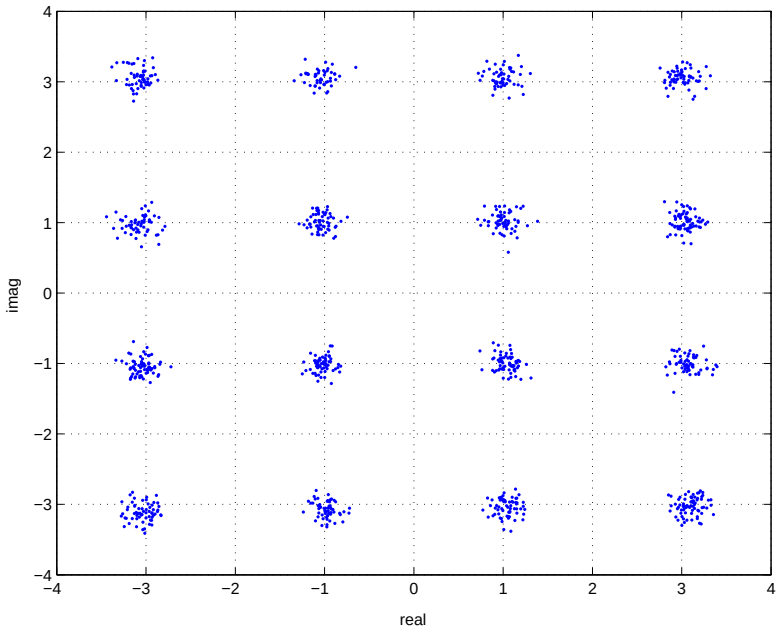

Figure 5.15: Constellation of 16-QAM signal after equalization when passed through complex channel-I as given by Picchi and Pratti [1] (last 1000 samples) for three constraints at $T/2$ spacing without the aid of decision directed mode

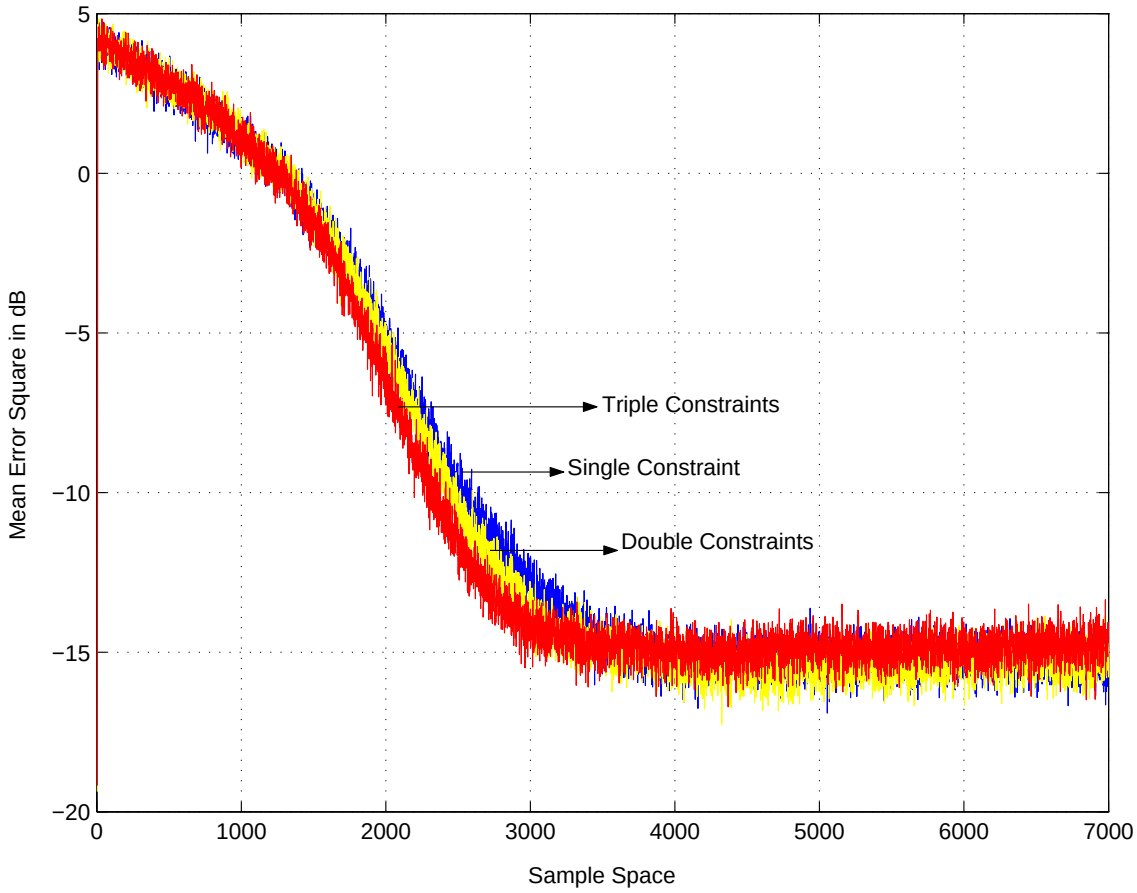

Figure 5.16: Comparison of the convergence rate for different constraints on complex channel-I as given by Picchi and Pratti [1] using the MSE for T/2 spaced equalizer without the aid of decision directed mode

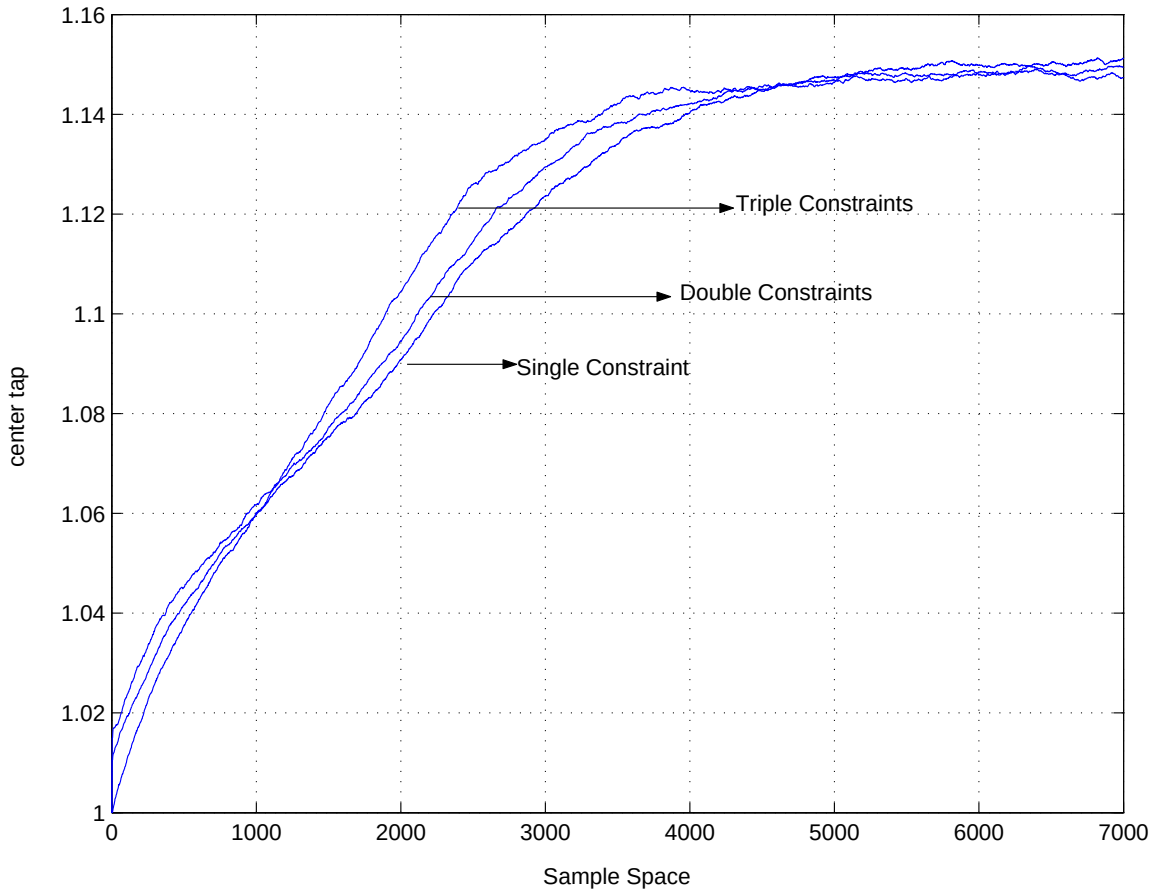

Figure 5.17: Comparison of the convergence rate for different constraints on complex channel-I as given by Picchi and Pratti [1] using the center tap of the T/2 spaced equalizer without the aid of decision directed mode

gests that introducing the fractional spacing concept in the equalizer which employs the newly derived scheme, not only gives better MSE but also better convergence rates. Also the signal constellations after the convergence are plotted for single, double and triple constraints in Figure 5.18, Figure 5.19 and Figure 5.20.

5.5 Summary

This chapter gives a brief over view about blind fractionally spaced equalization techniques, the conditions for their convergence and the performance of the newly derived scheme for $T/2$ spacing. As is evident from the simulation results the newly derived scheme can be implemented for fractional spacing also apart from baud spacing. In all the learning curves simulated, fractionally spaced equalizer performed better than the baud spaced equalizer.

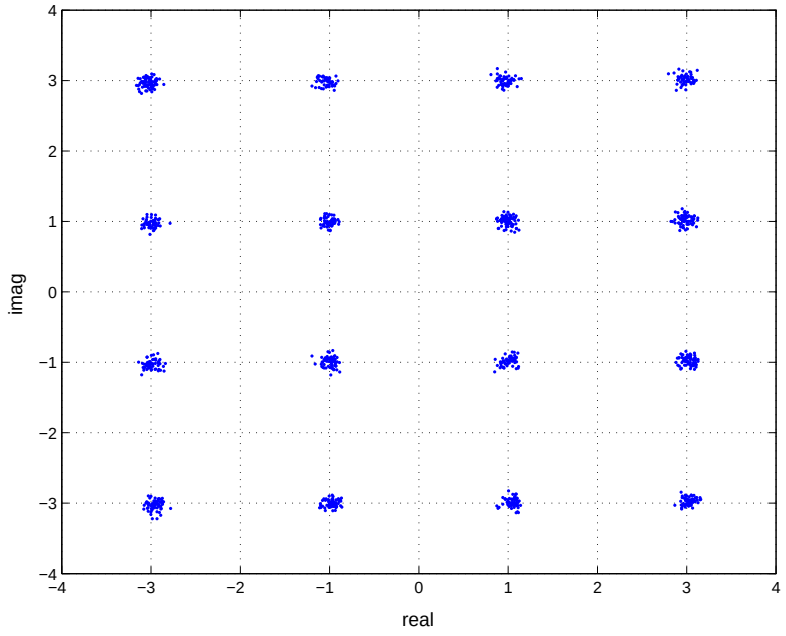

Figure 5.18: Constellation of 16-QAM signal after equalization when passed through complex channel-I as given by Picchi and Pratti [1] (last 1000 samples) effected by phase offset for single constraint at $T/2$ spacing

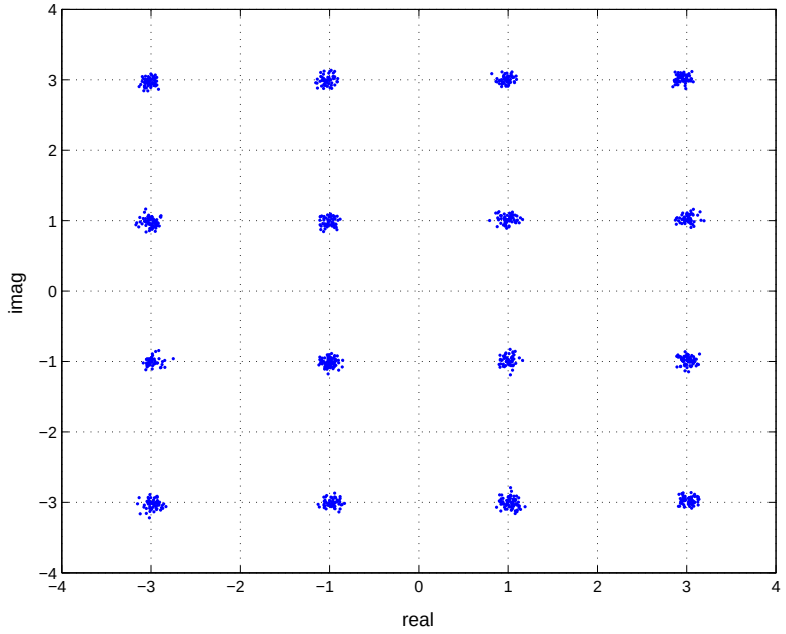

Figure 5.19: Constellation of 16-QAM signal after equalization when passed through complex channel-I as given by Picchi and Pratti [1] (last 1000 samples) effected by phase offset for double constraints at $T/2$ spacing

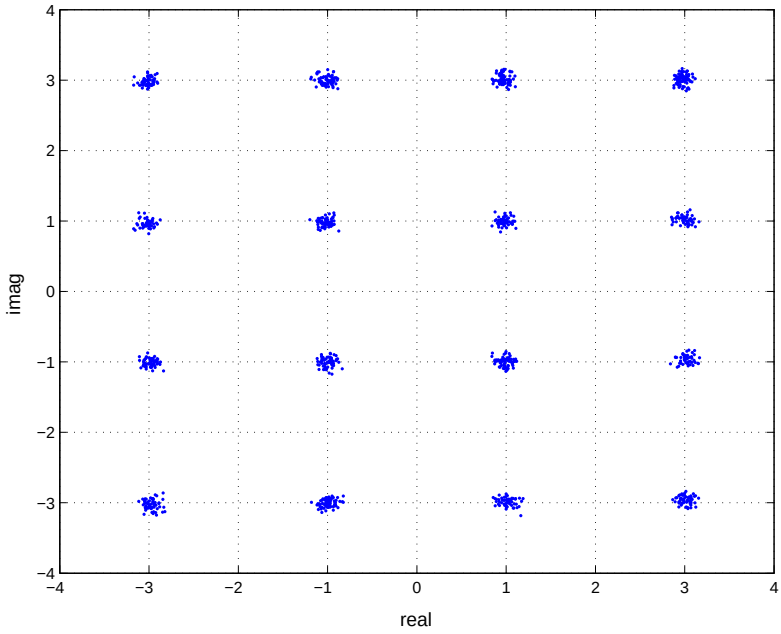

Figure 5.20: Constellation of 16-QAM signal after equalization when passed through complex channel-I as given by Picchi and Pratti [1] (last 1000 samples) effected by phase offset for triple constraints at $T/2$ spacing

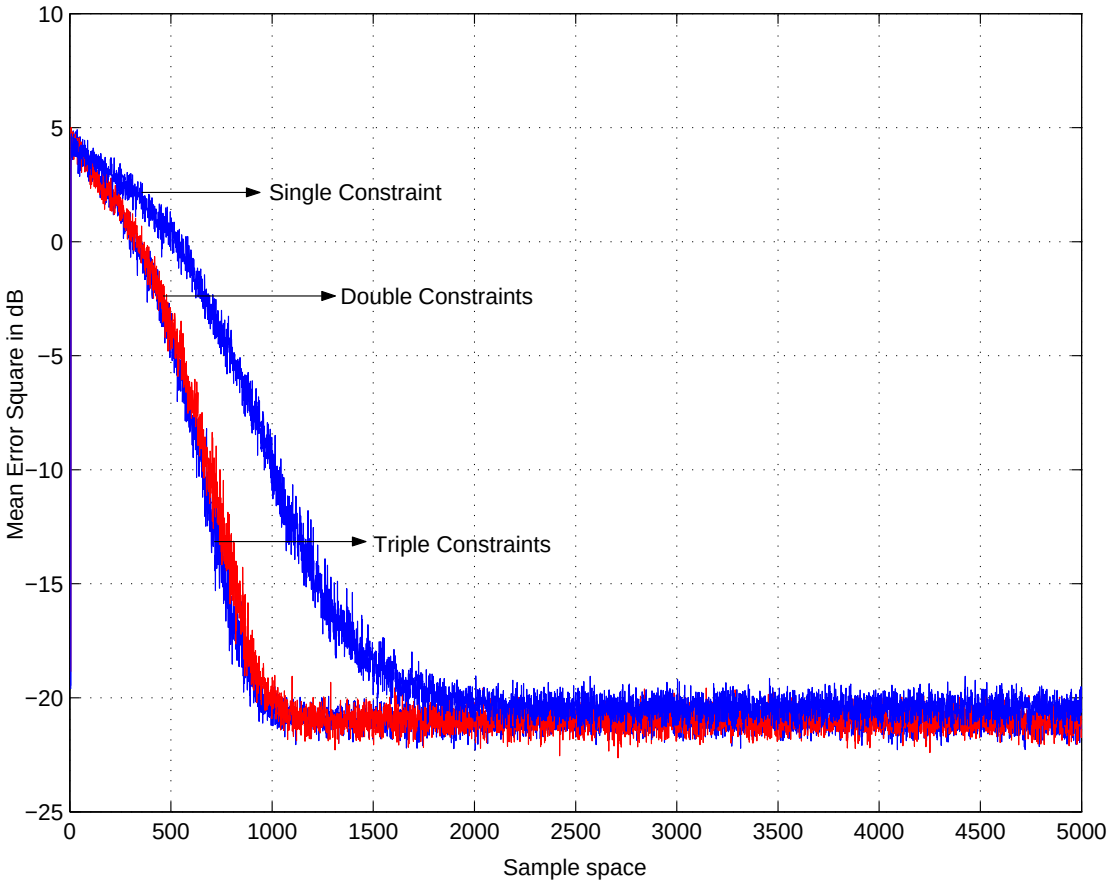

Figure 5.21: Comparison of the convergence rate for different constraints on complex channel-I as given by Picchi and Pratti [1] effected by phase offset using the MSE for T/2 spaced equalizer

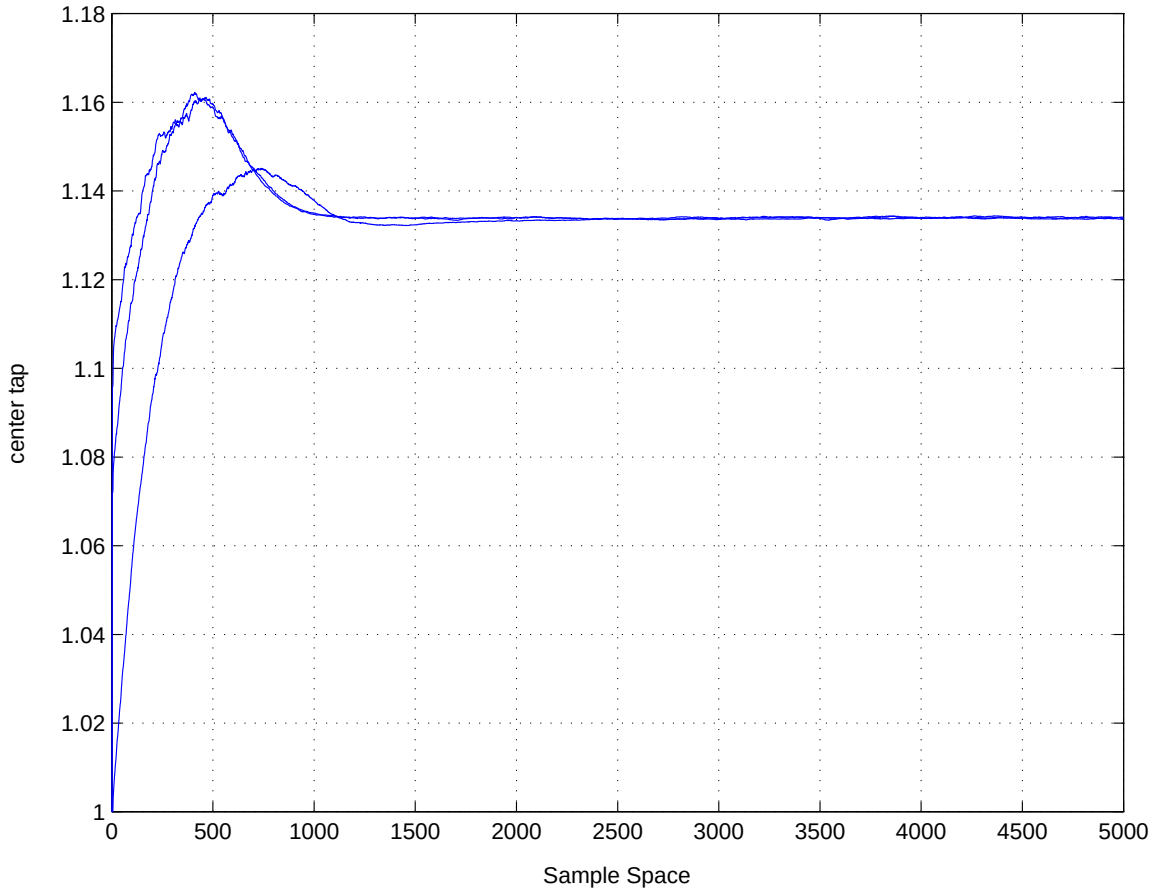

Figure 5.22: Comparison of the convergence rate for different constraints on complex channel-I as given by Picchi and Pratti [1] effected by phase offset using the center tap of the T/2 spaced equalizer

Chapter 6

Conclusions & Future Work

6.1 Conclusions

A new blind equalization scheme based on principle of minimal disturbance is successfully derived by introducing the concept of multiple constraints and using the method of Lagrange multipliers. The new scheme when compared with the existing similar schemes gives better convergence rates at the cost of complexity (from Table: 3.1). As more number of constraints are added, it is observed that the algorithm converges with an improved rate.

It is also seen that the algorithm performs well, only when used along with the decision directed mode. When the new scheme is simulated without the aid of the decision directed mode it gives results which are poorer to the existing similar algorithms. Also in the case of no decision directed mode a large impact of the

dispersion constant on convergence rates is observed. It can also be analyzed from the simulation results that the new algorithm performs better when a dispersion constant as used by Sato [6] is used than that as used by Godard [14]. Hence it can be concluded that the new algorithm has its basic traits in the R.C.A and not in C.M.A. However, when the decision directed mode is included and the dispersion constant is varied i.e. from the one used by Sato [6] to the one used by Godard [14], the algorithm exhibits no change. This is precisely due to the smooth shift of the algorithm into the decision directed mode. Hence it can be concluded that when the decision directed mode is used, the variation of the dispersion constant does not have any impact on the algorithm.

The algorithm follows the same pattern for a more severe channel, i.e. the convergence rate is improved as the number of constraints are increased. The difference between the convergence rate between the single and double constraints is also observed to increase. The main reason for the good performance of the algorithm is because of the utilization of the previous set of inputs which are left unused in the previous other algorithms and the application of the decision directed mode.

When the signal is affected by small values of phase offsets, the algorithm converges with a good rate and a steady state MSE . Hence this algorithm is also in a position to handle small phase offsets introduced by the channel apart from the phase error introduced by the complex nature of the channel. The algorithm does not shift into the decision directed mode unless and until both the real and the imag-

inary parts of the output of the equalizer are in the decision zone, whereas in the case of other algorithms the shift in the real and the imaginary parts is separate. In case of severity in the channel and phase offset those algorithms exhibit high MSE's than the new one.

Inspite of the algorithm being simulated for SNR = 20 dB, it still retained its nature of good convergence for higher number of constraints.

The algorithm is also simulated for fractionally spaced scenario Firstly, it can be concluded from the simulation results that the algorithm can be implemented for fractional spacing. Secondly, in the case of severe channels the results are promising, not only an improvement in the MSE but also an improvement in the convergence rate is observed. However, for the case of less severe channels and the without the aid of the decision directed mode the algorithm behaved in a similar manner from the convergence point of view. A difference of 2 dB is observed in the case of MSE when a comparison between baud spaced and fractionally spaced is made.

6.2 Future Work

All the constants that are present in the newly derived scheme can be varied in a optimal way to achieve better results

6.2.1 Step size parameter

The step size parameter in every algorithm controls the convergence speed, the greater the step size the more faster convergence rate is achieved. If this parameter is made to vary according to the shift in the newly derived algorithm from the blind mode to the decision directed mode, the algorithm should give better convergence rates. In order to maintain good steady state MSE, the value of the step size parameter should be varied in such a manner that in the blind mode it should be less than that in the decision directed mode.

6.2.2 Dispersion constant

The dispersion constants can be varied accordingly to the soft constraint approach as specified in the paper by Tanrikulu [11]. According to Tanrikulu the application of soft constraints to the algorithm gives better steady state MSE.

6.2.3 Application of DD mode

The other aspect which can be looked upon is the application of the decision directed mode. In the newly derived scheme the output of the algorithm is tested first for the decision zones, if the output is not in the decision zones, the algorithm is forced to use the blind mode tap update function. There exists a possibility that the decision directed mode can be applied to the algorithm simultaneously with that of the blind

mode, thus imparting greater stability and good convergence rate. However, at the rate of increased complexity.

6.2.4 Complexity

One of the major disadvantages of the newly derived scheme is the increment in the complexity. Further study can be carried out in order to reduce the complexity of the algorithm.

Bibliography

[1] G. Picchi and G. Prati. Blind equalization with carrier recovery using 'stop-and-go' decision-directed algorithm. *IEEE Trans. Commun.*, 35:877–887, September 1987.

[2] J.R Treichler and M.G. Larimore. New processing techniques based on constant modulus algorithm. *IEEE International Conference on Acoustics, Speech, and Signal Processing*, 33:420–431, April 1985.

[3] J.R.Treichler, V.Wolff, and C.R.Jhonson. Observed misconvergence in the constant modulus algorithm. *Proc. 25th Asilomar Conf. Signal, Syst., Computers*, pages 663–667, November 1991.

[4] G.Xu, H.Liu, L.Tong, and T.Kailath. A least squares approach to blind channel identification. *IEEE Trans. Signal Proc.*, 43:2982–2993, December 1995.

[5] Thomas Kailath. *Linear Estimation*. Prentice Hall, March 2000.

[6] Y. Sato. A method of self recovering equalization for multilevel amplitude modulation. *IEEE Trans. Commun.*, 23:679–682, June 1975.

[7] G. Ungerboeck. Fractional tap-spacing equalizer and consequences for clock recovery in data modems. *IEEE Trans. Commun.*, com-24,(8):856–864, August 1976..

[8] R.D.Gitlin and S.B.Weinstein. Fractionally-spaced equalizatioin : An improved digital transversal equalizer. *Bell Systems Technical Journal*, 60:275–296, February 1981.

[9] Simon Haykin. *Adaptive Filter Theory.* Prentice Hall, Englewood Cliffs, NJ, 4th edition, 2002.

[10] J.C.Lin. A blind equalisation technique based on improved constant modulus algorithm. *IEE Proceedings, Coomunications*, 149:45–50, February 2002.

[11] O.Tanrikulu, B.Baykal, A.G.Constantinides, and Jonathan A. Chambers. Soft constraint satisfaction (scs) blind channel equalization algorithms. *International Journal of Adaptive Control and Signal Processing*, 12:117–119, 1998.

[12] A. Benveniste and M. Goursat. Blind equalizers. *IEEE Trans. Commun.*, 32:871–882, August 1982.

[13] M. Goursat A. Benveniste and Ruget. Robust identification of non minimum phase system: Blind adjustment of linear equalizer in data communications. *IEEE Transaction on Automatic Control*, 25:385–389, June 1980.

[14] D. N. Godard. Self recovering equalization and carrier tracking in two-dimensional data communication systems. *IEEE Trans. Commun.*, 28:1867–1875, November 1980.

[15] Ding. Z and R.A. Kennedy. On the whereabouts of the local minima for blind adaptive equalizers. *IEEE Trans. Circuits Systems-II*, 40:119–123, 1992.

[16] K.J.R. Liu Y.Li and Z. Ding. On the convergence of blind equalization. *Technical Research Report,ISIR, Harvard University*, pages 1–22, April 1995.

[17] O. Macchi and E.Ewada. Convergence analysis of self-adaptive equalizers. *IEEE Transaction of Information and Theory*, IT-30:161–176, March 1984.

[18] G.J. Foschini. Equalization without altering or detecting data. *AT & T Tech. Journal*, pages 1885–1911, October 1985.

[19] Z. Ding, C.R Johnson, R. A. Kennedy, and B.D.O Anderson. On the ill convergence of godard blind equalizers in data communications. *IEEE Trans. Commun.*, 39:1313–1328, September 1991.

[20] K.Hilal and P.Duhammel. A convergence study of the constant modulus algorithm leading to normalized-cma and block-normalized-cma. *Euspico-92*, pages 135–138, August 1992.

[21] R.R.Bitmead and B.D.O Anderson. Performance of adaptive estimation algorithms in dependant random environments. *IEEE Transactions Automation and contrl*, AC-28:788–794, 1980.

[22] S.U.H. Qureshi. Adaptive equalization. *Proc. of the IEEE*, 40:119–123, September 1985.

[23] R. Godfrey and F. Rocca. Zero memory non-linear deconvolution. *Geophysical Prospecting*, 29:189–228, 1981.

[24] O. Shalvi and E. Weinstien. New criteria for blind deconvolution of non-minimum phase systems. *IEEE trans on Info Theroy*, 36:312–321, October 1990.

[25] O.Shalvi and E.Weinstein. Super exponential methods for blind equalization. *IEEE Transactions on Information Theory*, IT-39:504–519, March 1993.

[26] K. N Oh and Y.O Chin. Modified constant-modulus algorithm: blind equalization with carrier phase recovery algorithm. *Globecom 95.*, 29:498–502, 1995.

[27] Chii-Horng Chen Chong-Yung Chi, Ching-Yung Chen and Chih-Chun Feng. Batch proceesing algorithms using higher order statistics. *IEEE Signal Processing magazine*, pages 25–49, January 2003.

[28] O. Tanrikulu, A.G. Constantinides, and Jonathan A. Chambers. New normalized constant modulus algorithms with relaxation. *IEEE Signal Processing Letters*, 4(9):256–258, September 1997.

[29] Weerackody and Kassam. Dual-mode algorithms for blind equalization. *IEEE Transactions on Communications*, 42:22–28, January 1994.

[30] K. N. Oh and Y. Chin. New blind equalization scheme based on constantmodulus algorithm. *Globecom95*, page 865869, 1995.

[31] S. Cheng and E.S Ching. Concurrent costant modulus algorithm and soft decision-directed scheme for fractioanlly spaced blind equalization. *IEEE, ICC*, pages 2342–2345, June 2004.

[32] J.Yang, J-J.Werner, and G.A Dumont. The multi-modulus blind equalization algorithm. *IEEE International Conference od DSP*, 1:127–130, 1997.

[33] Y. Li and Z.Ding. Global convergence of fractionaly spaced godard equalizer. *Conference Record of the Twenty-Eighth Asilomar Conference*, 1:617 – 621, Oct-Nov 1994.

[34] Li. Y and Z.Ding. Global convergence of fractionally spaced godard(cma) adaptive equalizers. *IEEE Transactions on Signal Processing*, 44:818–826, 1996.

[35] Li. Y and Z.Ding. Convergence analysis of finite length blind adaptive equalizers. *IEEE Transactions for Signal Processing*, SP-43(2120-2129), 1995.

[36] L.M. Garth, J. Yang, and J-J Werner. Blind equalization algorithm for dual-mode cap-qam reception. *IEEE Trans. Commun.*, 49:455–466, March 2001.

[37] Simon Haykin. *Blind Deconvlution*. Prentice Hall, Englewod Cliffs, New Jersey, 1994.

[38] C.R.Johnson, P.Schniter, T.J.Endres, D.R.Brown, and R.A.Casas. Blind equalization using the constant modulus criterion: A review. *Proceedings of the IEEE*, 86(10):1927–1950, October 1998.

[39] D.L.Jones. A normalised constant modulus algorithm. *IEEE Proceedings ASILOMAR-29*, pages 694–679, 1996.

[40] L.B. White. Blind equalization of constant modulus signals using an adaptive observer approach. *IEEE Trans. Commun.*, 44(2):134–136, February 1996.

[41] H.Luo and R.W. Liu. Blind equalizers for multipath chanels with best equalization delay. *Proc. of ICASSP'99, Phoenix, AZ,USA.*, 5:2511–2514, May 1999.

[42] Michail K. Tsatsanis and Zhengyuan Xu. Constrained optimization methods for direct blind equalization. *IEEE Journal on selected areas of communications*, 17(3), March 1999.

[43] C. Papadias and D. Slock. On the convergence of normalized constant modulus algorithms. *Proc. International Conference on Digital Signal Processing (Nicosia-Cyprus)*, pages 245–250, July 1993.

[44] C.B.Papadias and D.T.M Slock. Normalized sliding window constant modulus and decision-directed algorithms: A link between blind equalization and classical adaptive filtering. *IEEE Transactions on Signal Processing*, 45(1):231–235, January 1997.

[45] M.Rupp and S.C Douglas. A posteriori analysis of adaptive blind equalizers. *32 and Asilomar Conference on Signals, Systems and Computers*, 1:369–373, 1998.

[46] G.Ungerboek. Theory on the speed of convergence in adaptive equalizers for digital communications. *IBM Journal Res. Develop.*, 11:546–555, November 1972.

[47] K. Wesolowsky. Analysis and properties of modified constant modulus algorithm. *Communication Theory*, 49:225–230, May-June 1992.

[48] H.H.Zeng and L.Tong. Blind equalization using the constant modulus alogrithm. *Proceedings of International Conference on Signal Processing*, pages 400–403, 1996.

Vitae

- Bakhtiar Qutub Ali.
- Born in Raichur, Karnataka, India on January 17th, 1980.
- Received Bachelor of Technology (B.E) degree in Electronics and Communication Engineering from Jawahar Lal Nehru Technological University, Hyderabad, Andhra Pradesh, India in 2001.
- Joined King Fahd University of Petroleum and Minerals in September 2002.
- Email: bqutub@kfupm.edu.sa